

**SHEAR AND BENDING RESPONSE
OF INELASTIC STRUCTURES
TO DYNAMIC LOAD**

KADRE TORN



TARTU UNIVERSITY
PRESS

Department of Mathematics, University of Tartu, Tartu, Estonia

Dissertation is accepted for the commencement of the degree of Doctor of Philosophy (PhD) on March 24, 2006 by the Council of the Department of Mathematics, University of Tartu.

Supervisor:

Dr. Sci., Professor

Jaan Lellep
University of Tartu
Estonia

Opponents:

Dr. Techn., Professor

Janis Brauns
Latvian Agricultural University
Latvia

Dr. Techn., Professor Emeritus

Jakub Kõo
Estonian University of Life Sciences
Estonia

Commencement will take place on May 9, 2006.

Publication of this dissertation is granted by the Institute of Applied Mathematics, University of Tartu (project HMTRM)

ISSN 1024-4212

ISBN 9949-11-300-8 (trükis)

ISBN 9949-11-301-6 (PDF)

Autoriõigus Kadre Torn, 2006

Tartu Ülikooli Kirjastus

www.tyk.ee

Tellimus nr. 225

Department of Mathematics, University of Tartu, Tartu, Estonia

Dissertation is accepted for the commencement of the degree of Doctor of Philosophy (PhD) on March 24, 2006 by the Council of the Department of Mathematics, University of Tartu.

Supervisor:

Dr. Sci University of Tartu, Estonia, Professor Jaan Lellep

Opponents:

Dr. Techn., Professor

Janis Brauns

Latvian Agricultural University

Latvia

Dr. Techn., Professor Emeritus

Jakub Kõo

Estonian University of Life Sciences

Estonia

Commencement will take place on May 9, 2006.

Publication of this dissertation is granted by the Institute of Applied Mathematics, University of Tartu (research project TMTRM0066)

Kadre Torn, 2006

Tartu Ülikooli Kirjastuse trükikoda
Tiigi 78, 50410 Tartu
Tellimus nr.

CONTENTS

INTRODUCTION	7
1 Basic equations	13
1.1 Beams	15
1.1.1 Geometry of the beam	15
1.1.2 Equilibrium equations	15
1.1.3 Strain components	17
1.1.4 Principle of virtual work	17
1.1.5 Yield surfaces and associated flow law	18
1.2 Annular and circular plates	19
1.2.1 Geometry of the plate	19
1.2.2 Equilibrium equations	20
1.2.3 Strain components	20
1.2.4 Principle of virtual work	21
1.2.5 Yield condition	21
1.3 Circular cylindrical shells	22
1.3.1 Geometry of the shell	22
1.3.2 Equilibrium equations	22
1.3.3 Strain components	24
1.3.4 Principle of virtual work	24
1.3.5 Yield surface and associated flow law	25
2 Shear and bending response of a rigid-plastic beam subjected to impulsive loading	31
2.1 Introduction	34
2.2 Basic equations	35
2.3 Theoretical solution for the beam subjected to an impulsive velocity	36
2.3.1 Case I	36
2.3.2 Case II	39

2.3.3	Case III	44
2.3.4	Case IV	46
2.3.5	Case V	49
2.4	Discussion	50
2.5	Concluding remarks	53
2.6	References	54
3	Dynamic plastic behaviour of annular plates with transverse shear effects	63
3.1	Introduction	66
3.2	Governing equations	68
3.3	Solution of governing equations	70
3.3.1	Case I	70
3.3.2	Case II	71
3.3.3	Case III	74
3.4	Discussion	79
3.5	Concluding remarks	82
3.6	References	84
4	Plastic response of a circular cylindrical shell to dynamic loadings	95
4.1	Introduction	98
4.2	Governing equations	99
4.3	Theoretical prediction of the response to impulsive loading .	101
4.3.1	Case I	101
4.3.2	Case II	103
4.3.3	Case III	107
4.3.4	Case IV	109
4.3.5	Case V	112
4.4	Discussion	114
4.5	Concluding remarks	116
4.6	References	118
	REFERENCES	127
	SUMMARY	135
	KOKKUVÕTE	136
	ACKNOWLEDGEMENT	137
	CURRICULUM VITAE	138
	CURRICULUM VITAE	139

INTRODUCTION

The concept of a rigid-plastic body has received a great deal of attention among researchers in the field of mechanical engineering and practical engineers. This concept is useful not only in the theory of applied plasticity but in the limit analysis as well as in the dynamic plasticity of inelastic structures. Foundations of theoretical concepts and solutions of practical problems of limit analysis can be found in the books by Calladine (1985), Horne (1971), Kaliszky (1989), Martin (1975), Skrzypek and Hetnarski (1993), Źyczkowski (1981), Johnson and Mellor (1986), Chakrabarty (2000). Many authors like Hodge (1981), Erkhov (1978), Sawczuk (1989), Sawczuk and Sokół-Supel (1993), Yu and Zang (1996), Lin (1968), Save, Massonnet, Saxce (1997) and others concentrated on the thin walled plate and shell problems; applications of the limit analysis in the soil mechanics have studied by Chen and Liu (1990). Various aspects of dynamic loading of structures and media are presented in books by Jones (1989), Jones and Wierzbicki (1983, 1989), Stronge and Yu (1993), Lepik (1982), Komarov and Nemirovsky (1984), Campbell (1972) and of shakedown analysis by Nguyen Dang (1995).

Analytical solutions for dynamically loaded beams fixed at both ends are given by Symonds (see Jones (1989)) making use of the hypothesis of the classical bending theory of plates. Beams subjected to impulsive loading and resting on $n + 2$ supports were considered by Lellep (1978).

Comparison of theoretical predictions with experimental data lead to the conclusion that the transverse shear forces can exercise an important role in the dynamic plastic behaviour of beams, plates and shells as discussed by Jones (1989), Stronge and Yu (1993) and others. The influence of the transverse shear on the dynamic behaviour of rigid-plastic beams has been studied by several authors. Symonds (1968) has examined the influence of shear forces on the plastic response of an infinitely long beam struck by a mass travelling with an initial velocity. In the paper by Symonds (1968) a fully clamped beam of finite length that is subjected to an impulsive pressure loading has been studied also. Symonds (1968) used an approximate square instead of the exact yield locus. He concluded that a transverse shear hinge is always stationary in a rigid perfectly plastic beam. This implies that transverse shear is localized within the initially formed zone when material strain hardening is neglected. Later Symonds' conclusion has been extended to arbitrary regular and singular yield conditions. Li (2000) showed that this is true for symmetrically loaded circular plates and cylindrical shells, as well. Nonaka (1967, 1977) has presented the solutions for simply supported beams subjected to uniformly distributed blast pressure loading. Nonakas results were extended to the case when the blast pressure loading is uniformly distributed over a portion of the span by Jones and Song (1986). Nine different patterns of motion are obtained whereas the cases of rectangular, triangular and exponential pulse loadings

are examined. Theoretical solutions for fully clamped beams subjected to the blast pressure loading are presented by Li and Jones (1995), clamped beams under impulsive loading are studied by Yu and Chen (2000).

In these studies the bending moment as well as the transverse shear force are retained in the yield curve which is presented as a square yield curve. The accuracy of this approximation of the yield condition is discussed by de Oliveira and Jones (1978) on the basis of I-beams.

The influence of the rotatory inertia and transverse shear forces on the dynamic plastic response of rigid-plastic beams has been examined by Jones and de Oliveira (1979a,b). Jones (1985) has demonstrated that the simple bound theorems which were developed for rigid-plastic continua provide excellent estimates of the response durations and permanent displacements of impulsively loaded beams, circular plates and cylindrical shells when transverse shear effects are taken into account.

Jones and de Oliveira (1983), also Li and Jones (1995) have studied the plastic response of cylindrical shells to impulsive and blast loadings. The influence of transverse shear effects on the behaviour of circular plates was investigated by Jones and de Oliveira (1980) and by Li and Jones (1994).

In the investigations cited above the both ends of the beams under considerations are simply supported or fully clamped, respectively. In the paper by Lellep and Torn (2005) dynamic plastic response of beams clamped at left ends and simply supported at right hand ends will be investigated. The influence of the transverse shear is retained in the yield condition.

The first analytical work on dynamic plastic response of cylindrical shells was conducted by Hodge (1955). Song and Wang (1965) considered cantilever cylindrical shells.

In the paper by Lellep (1984) circular cylindrical shells reinforced with circumferential ribs were studied. Circular ribs were treated as absolutely rigid ring supports.

The influence of transverse shear forces on the dynamic plastic behaviour of beams, plates and shells subjected to impulsive and impact loading has attracted the interest of many researchers as discussed by Jones (1985, 1989a, b), Stronge and Yu (1993), Yu and Chen (2000).

The influence of shear forces on the limit load of cylindrical shells was investigated by Shablii and Zuk (1974), also by Haydl and Sherbourne (1973, 1979) making use of different non-linear approximations of the exact yield surface corresponding to Mises yield condition (Ilyushin, 1957).

The influence of both, transverse shear and rotatory inertia on the dynamic plastic behaviour of beams and circular plates was studied by Jones and Gomes de Oliveira (1979, 1980). Circular cylindrical shells subjected to impulsive and blast loading are studied by Duffey (1989), Li and Jones (1995), Jones and Oliveira (1983). In the above mentioned studies, the both ends of beams or cylindrical shells are fixed in the same manner. The exceptions are papers Lellep, Torn (2000) and Song, Wang (1965). In the

paper Lellep, Torn (2004), beams simply supported at the left and clamped at the right-hand end are considered. In the paper by Lellep, Torn (2005) the results of the previous paper are extended to circular cylindrical shells and in paper [46] - to annular plates.

The studies on dynamic plastic response of axisymmetric plates got its start by papers of Hopkins and Prager (1954) and Wang (1955). In these papers simply supported and clamped circular plates subjected to distributed loading and initial impulsive loading were studied resorting to the classical plate theory.

Hopkins and Prager considered circular plates made of an ideal rigid-plastic material which obeys Tresca's yield condition and associated flow law. This solution has been extended to plates subjected to the uniformly distributed transverse pressure and radial tension at the edge by Lellep (1971). It was assumed that the material of plate was an anisotropic material with different yield stresses in tension and compression.

Rigid-plastic annular plates (e.g. circular plates with a central hole) subjected to dynamical loadings have been considered by Jones (1968, 1989), Mroz (1958), Aggarwal and Ablow (1971), Mazalov and Nemirovsky (1976) using the bending theory of plates. In the case of a rigid-plastic material this concept includes stationary and moving hinge circles separating adjacent annuli of the plate which can deform in different manner.

An annular plate clamped at the inner boundary with its free outer edge given a constant velocity for a short time was studied by Shapiro (1959). Later an annular plate with a uniform transverse impulse on a narrow annular area near the outer edge was investigated by Florence (1965). Florence considered the annular plate clamped at the inner edge with free outer edge using Tresca's yield hexagon. In the subsequent papers by Florence (1966, 1977) rigid-plastic circular plates subjected blast loadings distributed over the entire plate or over a central area, respectively, are investigated. Annular plates fixed at the inner edge were studied also by Niepostyn and Stańczyk (1979, 1982) in the cases of various loadings.

Recently Guowei Ma et al (1999), Yan-bin Wang et al (2005) employed the concept of a unified strength theory in the analysis of dynamic plastic response of circular plates.

Wen, Yu, Reddy (1995,b) developed an approximate theory to examine the dynamic inelastic deformation and failure of clamped circular plates subjected to uniformly distributed impulsive loads. Resorting to the previous work by Wen, Yu, Reddy (1995,a) it was shown that the failure modes are: large inelastic deformations (Mode I), tensile tearing (Mode II) and transverse shear (Mode III).

The influence of shear forces on the static collapse pressure was investigated by Sawczuk and Duszek (1963), Haydl and Sherbourne (1973, 1979), Zhuk and Shablii (1972, 1973), Mohaghegh and Coon (1973), Dinno and Robinson (1976).

Shablii and Zhuk (1974) investigated problems of limit analysis of circular cylindrical shells accounting for shear forces.

Probably the first paper devoted to the investigation of rigid-plastic motion of axisymmetric plates accounting for transverse shear effects is due to Nemirovski and Skovoroda (1978). In this paper fully clamped and simply supported circular plates subjected to a distributed transverse loading are considered. The time history of the load intensity is assumed to be prescribed with a non-increasing function.

Jones and Oliveira (1980) studied the influence of the rotatory inertia and shear forces on the dynamic plastic response of circular plates to dynamic loads. This study revealed the influence of shear forces on the behaviour of plates in the case of small values of the parameter ν . Li and Jones (1994) investigated clamped circular plates subjected to blast loading distributed uniformly over the entire area of the plate. Theoretical solutions are obtained for a general blast loading for a plate made of a Johansen's material. The effects of different boundary conditions, pressure pulse loading shapes and the influence of the transverse shear force on the dynamic plastic response of circular plates are explored. The applicability of Youngdahl's correlation parameter is stated for circular plates. The case of a central pressure pulse distributed over a central part was investigated by Liu and Stronge (1996). Komarov and Nemirovski (1984), resorting to the paper by Nemirovski and Skovoroda (1978) gave solutions for clamped circular plates accounting for shear stresses.

The motion of a simply supported circular plate subjected to a rectangular loading was studied by Kumar and Krishka Reddy (1986). In a similar study under taken by Jones and Oliveira (1980) for circular plates subjected to blast loading idealized by an instantaneous uniform velocity, it was concluded that the velocity pattern depends on a parameter $\nu = RQ_0/2M_0$. Here R is the radius of the plate, Q_0 and M_0 stand for the limit shear force and limit bending moment, respectively. Following a procedure similar to that by Jones and Oliveira (1980) the expressions for the shear force, bending moment and the plate deflection have been obtained. It appeared that the solution of the problem including shear showed greater radial moments throughout the plate when compared with the pure bending solution. The transverse shear failure of infinitely large circular plates with a central boss which is subjected to an initial impulsive velocity was studied by Zhao et al (1994).

Clamped circular plates made of work-hardening materials were studied by Wen (1998). An approximate theory was developed to predict the deformations and tearing of plates for power-law stress-strain relationship. Theoretical predictions are shown to be in good agreement with experimental data. Viscoplastic metallic circular plates subjected to impulsive loading are considered by Zaera, Arias and Navarro (2002) making use of various non-linear approximations of the actual yield surface.

Li and Jones (2000,a), also Hu (2000) used the dimensionless damage

number $D = \rho V_0^2 / \sigma_0$ (where ρ is material density, V_0 - initial velocity and σ_0 - yield stress) in order to assess the dynamic behaviour of plastic plates. The dynamic plastic response number was generalized for spherical and cylindrical shells by Shi and Gao (2001).

Li and Jones (2000,b) investigated the formation of a transverse shear localization (shear hinge) in a structural element made of a ductile material and subjected to transverse loading. A rigid-plastic beam element is considered in a greater detail. The current conclusions are applied to circular plates and cylindrical shells.

Li and Huang (1989, 1990) considered the case of a simply supported circular plate subjected to a uniformly distributed transverse pressure loading of rectangular shape. The basic equations established retain transverse shear forces and bending moments for an arbitrary loading case. Theoretical solutions are given for a rectangular shaped pressure loading and the effects of transverse shear and rotatory inertia are revealed in the comparisons with other solutions.

A theoretical study on the dynamic plastic response of aluminium alloy and mild steel circular plates struck normally by blunt solid cylindrical masses at the center of the plate is presented by Jones, Kim, Li (1997). Different failure mechanisms which have been revealed in previous experimental studies on aluminium and mild steel plates are compared by the proposed theory.

Dynamic bending of piece-wise non-homogeneous beams and circular plates has been investigated under different assumptions by Lepik (1982), Mazalov and Nemirovski (1973). The method of mode form motions suggested by Martin and Symonds (see Martin (1975)) was used in the dynamic plastic analysis of circular and annular plates by Lellep and Mürk (2003) and of reinforced cylindrical tubes by Lellep and Sakkov (1996).

In the present study dynamic plastic response of beams, annular plates and cylindrical shells is considered. The aim of the work is to investigate the influence of shear forces on the dynamic behaviour of structural elements. The attention is focused on beams and tubes with non-symmetrical end conditions, also on annular plates with supported outer edge and free inner edge.

Current study consists of the introduction and four chapters. In the introduction review of existing literature in this area is presented. The material presented in Chapter 1 is compiled on the basis of books by Chakrabarty (2000), Jones (1989), Kaliszky (1989), Skrzypek and Hetnarski (1993). In Chapters 2-4 corresponding papers of the author are presented; the paper regarding to annular plates (Chapter 3) is in press.

CHAPTER 1

Basic equations

In this chapter governing equations for investigation of the dynamic plastic behaviour of beams, plates and shells are presented. When preparing the material of this chapter the books by Jones (1989) etc where used.

1.1 Beams

1.1.1 Geometry of the beam

Let us consider beams of length l with different end conditions as shown in Fig. 1.1-1.4.

1.1.2 Equilibrium equations

The equations of motion of the beam may be written as (Jones, 1989)

$$\begin{aligned} \frac{\partial M}{\partial x} - Q &= 0 \\ \frac{\partial Q}{\partial x} &= \bar{m} \frac{\partial^2 W}{\partial t^2} - P. \end{aligned} \quad (1.1)$$

Here M and Q stand for the bending moment and shear force, respectively. Here P is the intensity of distributed transverse loading, whereas \bar{m} is the mass per unit length of the beam and W is the transverse displacement.

When deriving (1.1) shear forces are retained in the analysis but the rotatory inertia is neglected. The equilibrium equations will be solved making use of appropriate boundary conditions. Boundary conditions are following.

1) In the case of a beam simply supported at both ends (Fig. 1.1) one has

$$M(0, t) = M(l, t) = 0.$$

Kinematical boundary conditions are

$$W(0, t) = 0$$

if $|Q(0, t)| \neq Q_0$ and

$$W(l, t) = 0$$

if $|Q(l, t)| \neq Q_0$ where Q_0 is the limit value of the shear force.

If

$$Q(0, t) = \pm Q_0$$

or

$$Q(l, t) = \pm Q_0$$

then shear sliding takes place at supports and $W(0, t) \neq 0$, $W(l, t) \neq 0$.

2) In the case of a beam simply supported at the right end and fully clamped at the left end (Fig. 1.2) one has

$$M(l, t) = 0, \quad M(0, t) = -M_0.$$

Kinematical boundary conditions are

$$W(0, t) = 0$$

if $|Q(0, t)| \neq Q_0$ and

$$W(l, t) = 0$$

if $|Q(l, t)| \neq Q_0$.

3) In the case of a beam fully clamped at both ends (Fig. 1.3) one has

$$M(0, t) = M(l, t) = -M_0.$$

Kinematical boundary conditions are

$$W(0, t) = 0$$

if $|Q(0, t)| \neq Q_0$ and

$$W(l, t) = 0$$

if $|Q(l, t)| \neq Q_0$.

4) In the case of a beam fully clamped at the left end and free at the right hand end (Fig. 1.4) one has

$$M(0, t) = -M_0, \quad M(l, t) = 0, \quad Q(l, t) = 0.$$

Kinematical boundary conditions are

$$W(0, t) = 0$$

if $|Q(0, t)| \neq 0$.

1.1.3 Strain components

In the classical bending theory the only deformation component is the curvature of the middle line of the beam

$$\kappa = -\frac{\partial^2 W}{\partial x^2}. \quad (1.2)$$

However, if shear forces are taken into account then one has two components - κ and γ where

$$\gamma = \frac{\partial W}{\partial x} + \psi, \quad \kappa = \frac{\partial \psi}{\partial x}. \quad (1.3)$$

Here ψ is the rotation of an element of the center line due to bending only.

It can be easily seen from (1.2), (1.3) that when $\gamma = 0$, then $\psi = -\partial W/\partial x$ and κ is given by (1.2).

1.1.4 Principle of virtual work

Let the dissipation of the internal energy be denoted by \dot{D}_{int} and the power of external loads by \dot{D}_{ext} .

Evidently in the case of a distributed loading $p(x, t)$ the rate of the external work can be calculated as

$$\dot{D}_{ext} = \int_0^l (p - \bar{m} \frac{\partial^2 W}{\partial t^2}) \dot{W} dx. \quad (1.4)$$

The internal energy rate can be defined as

$$\dot{D}_{int} = \int_0^l (M \dot{\kappa} + Q \dot{\gamma}) dx - (M \dot{\psi} + Q \dot{W})|_0^l. \quad (1.5)$$

The principle of virtual work states that for each body being in an equilibrium state (Jones, 1989)

$$\dot{D}_{int} = \dot{D}_{ext}. \quad (1.6)$$

It appears that the principle of virtual work can be employed for deriving strain rate components making use of equilibrium equations. Indeed, it follows from (1.1) that

$$\begin{aligned} -\frac{\partial M}{\partial x} + Q &= 0 \\ -\frac{\partial Q}{\partial x} + \bar{m} \frac{\partial^2 W}{\partial t^2} - P &= 0. \end{aligned} \quad (1.7)$$

Multiplying the first equation in (1.7) with $\dot{\psi}$, the second with \dot{W} and integrating one obtains

$$\int_0^l \left\{ \left(-\frac{\partial M}{\partial x} + Q \right) \dot{\psi} + \left(-\frac{\partial Q}{\partial x} + \bar{m} \frac{\partial^2 W}{\partial t^2} - P \right) \dot{W} \right\} dx = 0.$$

Integrating by parts in the last equation yields

$$\int_0^l \left\{ M \frac{\partial \dot{\psi}}{\partial x} + Q \left(\dot{\psi} + \frac{\partial \dot{W}}{\partial x} \right) \right\} dx - (M \dot{\psi} + Q \dot{W}) \Big|_0^l = \int_0^l (P - \bar{m} \frac{\partial^2 W}{\partial t^2}) \dot{W} dx. \quad (1.8)$$

Comparing (1.8) with (1.4)-(1.6) one obtains

$$\dot{\kappa} = \frac{\partial \dot{\psi}}{\partial x}, \quad \dot{\gamma} = \dot{\psi} + \frac{\partial \dot{W}}{\partial x}$$

as it was predicted by (1.3).

1.1.5 Yield surfaces and associated flow law

Various yield curves are suggested for plastic beams by different authors (Fig. 1.5, 1.6). In Fig. 1.5 solid line 1 corresponds to Hodge (1981) yield curve, solid line 2 to square yield curve, dot-dashed line to Heyman (1970), dashed line to lower bound after Neal. In Fig. 1.6 solid line 1 corresponds to the approximation by Ilyushin and Shapiro (1957), dot-dashed line to Robinson (2000), dashed line to Drucker (1956), solid line 4 to Reckling (Zyczkowski, 1981).

Drucker (1956) suggested the yield curve for a beam of rectangular cross-section as

$$\left| \frac{M}{M_0} \right| + \left(\frac{Q}{Q_0} \right)^4 - 1 = 0$$

whereas Landgraf (1968) developed a curve in the form

$$\left(\frac{M}{M_0} \right)^2 + \frac{2}{3} \left(\frac{Q}{Q_0} \right)^2 + \frac{1}{3} \left(\frac{Q}{Q_0} \right)^4 = 1.$$

Robinson (1973, 2000) examined various approximations of the exact yield surface for beams and found that a reasonable approximation is

$$\left(\frac{M}{M_0} \right)^2 + \left(\frac{Q}{Q_0} \right)^2 = 1.$$

Heyman (1970) found for I-beams the yield curve

$$M = M_1 + \left[1 - \left(\frac{Q}{Q_0}\right)^2\right] M_2$$

where $M_1 + M_2 = M_0$.

It was established by Jones (1989) that the yield condition in the form of a square (Fig. 1.7) is a good approximation for engineering applications. It will be used in the present paper.

Let the yield curve be in a general form as

$$\Phi(M, Q) = 0.$$

According to the associated flow law the strain rate vector is directed along the outward normal to the yield curve at regular points of the curve. However, at a non-regular (Fig. 1.8) point the vector $\vec{\epsilon}$ must lie inside the angle formed by normals to the curve in both sides intersecting at the non-regular point. Thus

$$\dot{\gamma} = \lambda \frac{\partial \Phi}{\partial Q}$$

$$\dot{\kappa} = \lambda \frac{\partial \Phi}{\partial M}$$

where $\dot{\kappa}$, $\dot{\gamma}$ are corresponding strain rates and λ stands for a non-negative scalar multiplier.

For instance, for the side $Q = Q_0$ of the square (Fig. 1.7) it can be easily obtained

$$\dot{\gamma} = \lambda, \quad \dot{\kappa} = 0.$$

Similarly, for the side $M = M_0$ one has

$$\dot{\gamma} = 0, \quad \dot{\kappa} = \lambda.$$

Admissible directions of the strain rate vector $\vec{\epsilon}$ at non-regular points of the yield curve are shown on Fig. 1.8.

1.2 Annular and circular plates

1.2.1 Geometry of the plate

Let us consider an annular plate of radius R and inner radius a as shown in Fig. 1.9-1.10. The thickness of the plate is h .

1.2.2 Equilibrium equations

Neglecting the effect of rotatory inertia one can present equations of equilibrium of a plate element as (see Jones (1989))

$$\begin{aligned}\frac{\partial}{\partial r}(rQ_r) &= -pr + r\mu \frac{\partial^2 W}{\partial t^2} \\ \frac{\partial}{\partial r}(rM_r) - M_\theta + rQ_r &= 0.\end{aligned}\tag{1.9}$$

Here p stands for the intensity of a transverse loading.

1) In the case of a plate clamped at the outer edge and free at the inner edge boundary conditions at the inner edge are

$$M(a, t) = 0, \quad Q_r(a, t) = 0.\tag{1.10}$$

At the outer edge one has

$$W(R, t) = 0\tag{1.11}$$

if $|Q_r(R, t)| \neq Q_0$ and

$$M(R, t) = -M_0\tag{1.12}$$

2) In the case of a plate simply supported at the outer edge one has

$$M(R, t) = 0$$

whereas the conditions (1.10) and (1.11) hold good as well.

1.2.3 Strain components

When shear deformations are neglected the strain rate components are

$$\begin{aligned}\dot{\kappa}_r &= -\frac{\partial^2 W}{\partial r^2} \\ \dot{\kappa}_\theta &= -\frac{1}{r} \frac{\partial W}{\partial r}.\end{aligned}\tag{1.13}$$

However, when shear forces are retained in the yield condition one has

$$\dot{\gamma} = \dot{\psi} + \frac{\partial \dot{W}}{\partial r}$$

$$\begin{aligned}\dot{\kappa}_r &= \frac{\partial \dot{\psi}}{\partial r} \\ \dot{\kappa}_\theta &= \frac{\dot{\psi}}{r}.\end{aligned}\tag{1.14}$$

1.2.4 Principle of virtual work

Similarly to the case of inelastic beams the principle of virtual work (1.6) holds good in the case of plates and shells, as well. For annular plates the rate of the work done by external forces can be defined as

$$\dot{D}_{ext} = 2\pi \int_a^R (p - \mu \frac{\partial^2 W}{\partial t^2}) \dot{W} r dr.\tag{1.15}$$

The dissipation of the internal energy is

$$\dot{D}_{int} = 2\pi \int_a^R (M_r \dot{\kappa}_r + M_\theta \dot{\kappa}_\theta + Q_r \dot{\gamma}) r dr - 2\pi (r M_r \dot{\psi} + r Q_r \dot{W})|_a^r.\tag{1.16}$$

Multiplying equations (1.9) with \dot{W} and $\dot{\psi}$, respectively, after integration one obtains

$$\begin{aligned}2\pi \int_a^R \left\{ -\frac{\partial \dot{W}}{\partial r} Q_r - M_r \frac{\partial \dot{\psi}}{\partial r} - M_\theta \frac{\dot{\psi}}{r} - Q_r \dot{\psi} \right\} r dr + \\ + 2\pi \int_a^R (p - \mu \frac{\partial^2 W}{\partial t^2}) r dr + 2\pi (r Q \frac{\partial \dot{W}}{\partial r} + r M_r \frac{\partial \dot{\psi}}{\partial r})|_a^R = 0.\end{aligned}\tag{1.17}$$

When comparing (1.17) with (1.6) and taking (1.15), (1.16) into account one can see that the strain rate components have the form (1.14).

1.2.5 Yield condition

In the present study the yield surface in the form of a cube will be used. However, in a general case a yield surface for axisymmetric plates can be presented as

$$\Phi(M_r, M_\theta, Q_r) = 0\tag{1.18}$$

provided membrane forces can be neglected. According to the associated flow law at a regular point of the yield surface (Jones, 1989)

$$\begin{aligned}
\dot{\kappa}_r &= \lambda \frac{\partial \Phi}{\partial M_r}, \\
\dot{\kappa}_\theta &= \lambda \frac{\partial \Phi}{\partial M_\theta}, \\
\dot{\gamma} &= \lambda \frac{\partial \Phi}{\partial Q_r},
\end{aligned} \tag{1.19}$$

where λ is a non-negative scalar multiplier. At non-regular points of the yield surface the vector $\vec{e} = (\dot{\kappa}_r, \dot{\kappa}_\theta, \dot{\gamma})$ lies inside the angle formed by normals to the adjacent parts of the surface.

1.3 Circular cylindrical shells

1.3.1 Geometry of the shell

Consider a circular cylindrical shell with different end conditions as shown in Fig. 1.11-1.12.

1.3.2 Equilibrium equations

Neglecting rotatory inertia effects the dynamic equilibrium equations for a shell element may be written in the form

$$\begin{aligned}
\frac{\partial M_x}{\partial x} + Q &= 0, \\
\frac{\partial Q}{\partial x} - \frac{N_\theta}{R} + p - \mu \frac{\partial^2 W}{\partial t^2} &= 0.
\end{aligned} \tag{1.20}$$

Here M and Q stand for the bending moment and shear force, respectively. The quantity N is the circumferential membrane force, R is the radius of the middle surface, whereas μ is the mass per unit length of the shell and W is the transverse displacement.

The equilibrium equations will be solved making use of boundary conditions and these are following.

- 1) In the case of a shell simply supported at both ends one has

$$M_x(0, t) = M_x(l, t) = 0.$$

Kinematical boundary conditions are

$$W(0, t) = 0$$

if $|Q(0, t)| \neq Q_0$ and

$$W(l, t) = 0$$

if $|Q(l, t)| \neq Q_0$. The quantity Q_0 is the limit value of the shear force.

If

$$Q(0, t) = \pm Q_0$$

or

$$Q(l, t) = \pm Q_0$$

then shear sliding takes place at supports and $W(0, t) \neq 0$, $W(l, t) \neq 0$.

2) In the case of a shell fully clamped at both ends (Fig. 1.11) one has

$$M_x(0, t) = M_x(l, t) = M_0.$$

Kinematical boundary conditions are

$$W(0, t) = 0$$

if $|Q(0, t)| \neq Q_0$ and

$$W(l, t) = 0$$

if $|Q(l, t)| \neq Q_0$.

3) In the case of a shell simply supported at the left hand end and fully clamped at the right end one has

$$M_x(0, t) = 0, \quad M_x(l, t) = M_0$$

Kinematical boundary conditions are

$$W(0, t) = 0$$

if $|Q(0, t)| \neq Q_0$ and

$$W(l, t) = 0$$

if $|Q(l, t)| \neq Q_0$.

4) In the case of a shell fully clamped at the left end and free at the right hand end (Fig. 1.12) one has

$$M_x(0, t) = M_0, \quad M_x(l, t) = 0, \quad Q(l, t) = 0.$$

Kinematical boundary condition is

$$W(0, t) = 0$$

if $|Q(0, t)| \neq Q_0$.

1.3.3 Strain components

In the classical bending theory the deformation components are

$$\kappa_x = \frac{\partial^2 W}{\partial x^2}, \quad \varepsilon_\theta = \frac{W}{R}$$

When the shear forces are taken into account then the deformation components are

$$\gamma = \frac{\partial W}{\partial x} - \psi, \quad \varepsilon_\theta = \frac{W}{R}, \quad \kappa_x = \frac{\partial \psi}{\partial x}.$$

1.3.4 Principle of virtual work

Similarly to the case of inelastic beams the principle of virtual work (1.6) holds good in the case of shells. For circular cylindrical shells the rate of the external work can be defined as

$$\dot{D}_{ext} = \int_0^l (p - \mu \frac{\partial^2 W}{\partial t^2}) 2\pi R dx. \quad (1.21)$$

The internal energy rate can be defined as

$$\dot{D}_{int} = \int_0^l (Q\dot{\gamma} + M_x\dot{\kappa}_x + N_\theta\dot{\varepsilon}_\theta) 2\pi R dx - (M_x\dot{\psi} + Q\dot{W})|_0^l 2\pi R. \quad (1.22)$$

Multiplying the equilibrium equations (3.1) with $\dot{\psi}$ and \dot{W} , respectively and integrating by parts one obtains

$$\begin{aligned} & 2\pi R \left(\int_0^l (M_x \frac{\partial \dot{\psi}}{\partial x} + Q(\dot{\psi} + \frac{\partial \dot{W}}{\partial x}) - N_\theta \frac{\partial \dot{W}}{R}) dx - \right. \\ & \left. - (M_x \dot{\psi} + Q \dot{W})|_0^l \right) = 2\pi R \int_0^l (p - \mu \frac{\partial^2 W}{\partial t^2}) \dot{W} dx. \end{aligned} \quad (1.23)$$

Comparing the last equation (1.23) with (1.21) and (1.22) one obtains

$$\begin{aligned}
\dot{\kappa}_x &= \frac{\partial \dot{\psi}}{\partial x} \\
\dot{\gamma} &= \frac{\partial \dot{W}}{\partial x} - \dot{\psi} \\
\dot{\varepsilon}_\theta &= \frac{\dot{W}}{r}.
\end{aligned} \tag{1.24}$$

1.3.5 Yield surface and associated flow law

In the present study the yield surface is presented in the form of a cube (Fig. 1.13) when shear forces are taken into account. This approach was suggested by Jones (1989) and it was used by many researchers.

The associated flow law is similar to that discussed in the case of axisymmetric plates.

If, for instance, the equation of the yield surface is

$$\Phi(M_x, N_\theta, Q) = 0$$

then at regular points of the surface

$$\begin{aligned}
\dot{\kappa}_x &= \lambda \frac{\partial \Phi}{\partial M_x} \\
\dot{\varepsilon}_\theta &= \lambda \frac{\partial \Phi}{\partial N_\theta} \\
\dot{\gamma} &= \lambda \frac{\partial \Phi}{\partial Q}.
\end{aligned}$$

Consider the particular case of the yield surface in the form of a cube (Fig. 1.13).

If the stress state corresponds to the plane

$$N_\theta = N_0$$

then one has

$$\dot{\kappa}_x = 0, \quad \dot{\gamma} = 0, \quad \dot{\varepsilon}_\theta \geq 0,$$

provided the current point is located in the internal region of this face.

At the edge of the cube the direction of the strain rate vector is not unique, as in the case of plates.

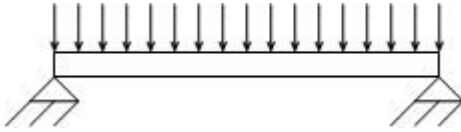


Figure 1.1: Simply supported beam.

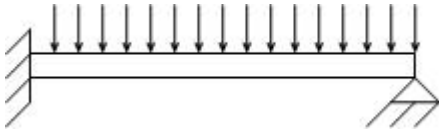


Figure 1.2: supported at the right end and fully clamped at the left end beam.

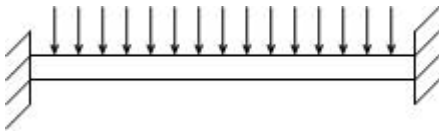


Figure 1.3: Fully clamped beam.

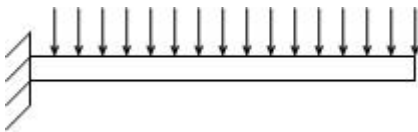


Figure 1.4: Cantilever beam.

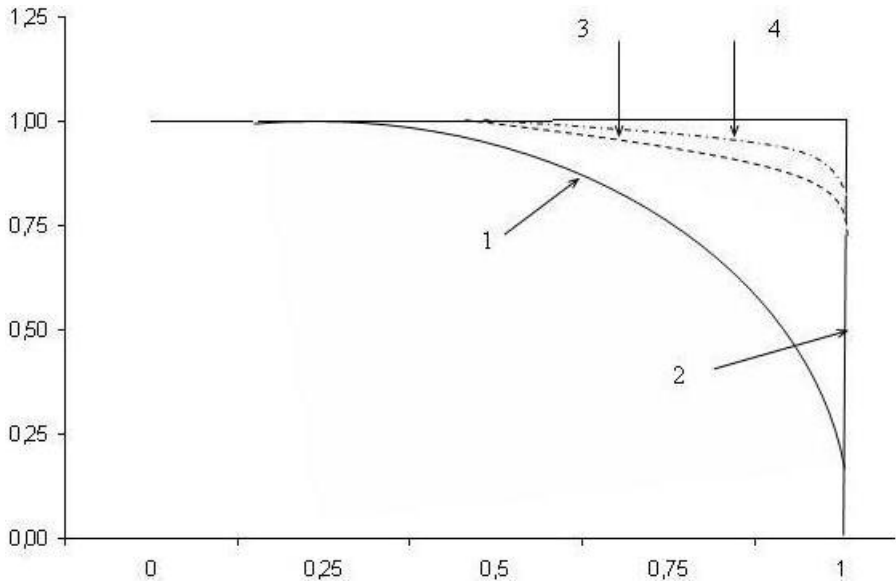


Figure 1.5: Approximations of the yield condition.

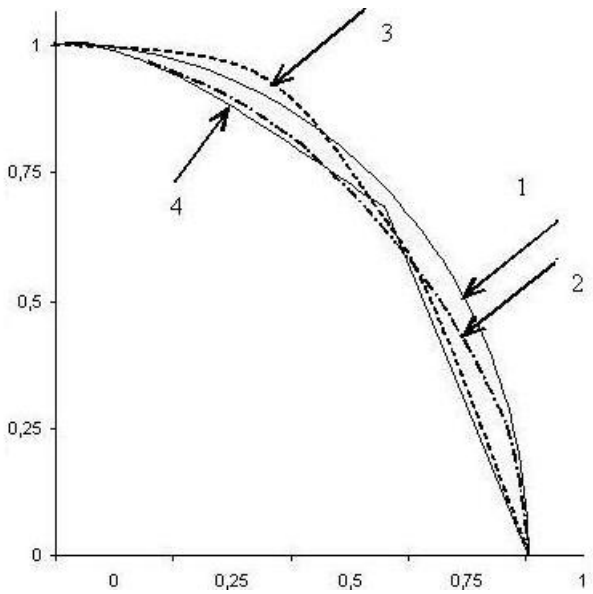


Figure 1.6: Comparison of yield curves

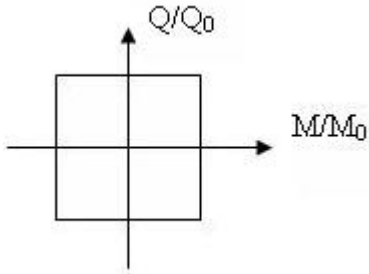


Figure 1.7: Square yield condition.

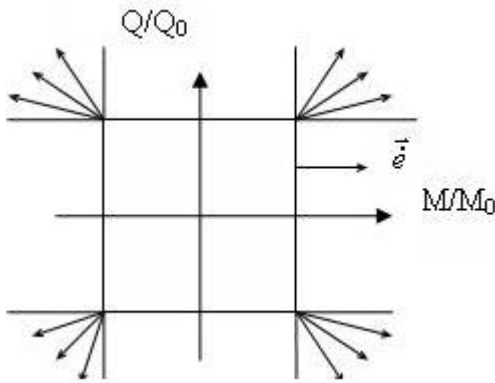


Figure 1.8: Associated flow law.

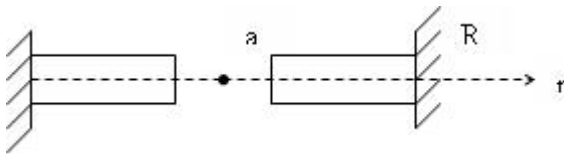


Figure 1.9: Plate clamped at the outer edge.

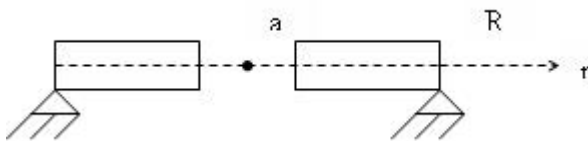


Figure 1.10: Plate simply supported at the outer edge.

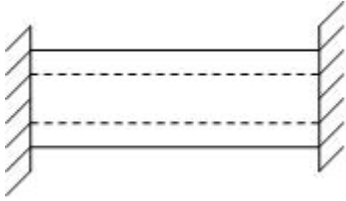


Figure 1.11: Fully clamped circular cylindrical shell.

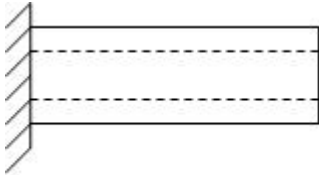


Figure 1.12: Cantilever cylindrical shell.

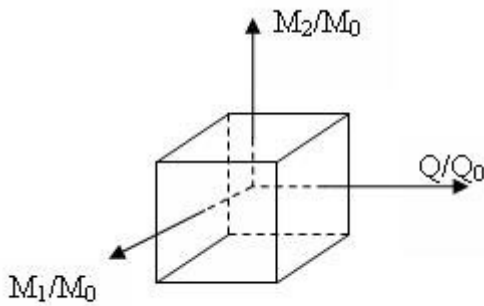


Figure 1.13: Cubic yield condition.

CHAPTER 2

Shear and bending response
of a rigid-plastic beam
subjected to impulsive
loading

International Journal of Impact Engineering
2005; 31(9): 1081-1105

Shear and bending response of a rigid-plastic beam subjected to impulsive loading

J. Lellep and K. Torn

Institute of Applied Mathematics, University of Tartu,
Tartu, 50409, 2 Liivi str., Estonia

Abstract

The dynamic response of a rigid-plastic beam is considered. The beam is subjected to the initial impulsive loading. Plastic yielding of the material is controlled by the square yield criterion which retains the transverse shear force as well as the bending moment. The beam under consideration is clamped at the left and simply supported at the right hand end.

Keywords:

Beam; Impulsive loading; Dynamic plasticity; Shear forces

Nomenclature

l	- length of the beam
$m = M/M_0$	- non-dimensional moment
\bar{m}	- mass per unit length
t	- time
u_i^f	- final displacements
v_0	- initial velocity
$w = M_0 W / \bar{m} v_0^2 l^2$	- non-dimensional displacement
$\dot{w}_0, \dot{w}_1, \dot{w}_2$	- transverse velocities
$\ddot{w}_0, \ddot{w}_1, \ddot{w}_2$	- accelerations
x	- coordinate
K_0	- kinetic energy
M	- bending moment
M_0	- yield moment
P	- distributed loading
Q	- shear force

Q_0	-	limit value of shear force
T_i	-	surface tractions
W	-	displacement
W_f	-	residual deflection
$\beta_1 = 6/\nu$	-	stationary hinge
$\beta_2 = 1 - 3/\nu$	-	stationary hinge
γ	-	transverse shear
η, η_1, η_2	-	travelling hinges
$\nu = Q_0 l / M_0$	-	parameter
$\xi = x/l$	-	non-dimensional coordinate
ξ_0, ξ_*	-	fixed points
$\tau = M_0 t / \bar{m} v_0 l^2$	-	new time-variable
$\tau_1, \tau_2, \tau_3, \tau_4$	-	moments of time
ψ	-	rotation angle

2.1 Introduction

It appeared that the transverse shear forces can exercise an important role in the dynamic plastic behaviour of beams, plates and shells as discussed by Jones [1, 2], Stronge and Yu [3] and others. The influence of the transverse shear on the dynamic behaviour of rigid-plastic beams has been studied by several authors. Symonds [4] has examined the influence of shear forces on the plastic response of an infinitely long beam struck by a mass travelling with an initial velocity. In [4] a fully clamped beam of finite length that is subjected to an impulsive pressure loading has been studied also. Nonaka [5, 6] has presented the solutions for simply supported beams subjected to uniformly distributed blast pressure loading. Nonakas results were extended to the case when the blast pressure loading is uniformly distributed over a portion of the span by Jones and Song [7]. Nine different patterns of motion are obtained whereas the cases of rectangular, triangular and exponential pulse loadings are examined. Theoretical solutions for fully clamped beams subjected to the blast pressure loading are presented by Li and Jones [8].

In these studies the bending moment as well as the transverse shear force are retained in the yield curve which is presented as a square yield curve. The accuracy of this approximation of the yield condition is discussed by de Oliveira and Jones [9] on the basis of I-beams.

The influence of the rotatory inertia and transverse shear forces on the dynamic plastic response of rigid-plastic beams has been examined by Jones and de Oliveira [10, 11]. Jones [12] has demonstrated that the simple bound theorems which were developed for rigid-plastic continua provide excellent estimates of the response durations and permanent displacements of impulsively loaded beams, circular plates and cylindrical shells when

transverse shear effects are taken into account.

Jones and de Oliveira [13], also Li and Jones [14] have studied the plastic response of cylindrical shells to impulsive and blast loadings. The influence of transverse shear effects on the behaviour of circular plates was investigated by Jones and de Oliveira [15] and by Li and Jones [16].

In the investigations cited above the both ends of the beams under considerations are simply supported or fully clamped, respectively. In the present study dynamic plastic response of beams clamped at left ends and simply supported at right hand ends will be investigated. The influence of the transverse shear is retained in the yield condition.

2.2 Basic equations

Let us consider a beam of length l fully clamped at the left end and simply supported at the right end as shown in Fig. 2.1.

When rotatory inertia is neglected the equations of motion of the beam may be written as

$$\begin{aligned} \frac{\partial M}{\partial x} - Q &= 0, \\ \frac{\partial Q}{\partial x} &= \bar{m} \frac{\partial^2 W}{\partial t^2} - P \end{aligned} \quad (2.1)$$

where M and Q stand for the bending moment and shear force, respectively. Here P is the intensity of the distributed transverse loading whereas \bar{m} stands for mass per unit length of the beam and W is the transverse displacement.

Since we shall consider the case of an impulsive loading of the beam one can take $P = 0$ in (2.1) whereas the initial impulsive velocity is v_0 .

The total slope of the axis of the beam is

$$\frac{\partial W}{\partial x} = \psi + \gamma$$

as shown in [1, 2]. Here ψ is the rotation of line elements along the center line due to bending and γ is the transverse shear strain.

The continuity requirements at a discontinuity interface have been discussed by Jones [1], Symonds [4] and others. When rotatory inertia is neglected but transverse shear effects are retained in the basic equations then the bending moment and shear force are continuous at travelling and stationary bending hinges as well as at shear slides [1]. However, the transverse displacement and displacement velocity are continuous at the bending hinges not at the shear slides.

The square yield curve presented in Fig. 2.2 will be used in the subsequent theoretical analysis. A detailed discussion on the accuracy of the square yield criterion is given by Jones and de Oliveira [9].

It appears to be convenient to use the following non-dimensional quantities

$$\begin{aligned}\xi &= \frac{x}{l}, & m &= \frac{M}{M_0}, & q &= \frac{Q}{Q_0}, \\ w &= \frac{M_0 W}{\bar{m} v_0^2 l^2}, & \tau &= \frac{M_0 t}{\bar{m} v_0 l^2}, & \nu &= \frac{Q_0 l}{M_0}\end{aligned}\tag{2.2}$$

where M_0 and Q_0 stand for the fully plastic capacity of a cross-section when subjected to a bending moment or transverse shear force, respectively.

Making use of the non-dimensional quantities the equilibrium equations (2.1) may be presented in the form

$$m' = \nu q, \quad q' = \frac{1}{\nu} \ddot{w}\tag{2.3}$$

where primes denote differentiation with respect to ξ and dots with respect to τ . Evidently $w = w(\xi, \tau)$ and

$$w(\xi, 0) = 0, \quad \dot{w}(\xi, 0) = 1.$$

2.3 Theoretical solution for the beam subjected to an impulsive velocity

It turns out that the pattern of initial motion of the beam depends on the parameter ν as it might be expected (see Refs [1, 2, 8]).

2.3.1 Case I

2.3.1.1 First phase of motion

If $\nu \geq 1$ and $\nu \leq \nu_2$ where ν is defined by (2.2) then the plastic response of the beam is governed by shear effects. It will be shown later that $\nu_2 = 5.6166$. The results are independent of rotatory inertia.

During the first phase shear sliding occurs at the supports. The transverse velocity distribution for this phase is presented in Fig. 2.3. According to Fig. 2.3 $\psi = 0$ and the transverse velocity may be written as

$$\dot{w} = \dot{w}_1 + (\dot{w}_2 - \dot{w}_1)\xi.\tag{2.4}$$

Here the quantities \dot{w}_1 and \dot{w}_2 depend only on τ . Thus the acceleration is

$$\ddot{w} = \ddot{w}_1 + (\ddot{w}_2 - \ddot{w}_1)\xi, \quad (2.5)$$

where \ddot{w}_1 and \ddot{w}_2 stand for the accelerations at the end points of the beam.

Substituting (2.5) in (2.3) and integrating with respect to the coordinate ξ under the conditions $q(0, \tau) = 1$, $q(1, \tau) = -1$ one obtains

$$q = \frac{1}{\nu}\ddot{w}_1\xi + \frac{1}{2\nu}(\ddot{w}_2 - \ddot{w}_1)\xi^2 + 1 \quad (2.6)$$

and

$$\frac{1}{\nu}\ddot{w}_1 + \frac{1}{2\nu}(\ddot{w}_2 - \ddot{w}_1) + 1 = -1. \quad (2.7)$$

Making use of (2.6) and integrating the first equation in (2.3) leads to the relation

$$m = \frac{\ddot{w}_1}{2}\xi^2 + \frac{1}{6}(\ddot{w}_2 - \ddot{w}_1)\xi^3 + \nu\xi - 1, \quad (2.8)$$

where the boundary condition $m(0, \tau) = -1$ is taken into account. Since bending moment must vanish at the simply supported end at $\xi = 1$ according to (2.8) one has

$$\frac{1}{2}\ddot{w}_1 + \frac{1}{6}(\ddot{w}_2 - \ddot{w}_1) + \nu - 1 = 0. \quad (2.9)$$

The set of equations (2.7), (2.9) may be solved with respect to the quantities \ddot{w}_1 and \ddot{w}_2 . After certain algebraic transformations one easily obtains

$$\ddot{w}_1 = -2\nu + 6 \quad (2.10)$$

and

$$\ddot{w}_2 = -2\nu - 6. \quad (2.11)$$

According to the initial condition $\dot{w}(\xi, 0) = 1$ one has

$$\dot{w}_1(0) = 1, \quad \dot{w}_2(0) = 1. \quad (2.12)$$

Since the beam is straight at the initial moment and shear sliding has not taken place yet one has

$$w_1(0) = 0, \quad w_2(0) = 0. \quad (2.13)$$

Integrating the equations (2.10) and (2.11) twice with respect to τ and satisfying the requirements (2.12), (2.13) one eventually obtains

$$\dot{w}_j(\tau) = \ddot{w}_j\tau + 1 \quad (2.14)$$

and

$$w_j(\tau) = \frac{1}{2}\ddot{w}_j\tau^2 + \tau \quad (2.15)$$

where the index j takes the values 1 and 2.

Evidently the first phase of motion ends when \dot{w}_2 vanishes. Let this happen at $\tau = \tau_1$. Thus it follows from (2.10), (2.11), (2.14), (2.15) that

$$\tau_1 = \frac{1}{2(\nu + 3)} \quad (2.16)$$

and

$$\dot{w}_1(\tau_1) = \frac{6}{\nu + 3}, \quad w_1(\tau_1) = \frac{\nu + 9}{4(\nu + 3)^2}. \quad (2.17)$$

Displacement at the right hand end of the beam becomes at the end of the first phase

$$w_2(\tau_1) = \frac{1}{4(\nu + 3)}. \quad (2.18)$$

2.3.1.2 Second phase of motion

During the second phase of motion shear sliding continues at the clamped edge and no shear occurs at the simply supported edge. Corresponding velocity distribution is depicted in Fig. 2.4. Thus the relations (2.4), (2.5), (2.6) and (2.8) hold good in the present case, provided $\dot{w}_2 = \ddot{w}_2 = 0$. Since $q(1, \tau) \neq -1$ and $m(1, \tau) = 0$ instead of (2.7) and (2.11) one has now a single equation

$$\ddot{w}_1 = 3(-\nu + 1). \quad (2.19)$$

Integrating (2.19) with respect to τ and taking (2.17) into account leads to the relations

$$\dot{w}_1 = 3(1 - \nu)(\tau - \tau_1) + \frac{6}{\nu + 3} \quad (2.20)$$

and

$$w_1 = \frac{3}{2}(1 - \nu)(\tau - \tau_1)^2 + \frac{6}{\nu + 3}(\tau - \tau_1) + \frac{\nu + 9}{4(\nu + 3)^2}. \quad (2.21)$$

The shear sliding at the left end of the beam ceases at the time $\tau = \tau_2$ when $\dot{w}_1(\tau_2) = 0$. According to (2.20)

$$\tau_2 = \tau_1 + \frac{2}{(\nu - 1)(\nu + 3)}. \quad (2.22)$$

Making use of (2.21), (2.22) one can find the maximal residual displacement at the clamped edge

$$w_1(\tau_2) = \frac{(\nu - 1)(\nu + 9) + 24}{4(\nu - 1)(\nu + 3)^2}. \quad (2.23)$$

The case I takes place for such values of the parameter ν for which the bending moment does not exceed unity. It can be seen from (2.10) that if $\nu \geq 3$ then $\ddot{w}_1 \leq 0$ in the present case.

It follows from (2.8)-(2.11) that the maximum of bending moment during the first phase is located at the point

$$\xi_0 = \frac{1}{6}(3 - \nu + \sqrt{9 + \nu^2}). \quad (2.24)$$

Making use of (2.8), (2.10), (2.11) and (2.24) one can check that the inequality $m(\xi, \tau) \leq 1$ is satisfied if $m(\xi_0, \tau) \leq 1$, or

$$\frac{1}{3}\nu^4 - 2\nu^3 + 3\nu^2 - 72 \leq 0, \quad (2.25)$$

e.g. for $\nu \leq \nu_2$ where $\nu_2 = 5.6166$.

2.3.2 Case II

2.3.2.1 First phase of motion

Assume that now $\nu > \nu_2$. During the first phase of motion shear sliding occurs at the both ends of the beam. At $\xi = \xi_*$ a stationary plastic hinge is located (Fig. 2.5). Thus the velocity distribution may be presented as

$$\dot{w} = \frac{1}{\xi_*}[\dot{w}_1(\xi_* - \xi) + \dot{w}_0\xi] \quad (2.26)$$

for $\xi \in [0, \xi_*]$ and

$$\dot{w} = \frac{1}{1 - \xi_*}[\dot{w}_2(\xi - \xi_*) + \dot{w}_0(1 - \xi)] \quad (2.27)$$

for $\xi \in [\xi_*, 1]$.

The set of equilibrium equations (2.3) will be integrated separately in the regions $[0, \xi_*]$ and $[\xi_*, 1]$, respectively, defining preliminarily the accelerations according to (2.26) and (2.27). For $\xi \in [0, \xi_*]$ the equations of motion (2.3) give

$$q = \frac{\ddot{w}_1}{\nu}\xi + \frac{\ddot{w}_0 - \ddot{w}_1}{2\nu\xi_*}\xi^2 + 1 \quad (2.28)$$

and

$$m = \frac{\ddot{w}_1}{2}\xi^2 + \frac{\ddot{w}_0 - \ddot{w}_1}{6\xi_*}\xi^3 + \nu\xi - 1. \quad (2.29)$$

When deriving (2.28) and (2.29) boundary conditions $q(0, \tau) = 1$ and $m(0, \tau) = -1$ are taken into account.

Similarly one eventually obtains for $\xi \in [\xi_*, 1]$

$$q = \frac{1}{\nu}\ddot{w}_2(\xi - 1) + \frac{\ddot{w}_0 - \ddot{w}_2}{2\nu(\xi_* - 1)}(\xi - 1)^2 - 1 \quad (2.30)$$

and

$$m = \frac{1}{2}\ddot{w}_2(\xi - 1)^2 + \frac{\ddot{w}_0 - \ddot{w}_2}{6(\xi_* - 1)}(\xi - 1)^3 - \nu(\xi - 1). \quad (2.31)$$

Evidently, (2.30), (2.31) meet the requirements $q(1, \tau) = -1$ and $m(1, \tau) = 0$. Since bending moment has its maximum at $\xi = \xi_*$ the requirements $q(\xi_*, \tau) = 0$, $m(\xi_*, \tau) = 1$ have to be satisfied also. The latter with (2.28)-(2.31) give respectively

$$\begin{aligned} \ddot{w}_1 &= -\frac{4\nu}{\xi_*} + \frac{12}{\xi_*^2}, \\ \ddot{w}_0 &= \frac{2\nu}{\xi_*} - \frac{12}{\xi_*^2} \end{aligned} \quad (2.32)$$

and

$$\begin{aligned} \ddot{w}_2 &= \frac{4\nu}{(\xi_* - 1)} + \frac{6}{(\xi_* - 1)^2}, \\ \ddot{w}_0 &= -\frac{2\nu}{(\xi_* - 1)} - \frac{6}{(\xi_* - 1)^2}. \end{aligned} \quad (2.33)$$

Due to uniqueness of the acceleration \ddot{w}_0 it follows from (2.32) and (2.33) that ξ_* must satisfy the equation

$$2\nu\xi_*^3 - 3(1 + \nu)\xi_*^2 + (\nu + 12)\xi_* - 6 = 0. \quad (2.34)$$

Numerical values of the quantity ξ_* are presented for several values of the parameter ν in Table 2.1. It may be seen from Table 1 that $\xi_* > 1/2$ for each value of ν .

According to (2.32), (2.33) $\ddot{w}_j = \text{const}$, where $j = 0, 1, 2$. Thus the velocities and displacements may be presented by (2.14) and (2.15) where the appropriate initial conditions are taken into account.

The first phase of motion ends at the moment $\tau = \tau_1$ when $\dot{w}_2(\tau_1) = 0$. Therefore (2.14) leads to the durability of the first phase

$$\tau_1 = \frac{(1 - \xi_*)^2}{4\nu(1 - \xi_*) - 6}. \quad (2.35)$$

At the final moment of the first phase according to (2.32)-(2.35) one has

$$\begin{aligned} \dot{w}_0(\tau_1) &= \left(\frac{2\nu}{\xi_*} - \frac{12}{\xi_*^2} \right) \tau_1 + 1, \\ w_0(\tau_1) &= \left(\frac{\nu}{\xi_*} - \frac{6}{\xi_*^2} \right) \tau_1^2 + \tau_1, \\ \dot{w}_1(\tau_1) &= \left(\frac{-4\nu}{\xi_*} + \frac{12}{\xi_*^2} \right) \tau_1 + 1, \\ w_1(\tau_1) &= \left(\frac{-2\nu}{\xi_*} + \frac{6}{\xi_*^2} \right) \tau_1^2 + \tau_1, \end{aligned} \quad (2.36)$$

and

$$w_2(\tau_1) = \left(\frac{2\nu}{\xi_* - 1} + \frac{3}{(\xi_* - 1)^2} \right) \tau_1^2 + \tau_1. \quad (2.37)$$

Note that the relations (2.36), (2.37) serve for the next phase of motion as initial conditions for appropriate displacements and velocities.

2.3.2.2 Second phase of motion

During the second phase of motion the plastic hinge which is located at $\xi = \xi_*$ when the first phase ends moves towards the clamped end. Corresponding distribution of velocities is presented in Fig. 2.6. Thus

$$\dot{w} = \frac{1}{\eta} [\dot{w}_1(\eta - \xi) + \dot{w}_0\xi] \quad (2.38)$$

for $\xi \in [0, \eta]$ and

$$\dot{w} = \dot{w}_0 \frac{\xi - 1}{\eta - 1} \quad (2.39)$$

for $\xi \in [\eta, 1]$.

Differentiating (2.38) and (2.39) with respect to time one easily obtains the acceleration

$$\ddot{w} = \ddot{w}_1 + (\ddot{w}_0 - \ddot{w}_1) \frac{\xi}{\eta} - \frac{\dot{\eta}}{\eta^2} (\dot{w}_0 - \dot{w}_1) \xi \quad (2.40)$$

for $\xi \in [0, \eta]$ and

$$\ddot{w} = \ddot{w}_0 \frac{\xi - 1}{\eta - 1} - \frac{\dot{w}_0(\xi - 1)}{(\eta - 1)^2} \dot{\eta} \quad (2.41)$$

for $\xi \in [\eta, 1]$.

Substituting (2.40) in (2.3) and integrating with respect to ξ leads to relations

$$q = \frac{\ddot{w}_1}{\nu} \xi + (\ddot{w}_0 - \ddot{w}_1) \frac{\xi^2}{2\nu\eta} - \frac{\dot{\eta}}{2\nu\eta^2} (\dot{w}_0 - \dot{w}_1) \xi^2 + 1 \quad (2.42)$$

and

$$m = \frac{1}{2} \ddot{w}_1 \xi^2 + (\ddot{w}_0 - \ddot{w}_1) \frac{\xi^3}{6\eta} - \frac{\dot{\eta}}{6\eta^2} (\dot{w}_0 - \dot{w}_1) \xi^3 + \nu\xi - 1 \quad (2.43)$$

for $\xi \in [0, \eta]$, where the conditions $q(0, \tau) = 1$ and $m(0, \tau) = -1$ are met.

Making use of (2.41) similarly one obtains for $\xi \in [\eta, 1]$

$$q = \frac{1}{\nu} \left[\frac{\ddot{w}_0}{\eta - 1} - \frac{\dot{w}_0 \dot{\eta}}{(\eta - 1)^2} \right] \left(\frac{1}{2} \xi^2 + \frac{1}{2} - \xi \right) + A \quad (2.44)$$

and

$$m = \frac{1}{6} \left[\frac{\ddot{w}_0}{\eta - 1} - \frac{\dot{w}_0 \dot{\eta}}{(\eta - 1)^2} \right] (\xi - 1)^3 + \nu(\xi - 1)A \quad (2.45)$$

where A is an unknown constant. In (2.45) the boundary condition $m(1, \tau) = 0$ is taken into account.

Satisfying the requirements $q(\eta, \tau) = 0$, $m(\eta, \tau) = 1$ one can get from (2.42)-(2.45)

$$\begin{aligned} \ddot{w}_1 \eta + (\ddot{w}_0 - \ddot{w}_1) \frac{\eta}{2} - \frac{\dot{\eta}}{2} (\dot{w}_0 - \dot{w}_1) + \nu &= 0, \\ \frac{1}{2\nu} \left(\frac{\ddot{w}_0}{\eta - 1} - \frac{\dot{w}_0 \dot{\eta}}{(\eta - 1)^2} \right) (\eta - 1)^2 + A &= 0, \\ \frac{1}{2} \ddot{w}_1 \eta^2 + \frac{1}{6} (\ddot{w}_0 - \ddot{w}_1) \eta^2 - \frac{1}{6} \dot{\eta} \eta (\dot{w}_0 - \dot{w}_1) + \nu \eta - 2 &= 0, \\ \frac{1}{6} \left(\frac{\ddot{w}_0}{\eta - 1} - \frac{\dot{w}_0 \dot{\eta}}{(\eta - 1)^2} \right) (\eta - 1)^3 + \nu(\eta - 1)A - 1 &= 0. \end{aligned} \quad (2.46)$$

It easily follows from (2.46) that

$$A = \frac{3}{2\nu(\eta - 1)} \quad (2.47)$$

and

$$\begin{aligned}
\dot{\eta} &= \frac{2(\eta - 1)(\nu - \frac{6}{\eta}) + \frac{3\eta}{\eta - 1}}{\eta\dot{w}_0 - (\dot{w}_1 - \dot{w}_0)(1 - \eta)}, \\
\ddot{w}_0 &= -\frac{3}{(1 - \eta)^2} + \frac{\dot{w}_0\dot{\eta}}{\eta - 1}, \\
\ddot{w}_1 &= -\frac{4\nu}{\eta} + \frac{12}{\eta^2}.
\end{aligned} \tag{2.48}$$

The system of equations (2.48) is to be integrated numerically under the initial conditions (2.36) and $\eta(\tau_1) = \xi_*$. Integrating the set (2.48) at the time interval $[\tau_1, \tau_2]$ one obtains the values $w_0(\tau_2)$, $\dot{w}_0(\tau_2)$, $w_1(\tau_2)$, $\eta(\tau_2)$ which serve as the initial values of corresponding variables for the next phase of motion.

The second phase of motion ends at the moment when the non-stationary hinge at $\xi = \eta$ disappears. Thus the velocity field becomes that depicted in Fig. 2.4 and

$$\dot{w}_0(\tau_2) = \dot{w}_1(\tau_2)(1 - \eta(\tau_2)). \tag{2.49}$$

The condition (2.49) with the solution of (2.48) enables to define the final moment τ_2 of the second phase.

2.3.2.3 Third phase of motion

During the third phase the motion of the beam corresponds to triangular velocity pattern (Fig. 2.4). This type of motion was considered earlier (case I, second phase of motion). Thus the relation (2.19) holds good in the present case and

$$\begin{aligned}
\dot{w}_1 &= 3(1 - \nu)(\tau - \tau_2) + \dot{w}_1(\tau_2), \\
w_1 &= \frac{3}{2}(1 - \nu)(\tau - \tau_2)^2 + \dot{w}_1(\tau_2)(\tau - \tau_2) + w_1(\tau_2).
\end{aligned} \tag{2.50}$$

The third phase ends when motion stops, e.g. $\dot{w}(\tau_3) = 0$. Evidently, according to (2.50)

$$\tau_3 = \tau_2 + \frac{\dot{w}_1(\tau_2)}{3(\nu - 1)}$$

and

$$w_1(\tau_3) = -\frac{1}{2} \frac{\dot{w}_1^2(\tau_2)}{\ddot{w}_1} + w_1(\tau_2).$$

Statical admissibility of the stress state can be evaluated numerically. Calculations carried out showed that the bending moment satisfies the requirement $|m| \leq 1$, if $\nu_2 \leq \nu \leq \nu_3$ where $\nu_3 = 6.45$.

2.3.3 Case III

2.3.3.1 First phase of motion

The first phase of motion coincides completely with that corresponding to the case II. Thus the relations (2.26)-(2.37) hold good in the present case, as well.

2.3.3.2 Second phase of motion

The second phase of motion is also similar to the case 2.3.2.2. Thus the formulae (2.38)-(2.49) remain valid in the present case also. However, the second phase terminates now at the moment when the sliding stops at the clamped end of the beam. Thus at the final moment of the second phase $\dot{w}_1(\tau_2) = 0$.

2.3.3.3 Third phase of motion

Now the deformation of the beam takes place with a single moving hinge located at $\xi = \eta$ (Fig. 2.7). Thus the velocity distribution is specified by

$$\dot{w} = \frac{1}{\eta} \dot{w}_0 \xi \quad (2.51)$$

for $\xi \in [0, \eta]$ and by (2.39) for $\xi \in [\eta, 1]$. Accelerations are defined by

$$\ddot{w} = \ddot{w}_0 \frac{\xi}{\eta} - \frac{\dot{w}_0 \dot{\eta}}{\eta^2} \xi \quad (2.52)$$

for $\xi \in [0, \eta]$ and by (2.41) for $\xi \in [\eta, 1]$.

Substituting (2.41) and (2.52) in (2.3) and integrating twice with respect to ξ leads to the bending moment

$$m = \left(\frac{\ddot{w}_0}{\eta} - \frac{\dot{w}_0 \dot{\eta}}{\eta^2} \right) \left(\frac{\xi^3}{6} - \frac{\eta^3}{6} - \frac{\eta^2}{2} (\xi - \eta) \right) + 1 \quad (2.53)$$

for $\xi \in [0, \eta]$ and

$$m = \frac{1}{(\eta - 1)^2} (\ddot{w}_0(\eta - 1) - \dot{w}_0 \dot{\eta}) \left(\frac{\xi^3}{6} - \frac{\eta^3}{6} - \frac{\eta^2}{2} (\xi - \eta) - \frac{1}{2} (\xi - \eta)^2 \right) + 1 \quad (2.54)$$

for $\xi \in [\eta, 1]$. In (2.53), (2.54) the requirements $m'(\eta, \tau) = 0$, $m(\eta, \tau) = 1$ are taken into account. Taking $m(0, \tau) = -1$ and $m(1, \tau) = 0$ in (2.53) and (2.54), respectively, leads to a set of differential equations which may be presented as

$$\begin{aligned}\ddot{w}_0 &= 3\left(\frac{-2}{\eta} - \frac{1}{1-\eta}\right) \\ \dot{\eta} &= \frac{-3}{\dot{w}_0}\left(\frac{2(\eta-1)}{\eta} - \frac{\eta}{1-\eta}\right).\end{aligned}\tag{2.55}$$

The system of equations (2.55) is integrated numerically. This phase of motion ends at the moment $\tau = \tau_3$ when $\eta(\tau_3) = \beta$, where $\beta = \sqrt{2}/(1+\sqrt{2})$. When integrating (2.55) one can find the values $w_0(\tau_3)$ and $\dot{w}_0(\tau_3)$ which serve as initial conditions for the next phase of motion.

2.3.3.4 Fourth phase of motion

During this phase the plastic hinge is stationary, e.g. $\eta = \beta = const$. Now the velocity pattern remains the same as presented in Fig. 2.7. However, accelerations are defined as

$$\ddot{w} = \frac{\ddot{w}_0}{\beta} \xi \tag{2.56}$$

for $\xi \in [0, \beta]$ and

$$\ddot{w} = \ddot{w}_0 \frac{\xi - 1}{\beta - 1} \tag{2.57}$$

for $\xi \in [\beta, 1]$.

Integrating the equations of motion taking (2.56) and (2.57) into account one obtains

$$\ddot{w}_0 = -\frac{6}{\beta^2}. \tag{2.58}$$

It follows from (2.58) that the displacement takes the form

$$w_0(\tau) = -\frac{3}{2}(1 + \sqrt{2})^2(\tau - \tau_3)^2 + \dot{w}_0(\tau_3)(\tau - \tau_3) + w_0(\tau_3). \tag{2.59}$$

The motion of the beam ceases at the moment $\tau = \tau_4$ when $\dot{w}_0(\tau_4)$ vanishes. Thus the maximal displacement may be presented as

$$w_0(\tau_4) = \frac{1}{6(1 + \sqrt{2})^2}(\dot{w}_0(\tau_3))^2 + w_0(\tau_3). \tag{2.60}$$

In (2.59) and (2.60) the quantities $w_0(\tau_3)$ and $\dot{w}_0(\tau_3)$ are the values of the solution of the system (2.55) at $\tau = \tau_3$.

2.3.4 Case IV

2.3.4.1 First phase of motion

If $\nu \geq \nu_4$, where $\nu_4 = 9$ then the motion of the beam takes place during five stages. In the first phase of motion shear sliding occurs at the supports. The corresponding transverse velocity distribution is presented in Fig. 2.8. Here β_1 and β_2 stand for locations of stationary plastic hinges. Thus

$$\ddot{w} = \ddot{w}_1 \frac{\beta_1 - \xi}{\beta_1} \quad (2.61)$$

for $\xi \in [0, \beta_1]$ and

$$\ddot{w} = \ddot{w}_2 \frac{\beta_2 - \xi}{\beta_2 - 1} \quad (2.62)$$

for $\xi \in [\beta_2, 1]$. Evidently, $\dot{w} \equiv 1$ if $\xi \in [\beta_1, \beta_2]$.

Substituting (2.61) in the equations of motion and integrating with respect to ξ one obtains for $\xi \in [0, \beta_1]$

$$q = \frac{\ddot{w}_1}{\nu} \xi - \frac{\ddot{w}_1}{2\nu\beta_1} \xi^2 + 1 \quad (2.63)$$

and

$$m = \frac{\ddot{w}_1}{2} \xi^2 - \frac{\ddot{w}_1}{6\beta_1} \xi^3 + \nu\xi - 1 \quad (2.64)$$

where the conditions $q(0, \tau) = 1$ and $m(0, \tau) = -1$ are taken into account.

Making use of the accelerations (2.62) and boundary conditions $q(1, \tau) = -1$, $m(1, \tau) = 0$ one can similarly obtain for $\xi \in [\beta_2, 1]$

$$q = \frac{1}{\nu} \ddot{w}_2 (\xi - 1) - \frac{\ddot{w}_2}{2\nu(\beta_2 - 1)} (\xi - 1)^2 - 1 \quad (2.65)$$

and

$$m = \frac{\ddot{w}_2}{2} (\xi - 1)^2 - \frac{\ddot{w}_2}{6(\beta_2 - 1)} (\xi - 1)^3 - \nu(\xi - 1). \quad (2.66)$$

Satisfying the requirements $q(\beta_1, \tau) = 0$, $q(\beta_2, \tau) = 0$, $m(\beta_1, \tau) = 1$, $m(\beta_2, \tau) = 1$ in (2.62)-(2.66) leads to the relations

$$\begin{aligned} \ddot{w}_1 &= -\frac{4\nu}{\beta_1} + \frac{12}{\beta_1^2} \\ \ddot{w}_2 &= \frac{4\nu}{\beta_2 - 1} + \frac{6}{(\beta_1 - 1)^2} \end{aligned} \quad (2.67)$$

and

$$\beta_1 = \frac{6}{\nu}, \quad \beta_2 = 1 - \frac{3}{\nu}. \quad (2.68)$$

It immediately follows from (2.68) that $\beta_1 \leq \beta_2$, if $\nu \geq 9$. Therefore, $\nu_4 = 9$.

The first phase of motion ends at the moment $\tau = \tau_1$ when $\dot{w}_2(\tau_1) = 0$. Since $\ddot{w}_1 = \text{const}$, $\ddot{w}_2 = \text{const}$ one can integrate the equations (2.67) twice with respect to time. Making use of the appropriate initial conditions one easily obtains

$$\begin{aligned} \dot{w}_1(\tau_1) &= \frac{4}{\beta_1} \left(-\nu + \frac{3}{\beta_1} \right) \tau_1 + 1, \\ w_1(\tau_1) &= \frac{2}{\beta_1} \left(-\nu + \frac{3}{\beta_1} \right) \tau_1^2 + \tau_1, \\ w_2(\tau_1) &= \frac{1}{(\beta_2 - 1)} \left(2\nu + \frac{3}{(\beta_2 - 1)} \right) \tau_1^2 + \tau_1, \end{aligned} \quad (2.69)$$

whereas

$$\tau_1 = \frac{(1 - \beta_2)^2}{4\nu(1 - \beta_2) - 6}. \quad (2.70)$$

2.3.4.2 Second phase of motion

During the second phase of motion the plastic hinge being stationary at $\xi = \beta_2$ during the first phase moves towards the center of the beam. The plastic hinge at $\xi = \beta_1$ remains stationary (Fig. 2.9).

Thus for $\xi \in [\eta_2, 1]$ the accelerations becomes as

$$\ddot{w} = -\frac{\dot{\eta}_2}{(\eta_2 - 1)^2} (\xi - 1). \quad (2.71)$$

Substituting (2.71) in (2.2) leads to the bending moment

$$m = -\frac{\dot{\eta}_2}{6(\eta_2 - 1)^2} [(\xi - 1)^3 - 3(\eta_2 - 1)^2(\xi - 1)]. \quad (2.72)$$

Taking $m(\eta_2) = 1$ one obtains

$$\dot{\eta}_2(\eta_2 - 1) = 3. \quad (2.73)$$

Integrating (2.73) under the initial condition $\eta_2(\tau_1) = \beta_2$ leads to the relation

$$\eta_2 = 1 - \sqrt{6(\tau - \tau_1) + \frac{9}{\nu^2}}. \quad (2.74)$$

However, the equations obtained for the region $(0, \beta_1)$ for the first phase of motion remain valid for this stage also. Therefore $\dot{w}_1 = -\nu^2/3$ and

$$\begin{aligned} \dot{w}_1 &= -\frac{\nu^2}{3}\tau + 1, \\ w_1 &= -\frac{\nu^2}{6}\tau^2 + \tau. \end{aligned} \quad (2.75)$$

The second phase of motion ends at the moment when $\eta_2(\tau_2) = \beta_1$. This condition with (2.68) and (2.74) gives the final moment of this phase

$$\tau_2 = \frac{1}{6\nu^2}(\nu - 6)^2. \quad (2.76)$$

2.3.4.3 Third phase of motion

This phase of motion is similar to the second phase for case III. Now the velocity pattern is presented in Fig. 2.6 where $\eta_2 = \eta$. Thus the relations (2.38)-(2.48) obtained above remain valid for this stage of motion. The quantities η , w_0 and w_1 may be obtained when integrating the system (2.48) numerically. This phase of motion ends at $\tau = \tau_3$ when $\dot{w}_1(\tau_3) = 0$.

2.3.4.4 Fourth phase of motion

During this phase of motion the velocity pattern is prescribed with single moving hinge (Fig. 2.7). This type of motion has been studied considering the third phase of motion in the case III. Thus the formulae (2.51)-(2.55) remain valid for the present case also.

2.3.4.5 Fifth phase of motion

The final phase of motion takes place with the stationary plastic hinge located at $\eta = \sqrt{2}/(1 + \sqrt{2})$. This phase of motion corresponds to the fourth phase in case III. So the relations (2.56)-(2.60) remain valid provided τ_3 and τ_4 are substituted with τ_4 and τ_5 , respectively.

Making use of (2.63)-(2.68) one can show that $|m| \leq 1$. Thus the solution is statically admissible. Case IV takes place if $\nu \leq \nu = 6 + 3\sqrt{2}$.

2.3.5 Case V

2.3.5.1 First phase of motion

If $\nu > 6 + 3\sqrt{2}$ then the motion of the beam may be divided into five stages like in the previous case. Moreover, the first phase of motion coincides with that studied in the case IV (Fig. 2.8). Thus the formulae (2.61)-(2.70) hold good in the present case also.

2.3.5.2 Second phase of motion

Now the velocity distribution corresponds to Fig. 2.9 where we have a moving plastic hinges at $\xi = \eta_2$ and a stationary hinge at $\xi = \beta_1$. The central part of the beam has constant velocity $\dot{w}_0 = 1$ as in case IV. Therefore the relations (2.71)-(2.75) remain valid in the present case.

However, in the present case the second phase of motion terminates at $\tau = \tau_2$ when $\dot{w}_1(\tau_2) = 0$. Thus at the final moment of this stage according to (2.74) and (2.70)

$$\eta_2(\tau_2) = 1 - \frac{3}{2}\sqrt{2}. \quad (2.77)$$

It follows from (2.68), (2.75) and (2.77) that

$$\tau_2 = \frac{3}{\nu^2} \quad (2.78)$$

and

$$w_1(\tau_2) = \frac{3}{2\nu^2}. \quad (2.79)$$

2.3.5.3 Third phase of motion

When the transverse shear motion at the clamped end of the beam ceases then the plastic hinge located during the second phase at $\xi = \beta_1$ becomes non stationary. Corresponding velocity distribution is depicted in Fig. 2.10. Here, both, η_1 and η_2 stand for moving hinges.

According to Fig. 2.10 for $\xi \in [0, \eta_1]$ one has

$$\ddot{w} = -\frac{\dot{\eta}_1}{\eta_1^2}\xi. \quad (2.80)$$

Substituting (2.80) in (2.2) and integrating with appropriate boundary conditions one obtains

$$\dot{\eta}_1 = \frac{6}{\eta_1}. \quad (2.81)$$

Integrating (2.81) with respect to time and satisfying the initial condition $\eta_1(\tau_2) = \beta_1$ leads to the relation

$$\eta_1 = \sqrt{12(\tau - \tau_2) + \frac{36}{\nu^2}}. \quad (2.82)$$

Evidently, for $\xi \in [\eta_2, 1]$ the acceleration field is given by (2.71). Thus the relations (2.71)-(2.74) derived earlier hold good in the present case also.

The third phase of motion terminates at $\tau = \tau_3$ when $\eta_1(\tau_3) = \eta_2(\tau_3)$. Making use of (2.68), (2.70), (2.74) and (2.82) one can state that

$$\tau_3 = \frac{1}{2} - \frac{\sqrt{2}}{3}. \quad (2.83)$$

2.3.5.4 Fourth phase of motion

In this phase of motion the velocity pattern is presented in Fig. 2.7 (triangular velocity field with single moving hinge). Thus this phase coincides with the fourth phase of motion studied in the case IV.

2.3.5.5 Fifth phase of motion

Evidently, this phase of motion coincides with the fifth phase in the case IV.

2.4 Discussion

The results of calculations are presented in Table 2.1 and Fig. 2.11-2.17. In Table 2.1 the values of ξ_0 and ξ_* are presented for different values of the parameter ν .

Bending moment and shear force are depicted in Fig. 2.11-2.13 corresponding to case I, case II and case V, respectively. Calculations carried out showed that m and q do not exceed the limit values.

The displacements w_0 , w_1 and w_2 as functions of time are presented in Fig. 2.14 and 2.15. Fig. 2.14 corresponds to the case I whereas Fig. 2.15 is associated with the case III. Solid lines in Fig. 2.14, 2.15 correspond to theoretical and numerical predictions obtained in the present paper; the dashed line in Fig. 2.16 presents an upper bound on displacements [1, 12].

The results in Fig. 2.14 reveal that shear sliding at supports leads to greater displacements in the case of smaller values of the parameter ν . The deflection of the central part of the beam is greater for larger values of ν , as might be expected (Fig. 2.15).

The upper bound is obtained according to Martin's upper bound theorem for permanent displacements [1]. It states that the final displacement field u_i^f satisfies the inequality

$$\int_S T_i u_i^f dS \leq K_0 \quad (2.84)$$

where K_0 is the initial kinetic energy and T_i is a set of safe time-independent surface tractions [12].

If, in particular case T_s is a concentrated load applied at the point where the displacement W_f is estimated then (2.84) takes the form

$$W_f \leq \frac{K_0}{T_s}. \quad (2.85)$$

Note that in (2.85) T_s is the limit static load applied at $\xi = \xi_*$ whereas $W_f = W(\xi_*, \tau_f)$. Evidently,

$$K_0 = \frac{1}{2} \bar{m} v_0^2 l.$$

It is easy to recheck that the maximal safe value for a concentrated load subjected to a beam simply supported at the right hand end and clamped at the left end is

$$T_s = 2Q_0 \quad (2.86)$$

if $\nu \leq 1 + \sqrt{2}$

$$T_s = \left[1 - \frac{1}{\nu(\xi_* - 1)} \right] Q_0 \quad (2.87)$$

if $1 + \sqrt{2} \leq \nu \leq 2 + \sqrt{2}$

$$T_s = \frac{1}{\nu} \left(\frac{2}{\xi_*} - \frac{1}{\xi_* - 1} \right) Q_0 \quad (2.88)$$

if $\nu \geq 2 + \sqrt{2}$.

The limit value (2.86) holds good in the case if shear sliding takes place at both ends of the beam whereas (2.87) corresponds to the situation where shear does not occur at the simply supported end and it does at the clamped end. Finally, (2.88) corresponds to the pure bending theory with bending hinges at the clamped end and at $\xi = \xi_*$.

According to (2.85)-(2.88) the maximal permanent deflections are bounded by

$$w_f = \frac{1}{4\nu}$$

if $\nu \leq 1 + \sqrt{2}$

$$w_f = \frac{1}{2\nu - \frac{1}{\xi_* - 1}}$$

if $1 + \sqrt{2} \leq \nu \leq 2 + \sqrt{2}$ and

$$w_f = \frac{\xi_*(\xi_* - 1)}{2(\xi_* - 2)}$$

if $\nu \geq 2 + \sqrt{2}$.

When calculating the upper bounds for cases IV and V one has to take $\xi_* = \beta$, evidently. The values of ξ_* for cases II and III are accommodated in Table 2.1.

Maximal displacements versus ν are plotted in Fig. 2.16, 2.17. Solid lines in Fig. 2.16, 2.17 correspond to numerical solutions obtained in the present paper. The upper bound is presented by the dashed line. It can be seen from Fig. 2.16 that for greater values of ν the maximal deflection does not depend on ν . The same matter was pointed out by N. Jones [1] in the case of simply supported beams and cylindrical shells. It also can be seen from Fig. 2.17 that the deflections tend to zero when ν tends to infinity.

Note that according to (2.19)-(2.23) the case I can not take place for very short beams for $\nu \leq 1$. However, in this case the ratio $l/h < 0.5$ and evidently the usual assumptions of the beam theory are also violated. In the present paper only moderately short beams are considered, assuming $\nu > 1$.

The case II takes place for $\nu_2 = 5.6166 \leq \nu \leq \nu_3$. The value of ν_3 is calculated as $\max \nu$ so that $\tau_2 \leq \tau_{23}$ where τ_2 is the solution of the equation

$$\frac{\dot{w}_0(\tau_2)}{\dot{w}_1(\tau_2)} = 1 - \eta(\tau_2)$$

and τ_{23} meets the constraint $\dot{w}_1(\tau_{23}) = 0$. Here \dot{w}_0, \dot{w}_1 and η are to be integrated according to (2.48), Calculations showed that

$$\nu_3 = 6.4515.$$

The case III holds good for $\nu \leq \nu_4$ where $\nu_4 = 9$ and case IV for $\nu \leq \nu_5$ where $\nu_5 = \max \nu$ for which η_2 reaches the value β_1 earlier than shear sliding stops at the clamped end of the beam. Making use of (2.74), (2.75), (2.78) one easily obtains

$$\nu_5 = 6 + 3\sqrt{2}.$$

The dependence of velocities on the parameter ν is presented on Fig. 2.18-2.20. The distributions of velocities are calculated at $\tau = \tau_1$. Fig. 2.18

corresponds to case I whereas Fig. 2.19 and Fig. 2.20 are associated with cases III and IV, respectively.

2.5 Concluding remarks

A method for investigation of rigid-plastic beams subjected to impulsive loading is developed. Theoretical solutions have been derived for beams made of a perfectly plastic material obeying the square yield condition. It is assumed that the left end of the beam is clamped whereas the right hand end is simply supported.

It is some what surprising that the present solution substantially differs from the solutions obtained for beams with both, simply supported or clamped ends, respectively.

Calculations carried out showed that the shear sliding is more essential for shorter beams. On the other hand, the first phase of motion includes shear sliding at supports equally in the case of short and long beams. However, the contribution of the shear sliding in the bulk deformation is less important for longer beams (for large values of the parameter ν).

Table 2.1. Values of ξ_0 and ξ_*

ν	ξ_0	ξ_*
3	0.7071	-
3.5	0.6849	-
4	0.6667	-
4.5	0.6514	-
5	0.6385	-
5.6166	0.6252	0.6252
6	-	0.6290
6.5	-	0.6344
7	-	0.6404
7.5	-	0.6464
8	-	0.6256
8.5	-	0.6594
9	-	0.6667

Acknowledgement

The support from Estonian Science Foundation by Grant Project 5693 is gratefully acknowledged.

2.6 References

1. Jones N. *Structural Impact*. Cambridge University Press, Cambridge, UK, 1989.
2. Jones N. On the dynamic inelastic failure of beams. In: *Structural Failure* (Eds T. Wierzbicki and N. Jones). Wiley, New York 1989; pp. 133-159.
3. Stronge WJ, Yu TX. *Dynamic Models for Structural Plasticity*. Springer, London, 1993.
4. Symonds PS. Plastic shear deformations in dynamic load problems. In: *Engineering Plasticity* (Eds J. Heyman and F.A. Leckie), Cambridge, CUP, 1968. p.647-664.
5. Nonaka T. Shear and bending response of a rigid-plastic beam to blast-type loading. *Ing.-Arch.* 1977; 46: 35-52.
6. Nonaka T. Some interaction effects in a problem of plastic beam dynamics. Parts 1-3. *ASME J. Appl. Mech.* 1967; 34: 623-643.
7. Jones N, Song B. Shear and bending response of a rigid-plastic beam to partly distributed blast-type loading. *J. Struct. Mech.* 1986; 14(3): 275-320.
8. Li QM, Jones N. Blast loading of fully clamped beams with transverse shear effects. *Mech. Struct. Mach.* 1995; 23(1): 59-86.
9. de Oliveira JG, Jones N. Some remarks on the influence of transverse shear on the plastic yielding of structures, *Int. J. Mech. Sci.* 1978; 20: 759-765.
10. Jones N, de Oliveira JG. The influence of rotatory inertia and transverse shear on the dynamic plastic behaviour of beams. *J. Appl. Mech.* 1979; 46: 303-310.
11. de Oliveira JG, Jones N. A numerical procedure for the dynamic plastic response of beams with rotatory inertia and transverse shear effects. *J. Struct. Mech.* 1979; 7: 193-2230.
12. Jones N. Bounds on the dynamic plastic behaviour of structures including transverse shear effects. *Int. J. Impact Eng.* 1985; 3(4): 273-291.
13. Jones N, de Oliveira JG. Impulsive loading of a cylindrical shell with transverse shear and rotatory inertia. *Int. J. Solids Struct.* 1983; 19: 263-279.
14. Li QM, Jones N. Blast loading of a "short" cylindrical shell with transverse shear effects. *Int. J. Impact Eng.* 1995; 16: 331-353.
15. Jones N, de Oliveira JG. Dynamic plastic response of circular plates with transverse shear and rotatory inertia. *J. Appl. Mech.* 1980; 47: 27-34.
16. Li QM, Jones N. Blast loading of fully clamped circular plates with transverse shear effects. *Int. J. Solids Struct.* 1994; 31: 1861-1876.

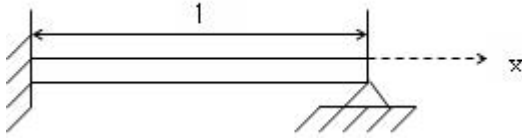


Figure 2.1: Geometry of the beam.

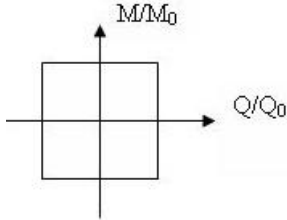


Figure 2.2: The yield surface.

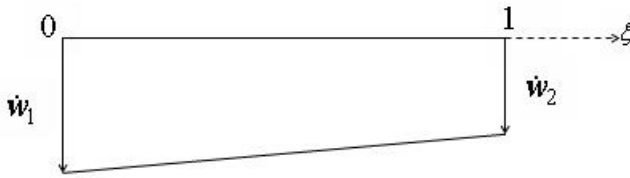


Figure 2.3: Velocity field for Case I, phase I.

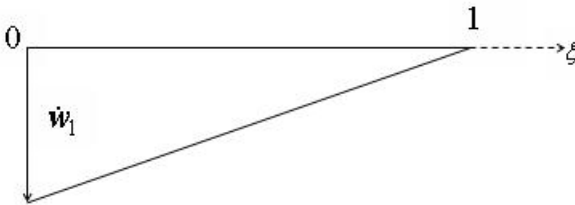


Figure 2.4: Velocity field for Case I, phase II.

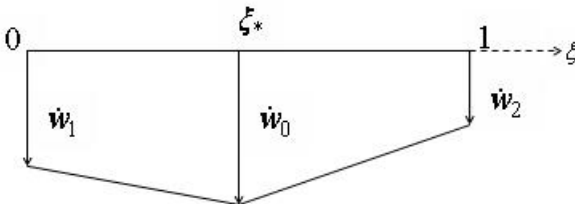


Figure 2.5: Velocity field for Case II, phase I.

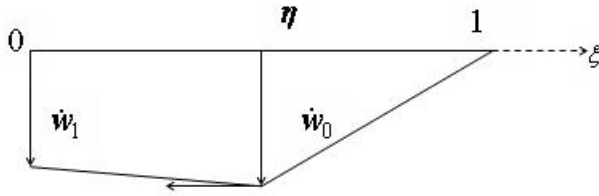


Figure 2.6: Velocity field for Case II, phase II.

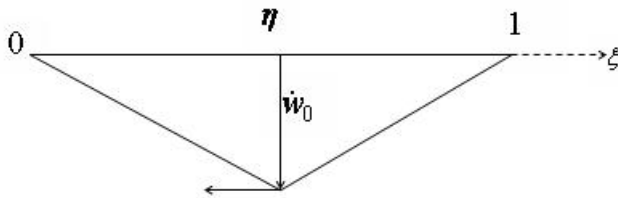


Figure 2.7: Velocity field for Case III, phase III.

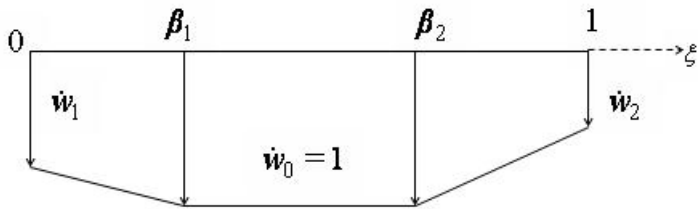


Figure 2.8: Velocity field for Case IV, phase I.

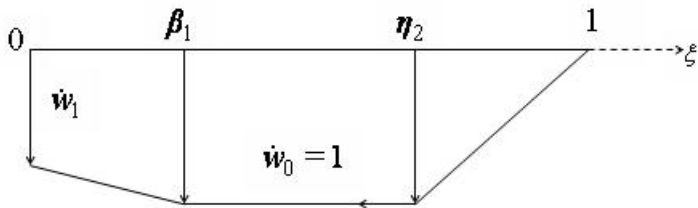


Figure 2.9: Velocity field for Case IV, phase II.

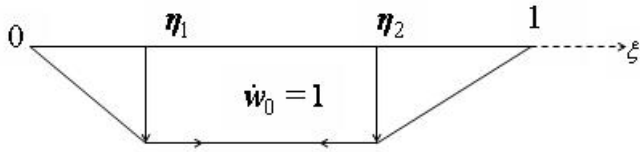


Figure 2.10: Velocity field for Case V, phase III.

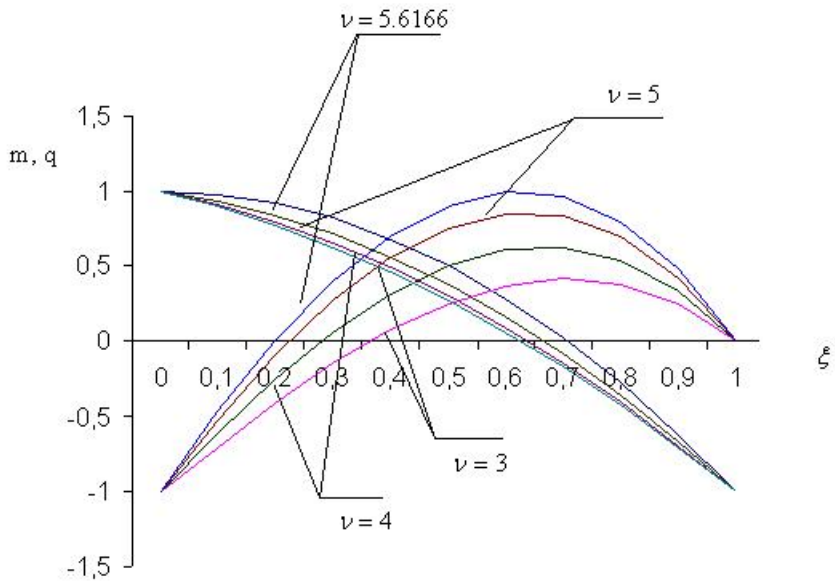


Figure 2.11: Bending moment and shear force (case I).

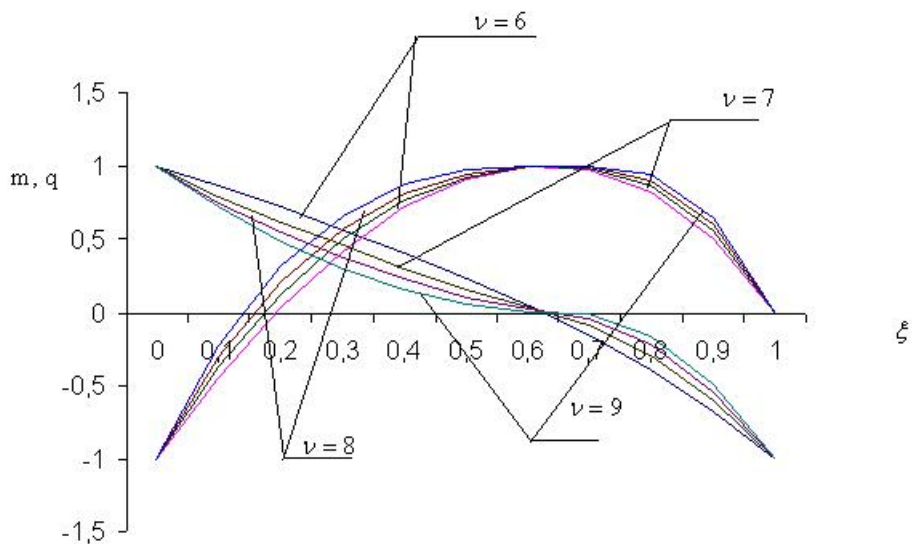


Figure 2.12: Bending moment and shear force (case III).

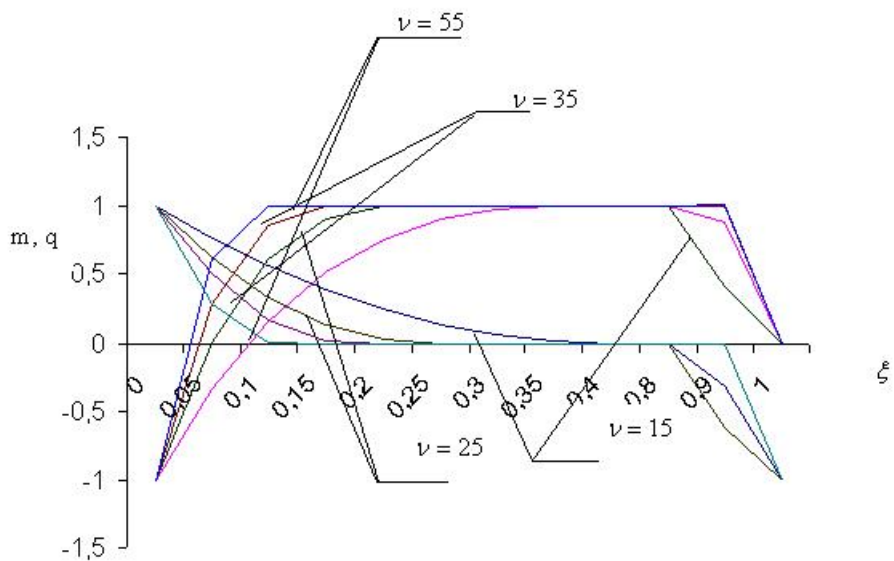


Figure 2.13: Bending moment and shear force (case V).

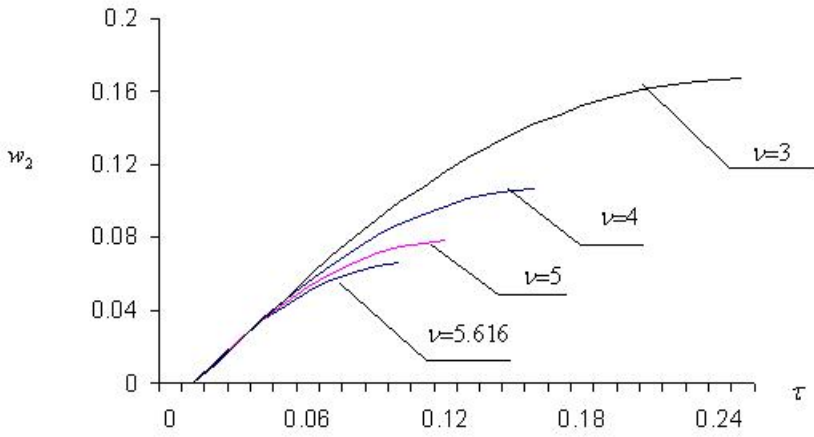


Figure 2.14: Maximal deflections (case I).

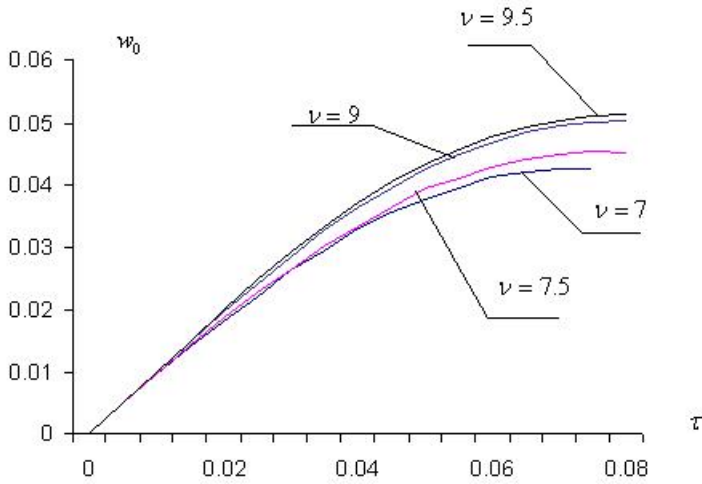


Figure 2.15: Maximal deflections (case III).

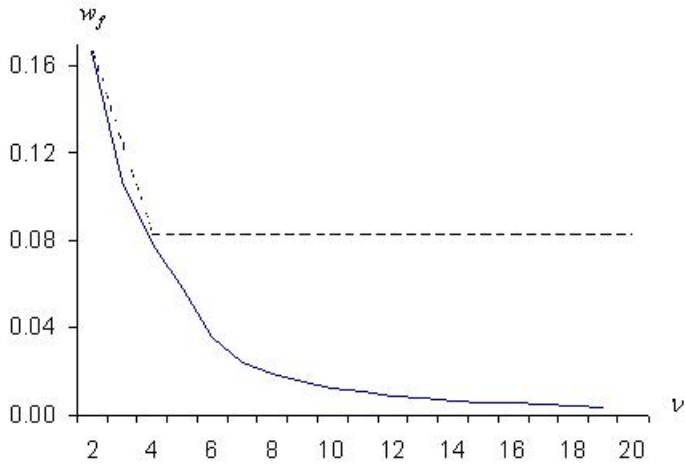


Figure 2.16: Maximal residual displacements.

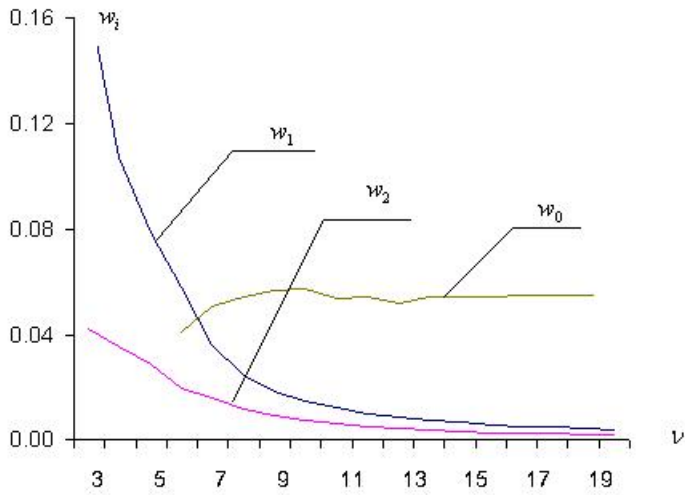


Figure 2.17: Displacements w_1 , w_2 , w_0 versus ν .

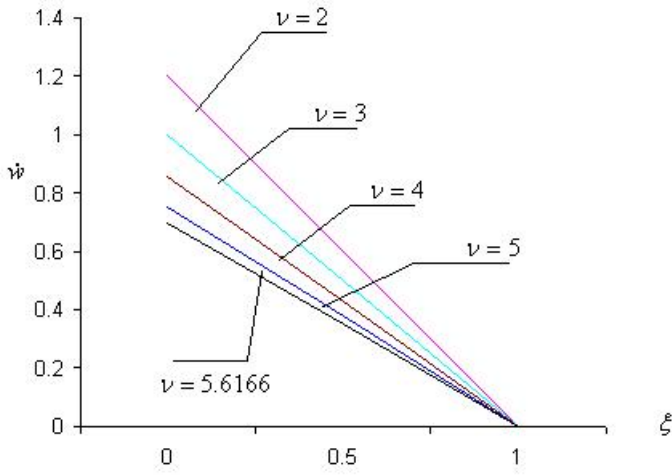


Figure 2.18: Velocity field at the end of the first stage (case I).

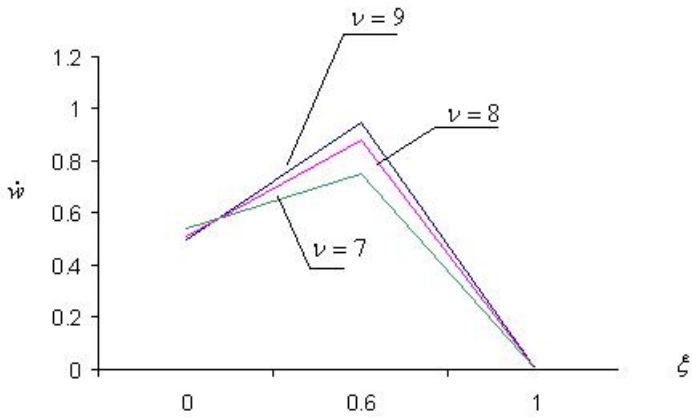


Figure 2.19: Velocity field at the end of the first stage (case III).

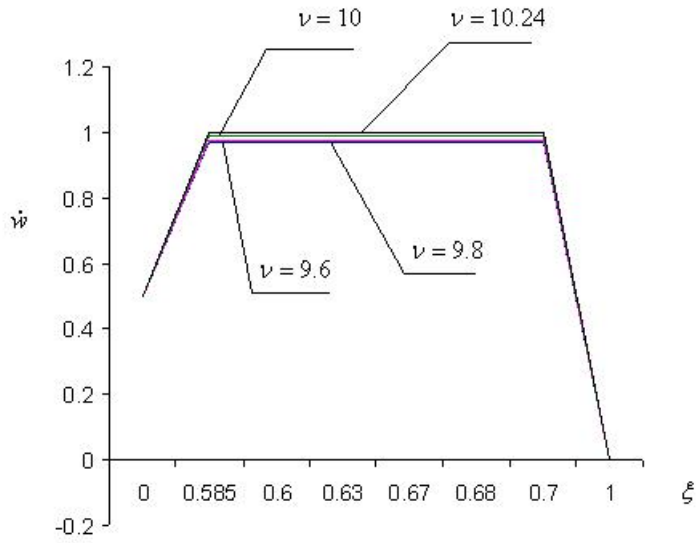


Figure 2.20: Velocity field at the end of the first stage (case IV).

CHAPTER 3

Dynamic plastic behaviour of annular plates with transverse shear effects

International Journal of Impact Engineering (in press)

Dynamic plastic behaviour of annular plates with transverse shear effects

J. Lellep, K. Torn

Institute of Applied Mathematics, University of Tartu,
2 Liivi str., Tartu 50409, Estonia
Tel. 3727375868, Fax 3727375862
E-mail: jaan.lellep@ut.ee, kadre@esttravel.ee

Abstract

The dynamic response of a rigid-plastic annular plate clamped at the outer edge and free at the inner edge is considered.

The plate is subjected to initial impulsive loading so that at the initial moment of time all points of the plate have the uniform transverse velocity. It is assumed that the behaviour of a rigid perfectly plastic material is controlled by a cubic yield condition and the associated flow law in the space of bending moments and the transverse shear force.

Theoretical predictions are developed and compared with an upper bound solution.

Key words:

Annular plate; Plasticity; Impulsive loading; Shear stresses

Notation

a	-	inner radius of annular plate
h	-	thickness of the plate
m_1, m_2, q	-	non-dimensional stress resultants
r	-	current radius
t, τ	-	time
\dot{u}_i^0	-	initial velocity
u_i^f	-	final displacement
v_0	-	initial transverse velocity
w	-	non-dimensional deflection
w_0, w_1, w_2	-	transverse deflections at fixed points
w_f	-	residual deflection
K_0	-	kinetic energy

M_r, M_θ	-	bending moment
Q_r	-	shear force
R	-	radius of annular plate
S	-	middle surface
T_i	-	surface tractions
V	-	volume
W	-	deflection
$\alpha = a/R$	-	non-dimensional coordinate
γ	-	transverse shear
$\rho = r/R$	-	non-dimensional coordinate
$\eta(\tau), \eta_0(\tau)$	-	travelling hinges
μ	-	mass per unit length
σ_0, τ_0	-	yield stresses
ν	-	parameters
τ_1, τ_2, τ_3	-	moments of time
ψ	-	rotation due to bending

3.1 Introduction

Analytical investigations of dynamic plastic response of axisymmetric plates made of an ideal plastic Tresca material got its start by papers of Hopkins and Prager (1954); Wang and Hopkins (1955). In these papers simply supported and clamped circular plates subjected to distributed loading and initial impulsive loading were studied resorting to the classical plate theory.

Rigid-plastic annular plates (e.g. circular plates with a central hole) subjected to dynamical loadings have been considered by Mroz (1958), Jones (1968, 1970, 1989) using the bending theory of plates. In the case of a rigid-plastic material this concept includes stationary and moving hinge circles separating adjacent annuli of the plate which can deform in different manner. Aggarwal and Ablow (1971) developed simplified approximate solution procedures for simply supported and clamped annular plates of a Tresca material subjected to initial impulsive loading; Mazalov and Nemirovski (1976) concentrated on the annular plates subjected to distributed transverse loadings.

An annular plate clamped at the inner boundary with its free outer edge given a constant velocity for a short time was studied by Shapiro (1959). Later an annular plate with a uniform transverse impulse on a narrow annular area near the outer edge was investigated by Florence (1965). Florence considered the annular plate clamped at the inner edge with free outer edge using Tresca's yield hexagon. Annular plates fixed at the inner edge were studied also by Niepostyn and Stańczyk (1979), Stańczyk (1982) in the cases of various loadings.

Recently Guowei Ma et al (1999), Yan-bin Wang et al (2005) employed

the concept of a unified strength theory in the analysis of dynamic plastic response of circular plates.

Clamped circular plates made of work-hardening materials were studied by Wen (1998). An approximate theory was developed to predict the deformations and tearing of plates for power-law stress-strain relationship. Theoretical predictions are shown to be in good agreement with experimental data. Viscoplastic metallic circular plates subjected to impulsive loading are considered by Zaera, Arias and Navarro (2002) making use of various non-linear approximations of the actual yield surface.

Wen, Yu, Reddy (1995,b) developed an approximate theory to examine the dynamic inelastic deformation and failure of clamped circular plates subjected to uniformly distributed impulsive loads. Resorting to the previous work by Wen, Yu, Reddy (1995,a) it was shown that the failure modes are: large inelastic deformations (Mode I), tensile tearing (Mode II) and transverse shear (Mode III).

Experiments conducted on circular plates made of metallic materials revealed significant discrepancies between theoretical predictions according to the bending theory and experimental data. This involves the need for retention of shear forces in the yield condition together with bending moments (and membrane forces in the case of large deflections).

The influence of shear forces on the static collapse pressure was investigated by Sawczuk and Duszek (1963), Haydl and Sherbourne (1979), Zhuk and Shablii (1973), Mohaghegh and Coon (1973), Dinno and Robinson (1976).

Jones and Oliveira (1980) studied the influence of the rotatory inertia and shear forces on the dynamic plastic response of simply supported circular plates to impulsive loading. This study revealed the influence of shear forces on the behaviour of plates in the case of small values of the parameter ν . Li and Jones (1994) investigated clamped circular plates subjected to blast loading distributed uniformly over the entire area of the plate. Theoretical solutions are obtained for a general blast loading for a plate made of a Johansen's material. The effects of different boundary conditions, pressure pulse loading shapes and the influence of the transverse shear force on the dynamic plastic response of circular plates are explored. The applicability of Youngdahl's correlation parameter is stated for circular plates. The case of a central pressure pulse distributed over a central part was investigated by Liu and Stronge (1996). Li and Huang (1989) considered the case of a uniformly distributed rectangular pulse loading; Komarov and Nemirovski (1984) gave solutions for clamped circular plates accounting for shear stresses.

The motion of a simply supported circular plate subjected to a rectangular loading was studied by Kumar and Krishna Reddy (1986). In a similar study under taken by Jones and Oliveira (1980) for circular plates subjected to blast loading idealized by an instantaneous uniform velocity, it was concluded that the velocity pattern depends on a parameter $\nu = RQ_0/2M_0$.

Following a procedure similar to that by Jones and Oliveira (1980) the expressions for the shear force, bending moment and the plate deflection have been obtained. It appeared that the solution of the problem including shear showed greater radial moments throughout the plate when compared with the pure bending solution. The transverse shear failure of infinitely large circular plates with a central boss which is subjected to an initial impulsive velocity was studied by Zhao et al (1994).

Shen and Jones (1993) presented a theoretical investigation on plastic response and failure of clamped circular plates under impulsive loading employing an interaction yield surface which combines the bending moments, membrane force and transverse shear force. Cowper-Symonds constitutive equation was used to cater for material strain rate effects.

It is somewhat surprising that despite a lot of attention is paid in the literature to beams, cylindrical shells and circular plates in the case when shear force is retained in the yield surface there are no works regarding to annular plates. In the case of annular plates yield mechanisms are often completely different from those taking place in the case of circular plates.

In earlier works by Lellep and Torn (2004, 2005) rigid plastic beams and circular cylindrical shells with non-symmetric end conditions have been studied accounting for shear forces in the yield condition. In the present study this concept is extended to circular plates with cutouts having free interior and clamped exterior edge, respectively.

3.2 Governing equations

Let us consider an annular plate of radius R and inner radius a (Fig. 3.1). The thickness of the plate is h . The plate is clamped at the outer edge and free at the inner edge.

Assume that at the initial moment of deformation the plate has a constant transverse velocity v_0 and the initial kinetic energy

$$K_0 = \mu \frac{\pi}{2} (R^2 - a^2) v_0^2. \quad (3.1)$$

Here μ stands for the mass per unit area of the plate.

The kinetic energy K_0 will be absorbed into plastic work which will be done by internal forces during subsequent plastic deformation of the plate. The generalized stresses contributing to the plastic dissipation are shear force Q_r and bending moments M_r, M_θ . Corresponding strain components are the transverse shear [5]

$$\gamma = \frac{\partial W}{\partial r} + \psi \quad (3.2)$$

and curvatures in the radial and circumferential directions, respectively

$$\begin{aligned} K_r &= \frac{\partial \psi}{\partial r}, \\ K_\theta &= \frac{\psi}{r} \end{aligned} \quad (3.3)$$

where $W = W(r, t)$ is the transverse displacement.

In (3.2) and (3.3) $\psi = \psi(r, t)$ is usual rotation of an element due to bending alone, while $\gamma(x, t)$ is the shear angle of the center line due to the transverse shear force alone. Here r stands for the current radius and t is time.

Neglecting the effect of rotatory inertia one can present equations of equilibrium of a plate element as [5]

$$\begin{aligned} \frac{\partial}{\partial r}(rQ_r) &= -pr + r\mu \frac{\partial^2 W}{\partial t^2} \\ \frac{\partial}{\partial r}(rM_r) - M_\theta + rQ_r &= 0. \end{aligned} \quad (3.4)$$

In (3.4) p stands for the intensity of a transverse loading. In the present case $p = 0$ as we are concentrating on the motion of the plate due to inertia only.

Let M_0, Q_0 stand for limit values of bending moments and the shear force, respectively. It appears that it will be reasonable to use following variables

$$\begin{aligned} \rho &= \frac{r}{R}, \quad \alpha = \frac{a}{R}, \quad m_1 = \frac{M_r}{M_0}, \quad m_2 = \frac{M_\theta}{M_0}, \\ q &= \frac{Q_r}{Q_0}, \quad \nu = \frac{Q_0 R}{M_0}, \quad w = \frac{M_0 W}{\mu v_0^2 R^2}, \quad \tau = \frac{M_0 t}{\mu v_0 R^2}. \end{aligned} \quad (3.5)$$

Making use of (3.5) one can present equations of motion (3.4)

$$\begin{aligned} (\rho m_1)' - m_2 &= \nu \rho q, \\ (\rho q)' &= \frac{\rho}{\nu} \ddot{w}. \end{aligned} \quad (3.6)$$

where dots denote differentiation with respect to τ , whereas primes - with respect to ρ .

Assume that the yield surface in the space m_1, m_2, q is approximated by a cube of unit volume (Fig. 3.2).

The theoretical analysis shows that the stress profile can be either inside of the cube or lie on the face $m_2 = 1$. On this face $|m_1| \leq 1$ and $|q| \leq 1$. According to the associated flow law

$$\dot{K}_r = 0, \quad \dot{\gamma} = 0, \quad \dot{K}_\theta \geq 0.$$

Therefore,

$$\frac{\partial \dot{\psi}}{\partial r} = 0, \quad \frac{\partial \dot{W}}{\partial r} = -\dot{\psi}. \quad (3.7)$$

It follows from (3.7) that

$$\dot{w} = C_1 \rho + C_2. \quad (3.8)$$

In other words, the transverse velocity distribution must be piece wise linear with respect to ρ .

Making use of (3.5) one can present the initial conditions as

$$w(\rho, 0) = 0, \quad \dot{w}(\rho, 0) = 1, \quad (3.9)$$

provided $w = w(\rho, \tau)$.

Boundary conditions are

$$m_1(\alpha, \tau) = 0, \quad q(\alpha, \tau) = 0 \quad (3.10)$$

at the free edge and

$$q(1, \tau) = -1 \quad (3.11)$$

if shear sliding takes place at the clamped edge. Otherwise

$$w(1, \tau) = 0, \quad \dot{w}(1, \tau) = 0 \quad (3.12)$$

and

$$m(1, \tau) = -1. \quad (3.13)$$

3.3 Solution of governing equations

3.3.1 Case I

If $1 \leq \nu \leq 6.75$ then during this case of motion the transverse velocity distribution is given by

$$\dot{w} = \dot{w}_0 \quad (3.14)$$

for the plate element (Fig. 3.3). In (3.14) \dot{w}_0 is certain function of time.

Differentiating (3.14) with respect to τ and substituting into (3.6) one can integrate the set (3.6) with respect to the coordinate ρ . Making use of boundary conditions $q(\alpha, \tau) = 0$ one has

$$q = \frac{\ddot{w}_0}{2\nu\rho}(\rho^2 - \alpha^2). \quad (3.15)$$

Making use of (3.15) and integrating the first equation in (3.6) leads to the relation

$$m_1 = 1 - \frac{\nu}{1 - \alpha^2} \left(\frac{\rho^2}{3} - \alpha^2 \right) + \frac{1}{\rho} \left(-\alpha - \frac{2\nu\alpha^3}{3(1 - \alpha^2)} \right), \quad (3.16)$$

where the boundary condition $m(\alpha, \tau) = 0$ is taken into account.

Taking $\rho = 1$ in the equation (3.15) after certain algebraic transformation one easily obtains

$$\ddot{w}_0 = \frac{-2\nu}{1 - \alpha^2}. \quad (3.17)$$

The motion of the plate according to case I ends at the moment τ_1 when the motion stops. Evidently (see Fig. 3.3, 3.8) case I takes place when $m_1(1, \tau) \geq -1$. Calculations carried out showed that this requirement is satisfied, if $\nu < \nu_1 = 6.75$.

3.3.2 Case II

3.3.2.1 First phase of motion

Assume that now $\nu > \nu_1 = 6.75$. During the first phase of motion shear sliding occurs at the clamped edge of the plate. The transverse velocity distribution for this phase is presented in Fig. 3.4. According to Fig. 3.4 the acceleration may be written as

$$\ddot{w} = \ddot{w}_0 \frac{1 - \rho}{1 - \alpha} + \ddot{w}_1 \frac{\rho - \alpha}{1 - \alpha}, \quad (3.18)$$

where \ddot{w}_0 and \ddot{w}_1 stand for the accelerations of points lying at the internal and external boundary, respectively.

Substituting (3.18) in (3.6) and integrating with respect to coordinate ρ under the conditions $q(\alpha, \tau) = 0$, $q(1, \tau) = -1$ one obtains

$$\rho q = \frac{1}{\nu(1 - \alpha)} \left[\ddot{w}_0 \left(\frac{\rho^2}{2} - \frac{\alpha^2}{2} - \frac{\rho^3}{3} + \frac{\alpha^3}{3} \right) + \ddot{w}_1 \left(\frac{\rho^3}{3} - \frac{\alpha^3}{3} - \frac{\alpha}{2} (\rho^2 - \alpha^2) \right) \right] \quad (3.19)$$

and

$$\frac{1}{\nu(1-\alpha)} \left[\frac{\ddot{w}_0}{6} (3(1-\alpha^2) - 2 + 2\alpha^3) + \frac{\ddot{w}_1}{6} (2 - 2\alpha^3 - 3\alpha(1-\alpha^2)) \right] = -1. \quad (3.20)$$

Making use of (3.19) and integrating the first equation in (3.6) leads to the relation

$$\begin{aligned} m_1 = & 1 + \frac{1}{\rho(1-\alpha)} \left\{ \ddot{w}_0 \left[\frac{\rho^3}{6} - \frac{\alpha^3}{6} - \frac{\alpha^2}{2}(\rho - \alpha) - \frac{\rho^4}{12} + \frac{\alpha^4}{12} + \frac{\alpha^3}{3}(\rho - \alpha) \right] + \right. \\ & \left. + \ddot{w}_1 \left[\frac{\rho^4}{12} - \frac{\alpha^4}{12} - \frac{\alpha}{6}(\rho^3 - \alpha^3) + \frac{\alpha^3}{6}(\rho - \alpha) \right] \right\} - \frac{\alpha}{\rho} \end{aligned} \quad (3.21)$$

where the boundary condition $m(\alpha, \tau) = 0$ is taken into account. Making use of boundary condition $m(1, \tau) = -1$ one has

$$\begin{aligned} & \ddot{w}_0 \left[\frac{1}{6}(1 + \alpha + \alpha^2) - \frac{\alpha^2}{2} - (1 + \alpha)(1 + \alpha^2) \frac{1}{12} + \frac{\alpha^3}{3} \right] + \\ & + \ddot{w}_1 \left[\frac{1}{12}(1 + \alpha)(1 + \alpha^2) - \frac{\alpha^2}{6} - (1 + \alpha + \alpha^2) + \frac{\alpha^3}{6} \right] - \alpha = -2. \end{aligned} \quad (3.22)$$

The set of equations (3.20), (3.22) with respect to the quantities \ddot{w}_0 and \ddot{w}_1 may be presented as

$$\ddot{w}_0(1 + 2\alpha) + \ddot{w}_1(\alpha + 2) = -\frac{6\nu}{1-\alpha} \quad (3.23)$$

and

$$\ddot{w}_0(1 + 3\alpha) + \ddot{w}_1(1 + \alpha) = \frac{12(\alpha - 2)}{(1 - \alpha)^2}. \quad (3.24)$$

It follows from (3.23), (3.24) that the accelerations can be defined as

$$\begin{aligned} \ddot{w}_0 &= \frac{6[\nu(1 - \alpha^2) + 2(\alpha^2 - 4)]}{(1 - \alpha)^2(1 + 4\alpha + \alpha^2)} \\ \ddot{w}_1 &= \frac{6[\nu(1 + 3\alpha)(1 - \alpha) + 2(\alpha - 2)(1 + 2\alpha)]}{(1 - \alpha)^2(1 - 4\alpha - \alpha^2)}. \end{aligned} \quad (3.25)$$

The first phase of motion ends at the moment $\tau = \tau_1$ when $\dot{w}_1(\tau_1) = 0$. Since $\ddot{w}_j(\tau) = \text{const}$ one has

$$\dot{w}_j = \ddot{w}_j \tau + 1 \quad (3.26)$$

and

$$w_j = \ddot{w}_j \frac{\tau^2}{2} + \tau.$$

Here $j = 0, 1$ and the initial conditions (3.9) are taken into account. Thus the first phase terminates at the moment when $\dot{w}_1(\tau_1) = 0$, e.g.

$$\tau_1 = -\frac{1}{\ddot{w}_1}.$$

Displacements at boundaries of the plate at moment τ_1 are

$$w_1(\tau_1) = -\frac{1}{2\ddot{w}_1}$$

$$w_0(\tau_1) = -\frac{1}{2\ddot{w}_0}$$

3.3.2.2 Second phase of motion

During the second phase of motion the acceleration may be written as (Fig. 3.5)

$$\ddot{w} = \ddot{w}_0 \frac{1 - \rho}{1 - \alpha} \quad (3.27)$$

Making use of (3.27) and integrating the system of equations (3.6) with modified boundary conditions (3.10)-(3.13) one obtains

$$q = \frac{\ddot{w}_0}{\rho\nu(1-\alpha)} \left(\frac{\rho^2}{2} - \frac{\alpha^2}{2} - \frac{\rho^3}{3} + \frac{\alpha^3}{3} \right) \quad (3.28)$$

$$m_1 = 1 + \frac{\ddot{w}_0}{\rho(1-\alpha)} \left(\frac{\rho^3}{6} - \frac{\alpha^3}{3} - \frac{\alpha^2}{2}(\rho - \alpha) - \frac{\rho^4}{12} + \frac{\alpha^4}{12} + \frac{\alpha^3}{3}(\rho - \alpha) \right) - \frac{\alpha}{\rho}$$

and

$$\ddot{w}_0 = \frac{12(\alpha - 2)}{(1 - \alpha)^2(1 + 3\alpha)}. \quad (3.29)$$

From the last equation one can easily find

$$\dot{w}_0 = \frac{12(\alpha - 2)}{(1 - \alpha)^2(1 + 3\alpha)}(\tau - \tau_1) + \dot{w}_0(\tau_1), \quad (3.30)$$

$$w_0 = \frac{6(\alpha - 2)}{(1 - \alpha)^2(1 + 3\alpha)}(\tau - \tau_1)^2 + \dot{w}_0(\tau_1)(\tau - \tau_1) + w_0(\tau_1)$$

where the initial values $\dot{w}_0(\tau_1)$, $w_0(\tau_1)$ are defined by corresponding quantities obtained for the first phase of motion.

The second phase of motion persists as long as $\dot{w}_0(\tau_2) = 0$. According to (3.30) the time of motion is

$$\tau_2 = \tau_1 - \frac{\dot{w}_0(\tau_1)}{\ddot{w}_0}.$$

Maximal residual deflection at the free edge of the plate equals

$$w_0(\tau_1) = -\frac{\dot{w}_0^2(\tau_1)}{2\ddot{w}_0} + w_0(\tau_1).$$

3.3.3 Case III

3.3.3.1 First phase of motion

If $\nu \geq \nu_2 = 22.1503$ the inequality $|m(\rho, \tau)| < 1$ is not satisfied for each $\rho \in [\alpha, 1]$. Calculations show that the maximum of $m(\rho, \tau)$ takes place at $\rho = \eta_0$. This means that at $\rho = \eta_0$ a hinge circle crops up. During the subsequent motion for $\tau \in [0, \tau_1]$ the hinge circle remains stationary.

For the first phase of motion the transverse velocity distribution is presented in Fig. 3.6, where \dot{w}_0 , \dot{w}_1 and \dot{w}_2 denote displacement rates at $\rho = \alpha$, $\rho = \eta_0$ and $\rho = 1$, respectively. As it reveals from Fig. 3.6 pure shear sliding takes place at the outer edge of the plate. According Fig. 3.6

$$\dot{w} = \frac{1}{\eta_0 - \alpha} [\dot{w}_2(\rho - \alpha) - \dot{w}_0(\rho - \eta_0)] \quad (3.31)$$

for $\rho \in [\alpha, \eta_0]$ and

$$\dot{w} = \frac{1}{1 - \eta_0} [\dot{w}_1(\rho - \eta_0) - \dot{w}_2(\rho - 1)] \quad (3.32)$$

for $\rho \in [\eta_0, 1]$.

Note that the acceleration distribution can easily be obtained from (3.31), (3.32) replacing velocities \dot{w}_0 , \dot{w}_1 , \dot{w}_2 by the accelerations \ddot{w}_0 , \ddot{w}_1 , \ddot{w}_2 , respectively.

Substituting (3.31) in (3.6) and integrating with respect to ρ one obtains the shear force

$$q = \frac{1}{6\rho\nu(\eta_0 - \alpha)} \{2(\ddot{w}_2 - \ddot{w}_0)(\rho^3 - \alpha^3) - 3\ddot{w}_0(\alpha - \eta_0)(\rho^2 - \alpha^2)\} \quad (3.33)$$

and the bending moment

$$\begin{aligned}
m_1 &= 1 - \frac{\alpha}{\rho} + \frac{1}{12\rho(\eta_0 - \alpha)} \{(\ddot{w}_2 - \ddot{w}_0)[\rho^4 - \alpha^4 - 4\alpha^3(\rho - \alpha)] + \\
&\quad + 2(\eta_0\ddot{w}_0 - \alpha\ddot{w}_2)[\rho^3 - \alpha^3 - 3\alpha^2(\rho - \alpha)]\} \quad (3.34)
\end{aligned}$$

for $\rho \in [\alpha, \eta_0]$. Note that when the system (3.6) is integrated boundary conditions (3.10) have been taken into account. At $\rho = \eta_0$ a stationary hinge circle is located. Thus $q(\eta_0, \tau) = 0$, $m_1(\eta_0, \tau) = 1$ and according to (3.33), (3.34) one has

$$\begin{aligned}
(\ddot{w}_2 - \ddot{w}_0)[\eta_0^4 - \alpha^4 - 4\alpha^3(\eta_0 - \alpha)] + 2(\eta_0\ddot{w}_0 - \\
- \alpha\ddot{w}_2)[\eta_0^3 - \alpha^3 - 3\alpha^2(\eta_0 - \alpha)] &= 12\alpha(\eta_0 - \alpha) \quad (3.35) \\
2(\ddot{w}_2 - \ddot{w}_0)(\eta_0^3 - \alpha^3) + 3(\eta_0\ddot{w}_0 - \alpha\ddot{w}_2)(\eta_0^2 - \alpha^2) &= 0.
\end{aligned}$$

Similarly, substituting (3.32) in (3.6) and taking into account that $m_1(\eta_0, \tau) = 1$, $q(\eta_0, \tau) = 0$ yields for $\rho \in [\eta_0, 1]$

$$q = \frac{1}{\nu\rho(1 - \eta_0)} \left\{ \frac{\ddot{w}_1}{3}[\rho^3 - \eta_0^3 - \frac{3}{2}\eta_0(\rho^2 - \eta_0^2)] - \frac{\ddot{w}_2}{3}[\rho^3 - \eta_0^3 - \frac{3}{2}(\rho^2 - \eta_0^2)] \right\} \quad (3.36)$$

and

$$\begin{aligned}
m_1 &= 1 + \frac{1}{12\rho(1 - \eta_0)} \{ \ddot{w}_1[\rho^4 - \eta_0^4 + 2\eta_0^3(\rho - \eta_0) - 2\eta_0(\rho^3 - \eta_0^3)] - \\
&\quad - \ddot{w}_2[\rho^4 - \eta_0^4 - 4\eta_0^3(\rho - \eta_0) - 2(\rho^3 - \eta_0^3) + 6\eta_0^2(\rho - \eta_0)] \}. \quad (3.37)
\end{aligned}$$

The boundary conditions (3.11) and (3.13) with (3.36) and (3.37) lead to the equations

$$\begin{aligned}
\ddot{w}_1[2(1 - \eta_0^3) - 3\eta_0(1 - \eta_0^2)] - \ddot{w}_2[2(1 - \eta_0^3) - 3(1 - \eta_0^2)] &= -6\nu(1 - \eta_0) \\
\ddot{w}_1[1 - \eta_0^4 - 2\eta_0(1 - \eta_0^3) + 2\eta_0^3(1 - \eta_0)] - \ddot{w}_2[1 - \eta_0^4 - 4\eta_0^3(1 - \eta_0) + \\
+ 6\eta_0^2(1 - \eta_0) - 2(1 - \eta_0^3)] &= -24(1 - \eta_0). \quad (3.38)
\end{aligned}$$

Solving equations (3.35) and (3.38) with respect to \ddot{w}_j , where $j = 0, 1, 2$ and η_0 one obtains

$$\begin{aligned}
\ddot{w}_0 &= \frac{12\alpha(2\eta_0 + \alpha)}{(\eta_0 - \alpha)^2(\eta_0^2 + 4\alpha\eta_0 + \alpha^2)} \\
\ddot{w}_1 &= \frac{-6\nu}{(1 - \eta_0)(2 + \eta_0)} + \frac{12\alpha(\eta_0 + 2\alpha)(2\eta_0 + 1)}{(\eta_0 - \alpha)^2(\eta_0^2 + 4\alpha\eta_0 + \alpha^2)(2 + \eta_0)} \\
\ddot{w}_2 &= \frac{-12\alpha(\eta_0 + 2\alpha)}{(\eta_0 - \alpha)^2(\eta_0^2 + 4\alpha\eta_0 + \alpha^2)} \quad (3.39)
\end{aligned}$$

and

$$\begin{aligned}
& 4(\eta_0 - \alpha)^2(\eta_0^2 + 4\alpha\eta_0 + \alpha^2) + \left[\frac{-\nu(\eta_0 - \alpha)^2}{(1 - \eta_0)(2 + \eta_0)}(\eta_0^2 + 4\alpha\eta_0 + \alpha^2) + \right. \\
& + \left. \frac{2\alpha}{2 + \eta_0}(\eta_0 + 2\alpha)(2\eta_0 + 1) \right] (1 - \eta_0)^2(1 + \eta_0) - \\
& - 2\alpha(\eta_0 + 2\alpha)(1 - \eta_0)^2(1 + 3\eta_0) = 0.
\end{aligned} \tag{3.40}$$

The last equation is to be solved numerically with respect to η_0 .

The accelerations \ddot{w}_j are constant as it can be seen from (3.39). Thus the relations (3.26) obtained for the Case II hold good for each $j = 0, 1, 2$ and

$$\begin{aligned}
w_0(\tau) &= \frac{6\alpha(2\eta_0 + \alpha)\tau^2}{(\eta_0 - \alpha)^2(\eta_0^2 + 4\alpha\eta_0 + \alpha^2)} + \tau \\
w_1(\tau) &= \left[\frac{-3\nu}{(1 - \eta_0)(2 + \eta_0)} + \frac{6\alpha(\eta_0 + 2\alpha)(2\eta_0 + 1)}{(\eta_0 - \alpha)^2(\eta_0^2 + 4\alpha\eta_0 + \alpha^2)(2 + \eta_0)} \right] \tau^2 + \tau \\
w_2(\tau) &= \frac{-6\alpha(\eta_0 + 2\alpha)}{(\eta_0 - \alpha)^2(\eta_0^2 + 4\alpha\eta_0 + \alpha^2)} \tau^2 + \tau.
\end{aligned} \tag{3.41}$$

The first phase of motion is completed at the time instant τ_1 when $\dot{w}_1(\tau_1) = 0$. According to (3.41)

$$\tau_1 = \left[\frac{6\nu}{(1 - \eta_0)(2 + \eta_0)} - \frac{12\alpha(\eta_0 + 2\alpha)(2\eta_0 + 1)}{(\eta_0 - \alpha)^2(\eta_0^2 + 4\alpha\eta_0 + \alpha^2)(2 + \eta_0)} \right]^{-1}. \tag{3.42}$$

The values of displacements at $\tau = \tau_1$ can be obtained from (3.41) and (3.42).

3.3.3.2 Second phase of motion

During the second phase of motion there is no more shear sliding at the clamped edge. However, a travelling bending hinge reveals at $\rho = \eta(\tau)$ (Fig. 3.7). The velocity distribution can be presented as

$$\dot{w} = \frac{1}{\eta - \alpha} [\dot{w}_2(\rho - \alpha) - \dot{w}_0(\rho - \eta)] \tag{3.43}$$

for $\rho \in [\alpha, \eta]$ and

$$\dot{w} = \dot{w}_2 \frac{\rho - 1}{\eta - 1} \tag{3.44}$$

for $\rho \in [\eta, 1]$.

Differentiating (3.43) and (3.44) with respect to time τ leads to the accelerations

$$\ddot{w} = \frac{1}{(\eta - \alpha)^2} \{ [\ddot{w}_2(\rho - \alpha) - \ddot{w}_0(\rho - \eta) + \dot{\eta}\dot{w}_0](\eta - \alpha) - \dot{\eta}[\dot{w}_2(\rho - \alpha) - \dot{w}_0(\rho - \eta)] \} \quad (3.45)$$

for $\rho \in (\alpha, \eta)$ and

$$\ddot{w} = \frac{\rho - 1}{(\eta - 1)^2} [\ddot{w}_2(\eta - 1) - \dot{w}_2\dot{\eta}] \quad (3.46)$$

for $\rho \in (\eta, 1)$.

Substituting (3.45) in (3.6) and integrating the system of equations with boundary conditions in (3.10) gives the shear force

$$q = \frac{1}{\nu\rho(\eta - \alpha)^2} \left\{ \left[\frac{1}{3}(\ddot{w}_2 - \ddot{w}_0)(\rho^3 - \alpha^3) + \frac{1}{2}(\ddot{w}_0\eta - \ddot{w}_2\alpha + \dot{\eta}\dot{w}_0)(\rho^2 - \alpha^2) \right](\eta - \alpha) - \dot{\eta} \left[\frac{1}{3}(\dot{w}_2 - \dot{w}_0)(\rho^3 - \alpha^3) + \frac{1}{2}(\dot{w}_0\eta - \dot{w}_2\alpha)(\rho^2 - \alpha^2) \right] \right\} \quad (3.47)$$

and the bending moment

$$m_1 = 1 + \frac{1}{12\rho(\eta - \alpha)^2} \left\{ [(\ddot{w}_2 - \ddot{w}_0)(\rho^4 - \eta^4 - 4\alpha^3(\rho - \eta)) + 2(\ddot{w}_0\eta - \ddot{w}_2\alpha + \dot{w}_0\dot{\eta})(\rho^3 - \eta^3 - 3\alpha^2(\rho - \eta))](\eta - \alpha) - \dot{\eta}[(\dot{w}_2 - \dot{w}_0)(\rho^4 - \eta^4 - 4\alpha^3(\rho - \eta)) + 2(\dot{w}_0\eta - \dot{w}_2\alpha)(\rho^3 - \eta^3 - 3\alpha^2(\rho - \eta))] \right\} \quad (3.48)$$

for $\rho \in [\alpha, \eta]$.

Similarly, the accelerations field (3.46) with equations of motion (3.6) yield the shear force

$$q = \frac{1}{6\nu\rho} [\ddot{w}_2(\eta - 1) - \dot{w}_2\dot{\eta}][2(\rho^3 - \eta^3) - 3(\rho^2 - \eta^2)] \quad (3.49)$$

and

$$m_1 = 1 + \frac{1}{12\rho} [\ddot{w}_2(\eta - 1) - \dot{w}_2\dot{\eta}][\rho^4 - \eta^4 - 2(\rho^3 - \eta^3) + (6\eta^2 - 4\eta^3)(\rho - \eta)] \quad (3.50)$$

for $\rho \in [\eta, 1]$. When deriving (3.48), (3.49), (3.50) the boundary conditions pertinent to plastic hinges

$$q(\eta, \tau) = 0, \quad m_1(\eta, \tau) = 1 \quad (3.51)$$

are satisfied.

Applying the first condition in (3.10) to (3.48), the first requirement in (3.51) to (3.47) and the boundary condition (3.13) to (3.50), respectively, yields

$$\begin{aligned} & [(\ddot{w}_2 - \ddot{w}_0)(\alpha^4 - \eta^4 - 4\alpha^3(\alpha - \eta)) + 2(\ddot{w}_0\eta - \ddot{w}_2\alpha + \dot{w}_0\dot{\eta})(\alpha^3 - \eta^3 - \\ & - 3\alpha^2(\alpha - \eta))](\eta - \alpha) - \dot{\eta}[(\dot{w}_2 - \dot{w}_0)(\alpha^4 - \eta^4 - 4\alpha^3(\alpha - \eta)) + 2(\dot{w}_0\eta - \\ & - \dot{w}_2\alpha)(\alpha^3 - \eta^3 - 3\alpha^2(\alpha - \eta))] = -12\alpha(\eta - \alpha)^2, \end{aligned} \quad (3.52)$$

$$[\ddot{w}_2(\eta - 1) - \dot{w}_2\dot{\eta}][1 - \eta^4 - 2(1 - \eta^3) + (6\eta^2 - 4\eta^3)(1 - \eta)] = -24(\eta - 1)^2,$$

$$\begin{aligned} & [2(\ddot{w}_2 - \ddot{w}_0)(\eta^3 - \alpha^3) + 3(\ddot{w}_0\eta - \ddot{w}_2\alpha + \dot{w}_0\dot{\eta})(\eta^2 - \alpha^2)](\eta - \alpha) - \\ & - \dot{\eta}[2(\dot{w}_2 - \dot{w}_0)(\eta^3 - \alpha^3) + 3(\dot{w}_0\eta - \dot{w}_2\alpha)(\eta^2 - \alpha^2)] = 0. \end{aligned}$$

The obtained set of equations can be solved with respect to accelerations \ddot{w}_0 , \ddot{w}_2 and the velocity of the travelling hinge $\dot{\eta}$. It can be rechecked that one obtains from (3.52) accelerations

$$\begin{aligned} \ddot{w}_0 &= \frac{\dot{\eta}(2\eta + \alpha)}{(\eta - 1)(\eta - \alpha)(\eta + 2\alpha)}[\dot{w}_2(\alpha - 1) - \dot{w}_0(\eta - 1)] + \frac{24(2\eta + \alpha)}{(1 - \eta)^2(1 + 3\eta)(\eta + 2\alpha)}, \\ \ddot{w}_2 &= \frac{\dot{w}_2\dot{\eta}}{\eta - 1} - \frac{24}{(1 - \eta)^2(1 + 3\eta)} \end{aligned} \quad (3.53)$$

where as $\dot{\eta}$ satisfies the equation

$$\begin{aligned} & \frac{\dot{\eta}}{(\eta - 1)(\eta - \alpha)(\eta + 2\alpha)} \{ \dot{w}_2(\eta + 3\alpha)(2\eta + \alpha)(\alpha - 1) + \\ & + \dot{w}_2(\eta + \alpha)(\eta + 2\alpha)(1 - \alpha) + \dot{w}_0(\eta - 1)(-\eta^2 - 4\alpha\eta - \alpha^2) \} = \\ & = \frac{12\alpha}{(\eta - \alpha)^2} + \frac{24(-\eta^2 - 4\alpha\eta - \alpha^2)}{(1 - \eta)^2(1 + 3\eta)(\eta + 2\alpha)}. \end{aligned} \quad (3.54)$$

The system of equations (3.53), (3.54) is to be integrated numerically. The initial values $w_0(\tau_1)$, $\dot{w}_0(\tau_1)$, $w_2(\tau_1)$, $\dot{w}_2(\tau_1)$ can be obtained from (3.41), (3.42) for the final time instant of the first phase of motion. Evidently, $\eta(\tau_1) = \eta_0$, where η_0 is defined by the solution for the first phase.

Let the second phase of motion be completed at $\tau = \tau_2$, whereas τ_2 is defined from the condition $\eta(\tau_2) = \alpha$.

Integrating (3.53), (3.54) on can determine quantities $w_0(\tau)$, $w_2(\tau)$ at each moment $\tau \in [\tau_1, \tau_2]$ and particularly values $w_0(\tau_2)$, $\dot{w}_0(\tau_2)$ which can be considered as initial values for the next phase of motion.

3.3.3.3 Third phase of motion

During the third phase of motion the velocity pattern corresponds to Fig. 3.5. Now the only hinge circle is located at the external edge of the plate. Thus

$$\dot{w}(\rho, \tau) = \dot{w}_0 \frac{1 - \rho}{1 - \alpha}$$

and the acceleration distribution corresponds to that for the second phase of motion for the case II. Evidently, relations (3.27)-(3.29) remain valid in the present case, as well.

However, instead of (3.30) on has now

$$\begin{aligned} \dot{w}_0 &= \frac{-12(2 - \alpha)}{(1 - \alpha)^2(1 + 3\alpha)}(\tau - \tau_2) + \dot{w}_0(\tau_2), \\ w_0 &= \frac{-6(2 - \alpha)}{(1 - \alpha)^2(1 + 3\alpha)}(\tau - \tau_2)^2 + \dot{w}_0(\tau_2)(\tau - \tau_2) + w_0(\tau_2) \end{aligned} \quad (3.55)$$

where the quantities $\dot{w}_0(\tau_2)$ and $w_0(\tau_2)$ are defined by the solution for the second phase of motion.

The motion of the plate ceases at the instant $\tau = \tau_3$, when \dot{w}_0 vanishes. Thus

$$\tau_3 = \tau_2 + \frac{(1 - \alpha)^2(1 + 3\alpha)}{12(2 - \alpha)}\dot{w}_0(\tau_2) \quad (3.56)$$

and the maximal residual displacement at the free edge of the plate attains the value

$$w_0(\tau_3) = \frac{(1 - \alpha)^2(1 + 3\alpha)}{24(2 - \alpha)}[\dot{w}_0(\tau_2)]^2 + w_0(\tau_2).$$

3.4 Discussion

Results of calculations are presented in Tables 3.1, 3.2 and Fig. 3.8-3.20. In Table 1 the values of the radius of the stationary hinge circle η_0 (Case III) are presented for different values of the parameter ν . Table 3.1 corresponds to the plate with the internal radius $a = 0.5R$ whereas Table 3.2 is associated with $a = 0.3R$.

Bending moment m_1 and shear force q are depicted in Fig. 3.8, Fig. 3.9 and Fig. 3.10 for initial stages of Cases I, II and III, respectively for plates with $\alpha = 0.5$. It transpires from Fig. 3.8 that the value of the radial bending moment at the clamped edge reaches to the limit value when the parameter ν tends to the value 6,75 (Case I, phase I). If the value $\nu_1 = 6.75$ is achieved then the motion takes place according to the velocity pattern for Case II (Fig. 3.4). Within the limits of Case II ($\nu_1 \leq \nu \leq \nu_2$) $m_1(1, \tau) = -1$, $q(1, \tau) = -1$ and $|m_1(\rho, \tau)| < 1$, $|q(\rho, \tau)| < 1$ elsewhere as it can be seen from Fig. 3.9. However, for a critical value $\nu = \nu_2 = 22.1503$ bending moment m_1 attains the upper limit at a certain point, e.g. $m_1(\eta_0, \tau) = 1$, if $\nu \geq \nu_2$ (Fig. 3.9). Such distributions of the bending moment m_1 and shear force q correspond to Case III with the velocity pattern presented in Figs 3.5-3.7. It can be seen from Fig. 3.8-3.10 that the stress distribution for Cases I-III are statically admissible, eg. the yield condition is violated nowhere.

Figs 3.8 and 3.9 show that for smaller and intermediate values of ν (cases I and II) shear force monotonically decreases from zero to -1. However, if $\nu > 22.1503$ then the shear force slowly increases near the free edge of the plate (Fig. 3.10). One can see from Fig. 3.10 that the point of maximum $\rho = \eta_0$ of the radial bending moment moves towards the outer edge when parameter ν increases.

The motion of points lying at the free edge of the plate is described in Figs 3.11-3.13 for Cases I-III, respectively. Distributions of transverse velocities during the first phase of motion are depicted in Fig. 3.14-3.18 for Case I-III. Maximal residual displacements at the free edge are plotted against ν in Fig. 3.19 (solid line). The dashed line in Fig. 3.19 presents an upper bound of Martin (1975) which is extended to the case when shear forces are retained in the yield condition by Jones (1985).

Upper bounds on the maximal residual deflection at the free edge of the plate are depicted in Fig. 3.20 for different ratios of internal and external radii, respectively.

Upper bounds on maximal displacements of structures subjected to initial impulsive loading are stated by Martin's upper bound theorems [34]. According to these theorems any kinematically admissible final displacement field u_i^f satisfies the inequality

$$\int_S T_i u_i^f dS \leq \int_V \frac{\mu}{2} \dot{u}_i^0 \dot{u}_i^0 dV$$

where \dot{u}_i^0 stand for the initial transverse velocities, S is the surface of the structure, V - its volume and T_i - surface tractions. It is reasonable to evaluate the final transverse displacements of the free edge of the plate and to present the last inequality as

$$2\pi \int_a^R T w_f r dr \leq K_0$$

where K_0 is the initial kinetic energy corresponding to the given initial velocity field.

Let T be the intensity of the ring load applied at the inner edge of the plate and w_f corresponding final displacement. Then evidently

$$2\pi a T w_f \leq K_0$$

and the upper bound can be defined as

$$\bar{w}_f = \frac{K_0}{2\pi T a}. \quad (3.57)$$

The load carrying capacity of the plate subjected to the ring load of intensity T will be evaluated in the cases of pure shear sliding with the velocity distribution presented in Fig. 3.3 and the triangular velocity distribution (Fig. 3.5), respectively. In the first case the kinematical method gives

$$T = \frac{R Q_0}{a}. \quad (3.58)$$

In the second case (Fig. 3.5) when deformations are caused by bending actions only one obtains the statical limit load as

$$T = \frac{M_0}{a} \frac{2R - a}{R - a}. \quad (3.59)$$

Direct calculations show that the velocity pattern depicted in Fig. 3.3 gives the kinetic energy

$$K_0 = \frac{\mu}{2} \pi h v_0^2 (R^2 - a^2) \quad (3.60)$$

whereas the second case is associated with

$$K_0 = \frac{\mu\pi}{2} v_0^2 R^2 \frac{R^2}{(R - a)^2}. \quad (3.61)$$

The upper bound defined by (3.57)-(3.61) is presented by the dashed line in Fig. 3.19 for $\alpha = 0.5$ and by solid lines in Fig. 20 for $\alpha = 0.2$; $\alpha = 0.3$; $\alpha = 0.5$; $\alpha = 0.6$.

Variation of the transverse velocity at the free edge in time is depicted in Fig. 3.11-3.13 for $a = R/2$. Fig. 11 corresponds to the Case I whereas Fig. 3.12 and 3.13 are associated with Cases II and III, respectively. It transpires from Fig. 3.13 that during the first phase the motion is not very sensitive with respect to the parameter ν . This matter can be explained by the obstacle that the early phase of motion is comparatively short and during this phase the most of the energy dissipation is caused by the shear sliding at the external support. Although the accelerations \ddot{w}_0 and \ddot{w}_1

explicitly do not depend on ν (see (3.39)) actually they do depend because the coordinate η_0 is a function of ν , as it can be seen from Tables 3.1, 3.2. Thus the lines corresponding to different values of ν are very near each other in the zone of small values of τ so that their coincidence is to be explained by the exactness of figures.

Variations of velocity patterns in time are presented in Fig. 3.14-3.18 for Cases I-III.

3.5 Concluding remarks

A theoretical solution has been developed for annular plates subjected to initial impulsive loading when the transverse shear force and bending moments are retained in the yield condition. It was shown that depending on the value of the parameter $\nu = Q_0 R / M_0$ three different types of the solution exist in the case of the uniform initial impulse. However, when the applied impulse is linear with respect to the coordinate the single yield mechanism takes place. In this case shear sliding occurs at the outer edge of the plate during the first phase whereas the motion is a modal one during the final phase.

Calculations carried out revealed the matter that shear stresses have greater influence on the plastic response of annular plates in the case of smaller values of the parameter ν . Maximal residual deflections have been compared with the upper bound method developed by J. Martin.

Numerical results showed that the solutions developed were statically admissible.

Tabel 3.1. Values of η_0 ($\alpha = 0.5$)

ν	η_0
22.1503	0.7759
25	0.7909
30	0.8153
35	0.8365
40	0.8542
45	0.8689
50	0.8812
55	0.8915
60	0.9002
65	0.9077
70	0.9142
75	0.9198
80	0.9248
85	0.9291
90	0.9331
95	0.9367
100	0.9397

Tabel 3.2. Values of η_0 ($\alpha = 0.3$)

ν	η_0
15.45941	0.6636
20	0.7157
25	0.7634
30	0.7997
35	0.8272
40	0.8484
45	0.8651
50	0.8786
55	0.8896
60	0.8988
65	0.9067
70	0.9134
75	0.9192
80	0.9243
85	0.9287
90	0.9327
95	0.9363
100	0.9395

Acknowledgement

The support from Estonian Science Foundation by Grant Project 5693 is gratefully acknowledged.

3.6 References

- [1] Hopkins HG, Prager W. On the dynamics of plastic circular plates. *J Appl Math Phys (ZAMP)* 1954; 5(4): 317-330.
- [2] Wang AJ, Hopkins HG. The plastic deformation of built-in circular plates under impulsive load. *J Mech Phys Solids* 1954; 3: 22-37.
- [3] Mroz Z. Plastic deformation of annular plates under dynamic loads. *Arch Mech Stosow* 1958; 10: 499-516.
- [4] Jones N. Finite deflections of a simply supported rigid-plastic annular plate loaded dynamically. *Int J Solids Struct* 1968; 4: 593-603.
- [5] Jones N. Rigid-plastic behaviour of plates. *Bull Mech Eng Educ* 1970; 9(3): 235-248.
- [6] Jones N. *Structural Impact*. Cambridge University Press. Cambridge. 1989.
- [7] Aggarwal HR, Ablow CM. Plastic bending of an annular plate by uniform impulse. *Int J Non-Linear Mech* 1971, 6(1): 69-80.
- [8] Mazalov VN, Nemirovsky J.V. Dynamical bending of rigid-plastic annular plates. *Int J Non-Linear Mech* 1976; 11(1): 25-39.
- [9] Shapiro GS. On a rigid-plastic annular plate under impulsive loading. *Prikl Mat Mekh* 1959; 23: 172-175.
- [10] Florence AL. Annular plate under a transverse line impulse. *AIAA J* 1965; 3(9): 1729-1732.
- [11] Niepostyn D, Stańczyk A. Impulsowe obciążenie plastycznej płyty pierścieniowej opartej na brzegu zewnętrznym. *Impuls ciśnienia. Biul WAT* 1979; 28(10): 61-76.
- [12] Stańczyk A. Impuls brzegowy w plastycznej płycie pierścieniowej. *Rozpr Inżyn* 1982; 30(2): 201-226.
- [13] Ma G, Iwasaki S, Miyamoto Y, Deto H. Dynamic plastic behavior of circular plate using unified yield criterion. *Int J Solids Struct* 1999; 36: 3257-3275.
- [14] Wang Y, Yu M, Xiao Y, Li L. Dynamic plastic response of a circular plate based on unified strength theory. *Int J Impact Eng* 2005; 31(1): 25-40.
- [15] Wen HM. Deformation and tearing of clamped circular work-hardening plates under impulsive loading. *Int J Pressure Vessels Piping* 1998; 75(1):

67-73.

[16] Zaera R, Arias A, Navarro C. Analytical modelling of metallic circular plates subjected to impulsive loads. *Int J Solids Struct* 2002; 39(3): 659-672.

[17] Wen HM, Yu TX, Reddy TY. A note on clamped circular plates under impulsive loading. *Mech Struct Mach* 1995; 23(3): 331-342.

[18] Wen HM, Yu TX, Reddy TY. Failure maps of clamped beams under impulsive loading. *Mech Struct Mach* 1995; 23(3): 453-472.

[19] Sawczuk A, Duszek M. A note on the interaction of shear and bending in plastic plates. *Arch Mech Stosow* 1963; 15: 411-426.

[20] Haydl HM, Sherbourne AN. Some approximations to the Ilyushin yield surface for circular plates and cylindrical shells. *Angew Math Mech* 1979; 59(2): 131-132.

[21] Zhuk NP, Shablii ON. Limit analysis of circular plates accounting for shear stresses. *Prikl Mekh* 1973; 9(3): 47-54.

[22] Mohaghegh MM, Coon MD. Plastic analysis of thick circular plates. *Int J Mech Sci* 1973; 15(11): 935-938.

[23] Dinno KS, Robinson M. Limit analysis of thick and thin circular plates subjected to transverse pressure. *World Conf Space Enclosures*. Montreal. 1976.

[24] Jones N, de Oliveira JG. Dynamic plastic response of circular plates with transverse shear and rotatory inertia. *ASME J Appl Mech* 1980; 47(1): 27-34.

[25] Li QM, Jones N. Blast loading of fully clamped circular plates with transverse shear effects. *Int J Solids Struct* 1994; 31(14): 1861-1876.

[26] Liu D, Stronge WJ. Shear and bending deformation of rigid-plastic circular plates by central pressure pulse. *Int J Impact Eng* 1996; 18(4): 383-402.

[27] Li QM, Huang YG. Dynamic plastic response of thin circular plates with transverse shear and rotatory inertia subjected to rectangular pulse loading. *Int J Impact Eng* 1989; 8: 219-228.

[28] Komarov KL, Nemirovskii YV. *Dynamics of Rigid-Plastic Structural Elements* (in Russian). Novosibirsk: Nauka; 1984.

[29] Kumar A, Reddy VVK. Dynamic plastic response of circular plates with transverse shear. *ASME J Appl Mech* 1986; 53: 952-953.

[30] Zhao Y-P, Fang J, Yu TX. Dynamic plastic shear failure analysis for an infinitely large plate with a centred cylinder under impulsive loading. *Int J Solids Struct* 1994; 31(11): 1585-1595.

[31] Shen WQ, Jones N. Dynamic response and failure of fully clamped circular plates under impulsive loading. *Int J Impact Eng* 1993; 13(2): 259-278.

[32] Lellep J, Torn K. Plastic response of a circular cylindrical shell to dynamic loadings. *Int J Impact Eng* 2004; 30: 555-576.

- [33] Lellep J, Torn K. Shear and bending response of a rigid-plastic beam subjected to impulsive loading. *Int J Impact Eng* 2005; 31: 1081-1105.
- [34] Martin JB. *Plasticity: Fundamentals and General Results*. Cambridge: MIT Press. 1975.
- [35] Jones N. Bounds on the dynamic plastic behaviour of structures including transverse shear effects. *Int J Impact Eng* 1985; 3: 273-291.

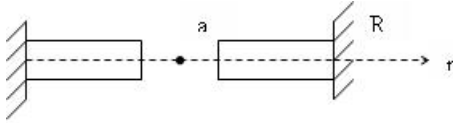


Figure 3.1: Annular plate.

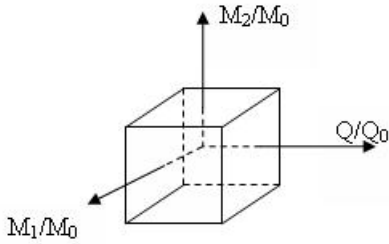


Figure 3.2: The yield surface.

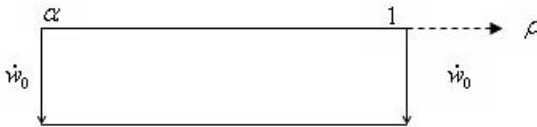


Figure 3.3: Velocity field for Case I.

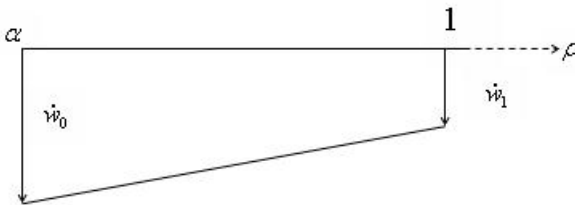


Figure 3.4: Velocity field for Case II, phase I.

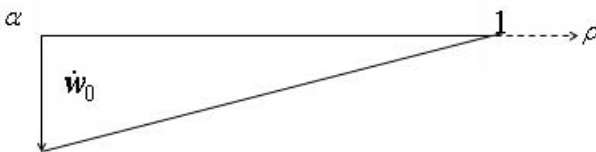


Figure 3.5: Velocity field for Case II, phase II and Case III, phase III.

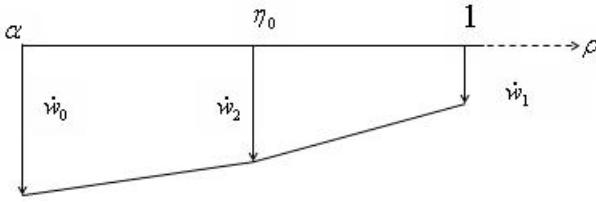


Figure 3.6: Velocity field for Case III, phase I.

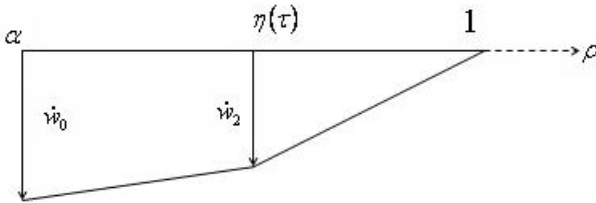


Figure 3.7: Velocity field for Case III, phase II.

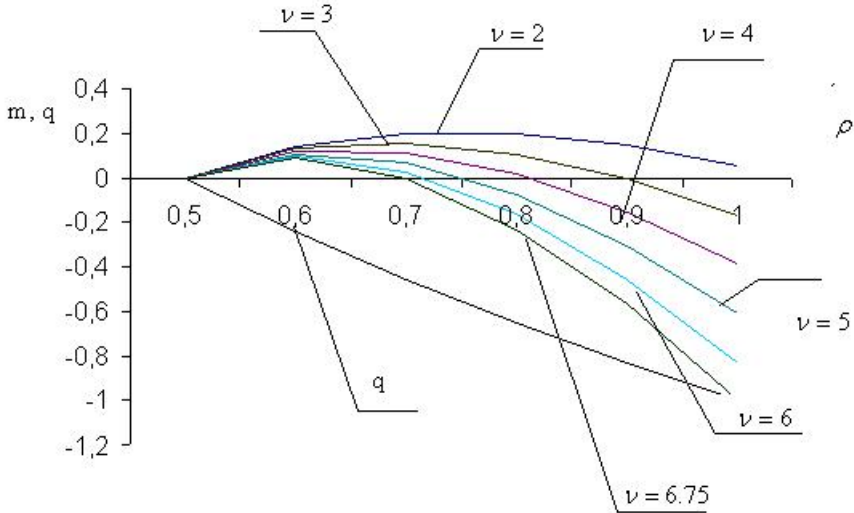


Figure 3.8: Bending moment and shear force (case I).

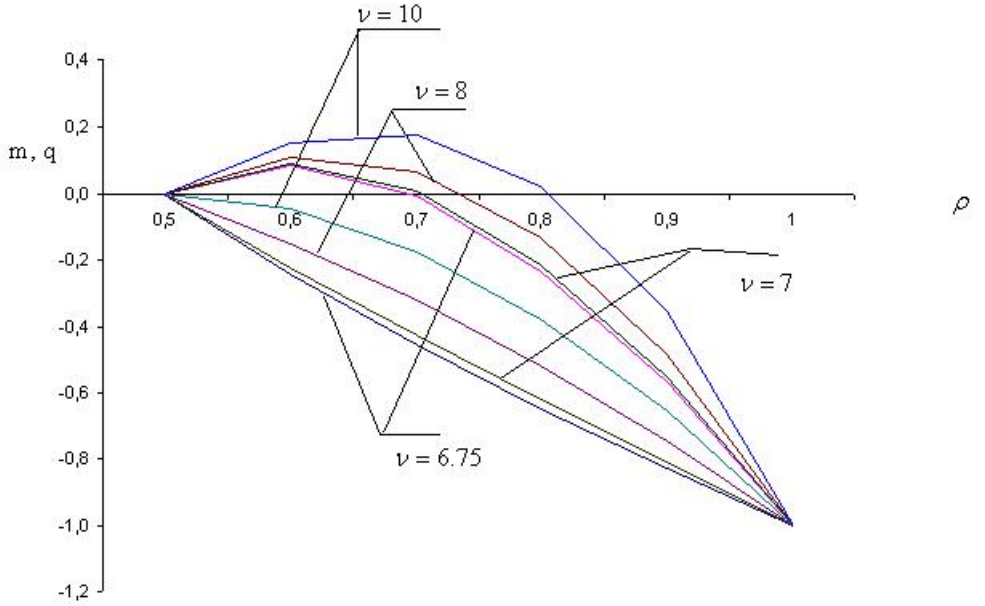


Figure 3.9: Bending moment and shear force (case II).

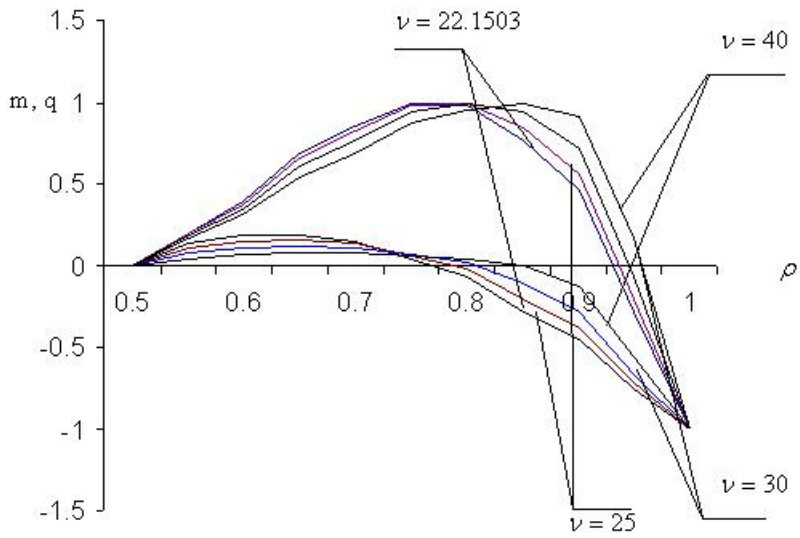


Figure.3.10: Bending moment and shear force (case III).

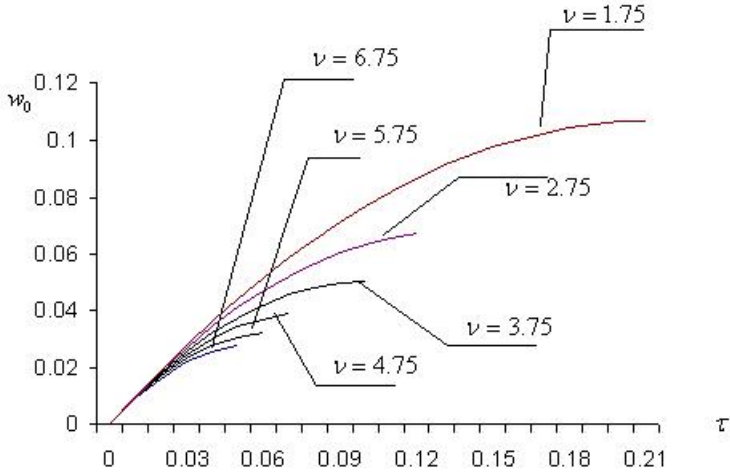


Figure 3.11: Maximal deflections (case I).

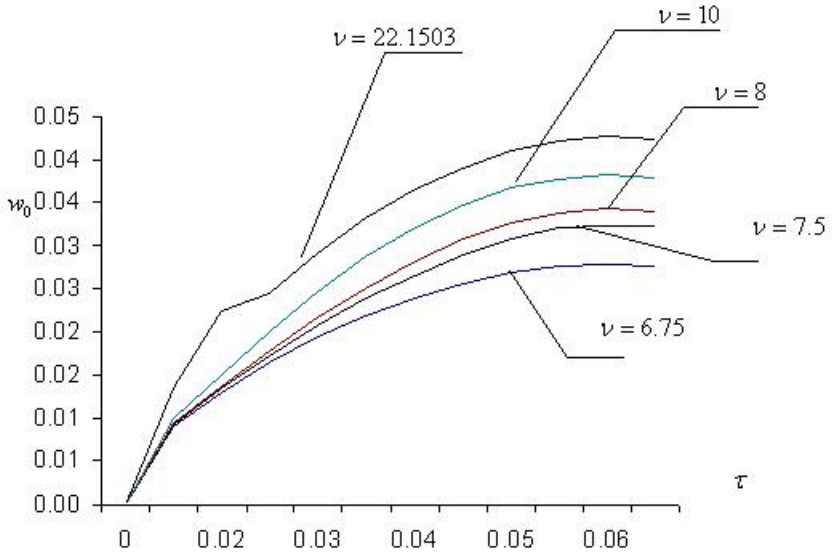


Figure 3.12: Maximal deflections (case II).

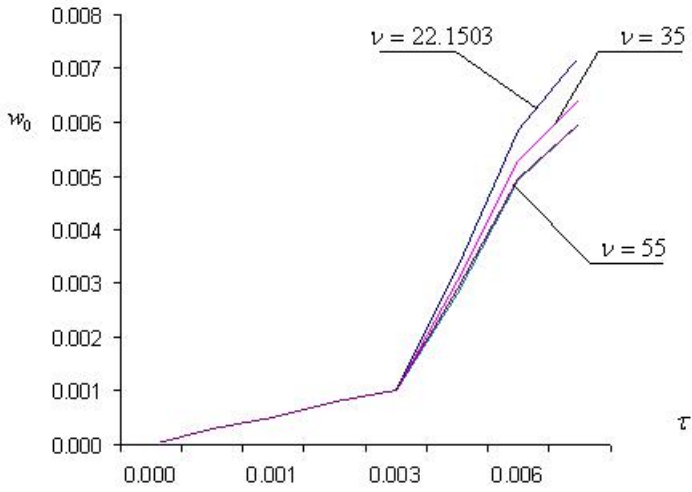


Figure 3.13: Maximal deflections (case III).

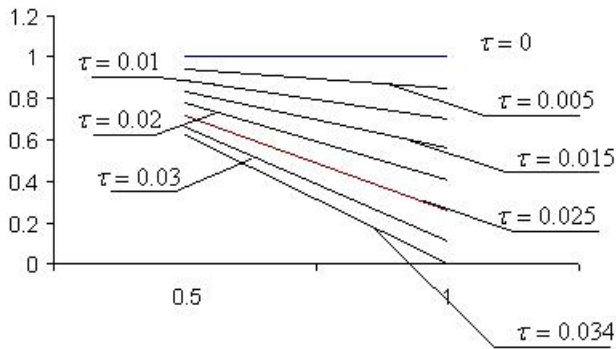


Figure 3.14: Velocity pattern Case II $\nu = 8$.

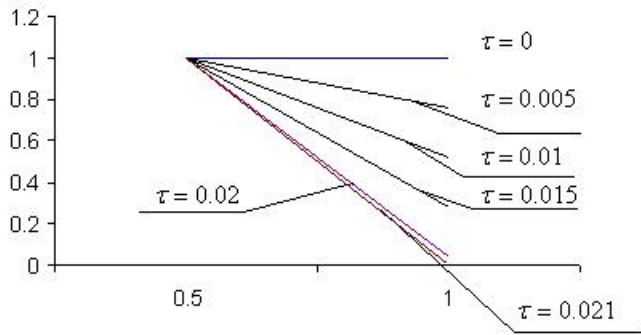


Figure 3.15: Velocity pattern Case II $\nu = 10$.

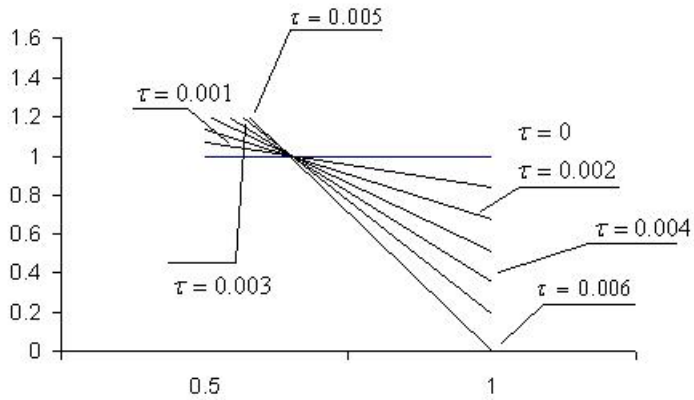


Figure 3.16: Velocity pattern Case II $\nu = 22.1503$.

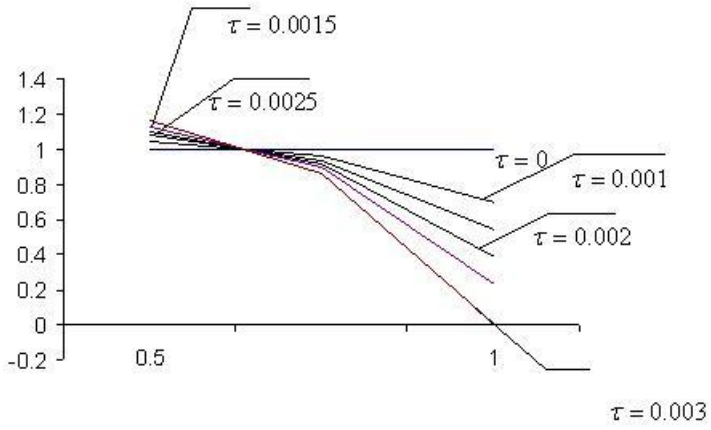


Figure 3.17: Velocity pattern Case II $\nu = 30$.

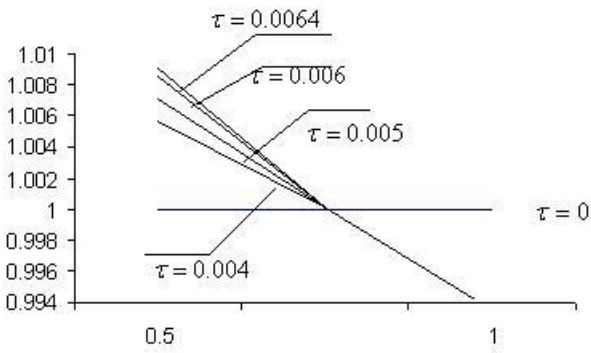


Figure 3.18: Velocity pattern Case III, phase 2.

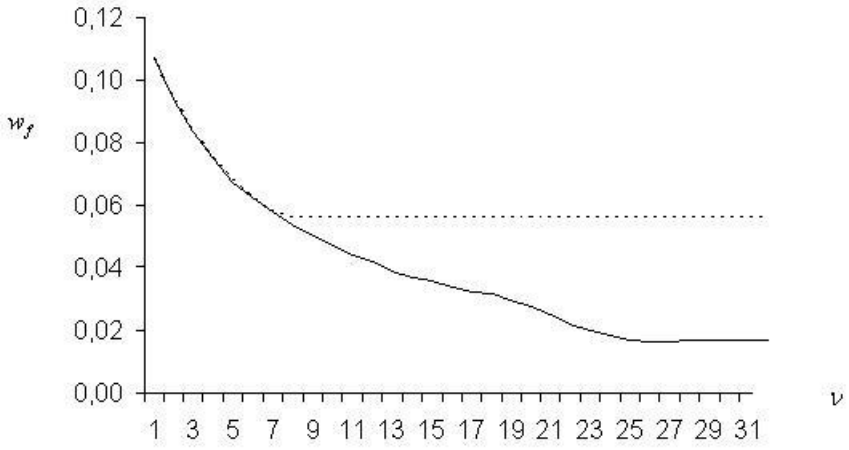


Figure 3.19: Maximal residual displacements.

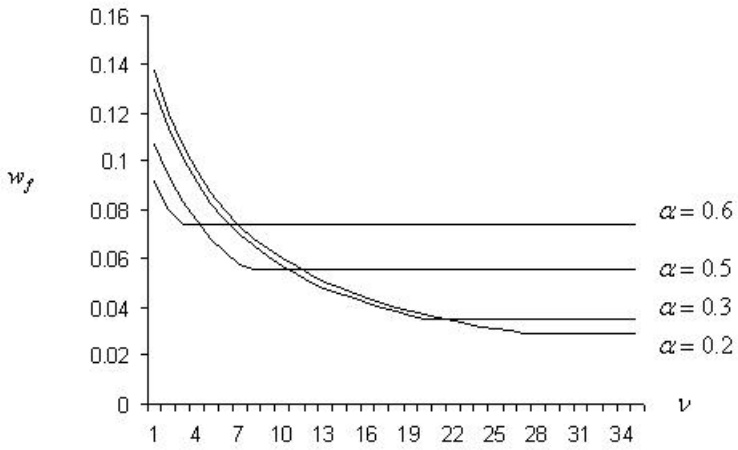


Figure 3.20: Upper bounds.

CHAPTER 4

Plastic response of a circular cylindrical shell to dynamic loadings

International Journal of Impact Engineering 2004; 30(5): 555-576.

Plastic response of a circular cylindrical shell to dynamic loadings

J. Lellep and K. Torn

Institute of Applied Mathematics, University of Tartu,
Tartu, 51014, 46 Vanemuise str., Estonia

Abstract

The dynamic plastic behaviour of a circular cylindrical shell subjected to an initial impulsive loading is studied. It is assumed that the thin walled tube is clamped at the left end and simply supported at the right-hand end. The behaviour of the rigid, perfectly plastic material is controlled by a cubic yield condition which retains the axial bending moment, circumferential membrane force as well as the transverse shear force. Theoretical predictions are presented for a wide range of geometrical and material parameters of the shell.

Keywords:

Cylindrical shell; Plasticity; Impulsive loading; Shear stresses

Notation

h	-	thickness of the shell wall
k	-	curvature
l	-	length of the shell
m, n, q	-	non-dimensional stress resultants
t, τ	-	time
w	-	non-dimensional deflection
w_0, w_1, w_2	-	transverse deflections at fixed points
x	-	coordinate
\dot{E}	-	energy dissipation
M	-	bending moment
M_0	-	yield moment
N	-	circumferential membrane force
N_0, Q_0	-	limit values of N, Q
P_j	-	generalized stresses
Q	-	shear force

R	- radius of the middle surface
W	- deflection
β, β_1, β_2	- stationary hinges
γ	- transverse shear
δ_j	- generalized strains
ε	- deformation component
ξ_0, ξ_*	- specific values of ξ
$\xi = x/l$	- non-dimensional coordinate
$\eta(\tau), \eta_1(\tau), \eta_2(\tau)$	- travelling hinges
μ	- mass per unit length
σ_0, τ_0	- yield stresses
ν, ω	- parameters
v_0	- initial transverse velocity
$\tau_1, \tau_2, \tau_3, \tau_4$	- moments of time
ψ	- rotation due to bending

4.1 Introduction

The first analytical work on dynamic plastic response of cylindrical shells was conducted by Hodge [1]. Song and Wang [2] considered cantilever cylindrical shells.

The influence of transverse shear forces on the dynamic plastic behaviour of beams, plates and shells subjected to impulsive and impact loading has attracted the interest of many researchers as discussed by Jones [3-5], Stronge and Yu [6], Yu and Chen [7].

Symonds [8] has examined the behaviour of a fully clamped beam subjected to impulsive loading and an infinitely long beam struck by a mass taking shear forces in the yield condition into account. Later different cases of beams subjected to distributed blast-type loadings were considered by Nonaka [9], Li and Jones [10], Jones and Song [11].

The influence of both, transverse shear and rotatory inertia on the dynamic plastic behaviour of beams and circular plates was studied by Jones and Gomes de Oliveira [12, 13]. Circular cylindrical shells subjected to impulsive and blast loading are studied by Duffey [14], Li and Jones [15], Jones and Oliveira [16]. In the above mentioned studies, the both ends of beams or cylindrical shells are fixed in the same manner. The exceptions are papers [17, 2]. In the paper [17], beams simply supported at the left and clamped at the right-hand end are considered. In the present paper the results of [17] are extended to circular cylindrical shells.

4.2 Governing equations

Consider a circular cylindrical shell clamped at the left end and simply supported at the right-hand end (Fig. 4.1). Assume that the shell is subjected to the uniformly distributed impulsive loading which imparts to a shell generator an initial transverse velocity v_0 .

Neglecting rotatory inertia effects but taking shear sliding caused by the shear force Q into account one can present the deflection slope as

$$\frac{\partial W}{\partial x} = \psi + \gamma. \quad (4.1)$$

Here γ stands for the transverse shear strain and ψ is the rotation of the mid-surface due to bending.

The dynamic equilibrium equation for a shell element may be written in the form

$$\begin{aligned} \frac{\partial M}{\partial x} + Q &= 0, \\ \frac{\partial Q}{\partial x} - \frac{N}{R} - \mu \frac{\partial^2 W}{\partial t^2} &= 0. \end{aligned} \quad (4.2)$$

The limit values of M , N and Q are

$$M_0 = \frac{\sigma_0}{4} h^2, \quad N_0 = \sigma_0 h, \quad Q_0 = \tau_0 h$$

for a solid shell wall with thickness h .

Making use of non-dimensional quantities

$$\begin{aligned} m &= \frac{M}{M_0}, \quad q = \frac{Q}{Q_0}, \quad n = \frac{N}{N_0}, \\ \nu &= \frac{Q_0 l}{M_0}, \quad \omega = \frac{N_0 l^2}{M_0 R}, \quad \xi = \frac{x}{l}, \\ w &= \frac{M_0 W}{\mu v_0^2 l^2}, \quad \tau = \frac{M_0 t}{\mu v_0 l^2} \end{aligned} \quad (4.3)$$

one can present the equations of motion (4.2) as

$$\begin{aligned} m' &= -\nu q, \\ q' &= \frac{1}{\nu} (\ddot{w} + \omega n). \end{aligned} \quad (4.4)$$

In Eq. (4.4) and henceforth primes and dots denote the differentiation with respect to ξ and τ , respectively.

As the shell is not deformed at the initial moment $\tau = 0$, but each point of a generator has velocity v_0 initial conditions to the system of Eqs. (4.4) have according to (4.3) the form

$$w(\xi, 0) = 0, \quad \dot{w}(\xi, 0) = 1. \quad (4.5)$$

Boundary conditions for the clamped and simply supported end of the shell, respectively, are

$$m(0, \tau) = 1, \quad m(1, \tau) = 0. \quad (4.6)$$

If shear sliding takes place at supports then one has

$$q(0, \tau) = 1, \quad q(1, \tau) = -1. \quad (4.7)$$

Yield surfaces for circular cylindrical shells which retain circumferential membrane force and longitudinal bending moment as well as the transverse shear force have been discussed by Haydl and Sherbourne [18], Ilyushin [19], Jones [3], Robinson [20], Zyczkowski [21]. However, as it was mentioned by Li and Jones [10] the most of theoretical studies on the dynamic response of rigid-plastic shells which retain transverse shear force effects have employed a simplified yield surface in order to obtain a complete theoretical solution of the problem. Following this idea in the present paper the cubic-shaped yield surface (Fig. 4.2) will be used.

According to the associated flow law the strain rate vector with components

$$\dot{\epsilon} = \frac{\dot{W}}{R}, \quad \dot{\kappa} = \frac{\partial \dot{\psi}}{\partial x}, \quad \dot{\gamma} = \frac{\partial \dot{w}}{\partial x} - \dot{\psi} \quad (4.8)$$

is to be directed along the outward normal to the surface at the current point.

On the edges of the cube the strain rate vector must lie between normals to adjacent faces of the edge.

It is reasonable to assume that $\dot{W} \geq 0$ and $\dot{\epsilon} \geq 0$. Thus the stress state of the tube corresponds to the face $n = 1$ of the yield surface. This face can be depicted as a square $|m| \leq 1$, $|q| \leq 1$ on $m - q$ plane. At each interior point of the square according to the flow law one has

$$\dot{\kappa} = \dot{\gamma} = 0. \quad (4.9)$$

It immediately follows from (4.8) and (4.9) that $\dot{w}'' = 0$. Thus

$$\dot{w} = C_1 \xi + C_2. \quad (4.10)$$

According to (4.10) in the following analysis it is assumed that the transverse velocity distribution is piece wise linear with respect to the axial coordinate ξ . Particular form of the velocity distribution depends on the value of the parameter ν .

4.3 Theoretical prediction of the response to impulsive loading

4.3.1 Case I

4.3.1.1 First phase of motion

If $2 \leq \nu \leq 5.6166$ then during the first stage of motion the transverse velocity distribution is given by

$$\dot{w} = \dot{w}_1 + (\dot{w}_2 - \dot{w}_1)\xi \quad (4.11)$$

for entire shell (Fig. 4.3). In Eq. (4.11) \dot{w}_1 and \dot{w}_2 are certain functions of time. Thus shear sliding takes place at both ends of the shell until the end of the first phase.

Differentiating (4.11) with respect to τ and substituting into (4.4) one can integrate the set (4.4) with respect to the coordinate ξ . Making use of boundary conditions (4.6) and (4.7) one has

$$\begin{aligned} q &= \frac{1}{\nu} \left(\ddot{w}_1 \xi + (\ddot{w}_2 - \ddot{w}_1) \frac{\xi^2}{2} + \omega \xi \right) + 1, \\ m &= -\frac{\ddot{w}_1}{2} \xi^2 + (\ddot{w}_1 - \ddot{w}_2) \frac{\xi^3}{6} - \frac{\omega}{2} \xi^2 - \nu \xi + 1 \end{aligned} \quad (4.12)$$

and

$$\begin{aligned} \ddot{w}_1 + \ddot{w}_2 &= -2(2\nu + \omega), \\ 2\ddot{w}_1 + \ddot{w}_2 &= 6\left(-\nu - \frac{\omega}{2} + 1\right). \end{aligned} \quad (4.13)$$

It follows from (4.13) that the accelerations \ddot{w}_1 and \ddot{w}_2 are constant, e.g.

$$\begin{aligned} \ddot{w}_1 &= -2\nu - \omega + 6, \\ \ddot{w}_2 &= -2\nu - \omega - 6. \end{aligned} \quad (4.14)$$

Integrating (4.14) with respect to time τ and taking into account that according to (4.5)

$$\dot{w}_1(0) = \dot{w}_2(0) = 1 \quad (4.15)$$

and

$$w_1(0) = w_2(0) = 0 \quad (4.16)$$

one easily obtains

$$\begin{aligned} \dot{w}_1 &= (-2\nu - \omega + 6)\tau + 1, \\ \dot{w}_2 &= (-2\nu - \omega - 6)\tau + 1 \end{aligned} \quad (4.17)$$

and

$$\begin{aligned} w_1 &= (-2\nu - \omega + 6)\frac{\tau^2}{2} + \tau, \\ w_2 &= (-2\nu - \omega - 6)\frac{\tau^2}{2} + \tau. \end{aligned} \quad (4.18)$$

The first phase ends at the moment τ_1 when the motion at the simply supported end stops. Thus

$$\tau_1 = \frac{1}{2\nu + \omega + 6} \quad (4.19)$$

and

$$\begin{aligned} w_1(\tau_1) &= \frac{2\nu + \omega + 18}{2(2\nu + \omega + 6)^2}, & \dot{w}_1(\tau_1) &= \frac{12}{2\nu + \omega + 6}, \\ w_2(\tau_1) &= \frac{1}{2(2\nu + \omega + 6)}, & \dot{w}_2(\tau_1) &= 0. \end{aligned} \quad (4.20)$$

4.3.1.2 Second phase of motion

During the second phase of motion shear sliding continues at the clamped end. At the same time each generator of the shell rotates around the simply supported right end (Fig. 4.4). The transverse velocity field can be presented as

$$\dot{w} = \dot{w}_1(\tau)(1 - \xi) \quad (4.21)$$

for $\xi \in (0, 1)$.

Making use of (4.21) and integrating the system of Eqs. (4.4) with modified boundary conditions (4.6) and (4.7) (where $q(1, \tau) \neq -1$) one obtains

$$\begin{aligned}
q &= \frac{1}{\nu} \left[\omega \xi + \ddot{w}_1 \left(\xi - \frac{\xi^2}{2} \right) \right] + 1, \\
m &= -\frac{\omega}{2} \xi^2 - \frac{\dot{w}_1}{6} (2\xi^2 - \xi^3) - \nu \xi + 1
\end{aligned} \tag{4.22}$$

and

$$\ddot{w}_1 = -3\nu - \frac{3}{2}\omega + 3. \tag{4.23}$$

From (4.23) one can easily find

$$\begin{aligned}
\dot{w}_1 &= \left(-3\nu - \frac{3}{2}\omega + 3 \right) (\tau - \tau_1) + \dot{w}_1(\tau_1), \\
w_1 &= \frac{1}{2} \left(-3\nu - \frac{3}{2}\omega + 3 \right) (\tau - \tau_1)^2 + \dot{w}_1(\tau_1) (\tau - \tau_1) + w_1(\tau_1)
\end{aligned} \tag{4.24}$$

where the initial values $\dot{w}_1(\tau_1)$, $w_1(\tau_1)$ are defined by (4.17)-(4.20).

The second phase of motion persists as long as $\dot{w}_1(\tau_2) = 0$. According to (4.24) the time of motion is

$$\tau_2 = \tau_1 + \frac{\dot{w}_1(\tau_1)}{3\nu + \frac{3}{2}\omega - 3}. \tag{4.25}$$

The motion prescribed in case I takes place if the limit moment is maintained elsewhere than at the clamped end of the shell. Making use of (4.12) and (4.22) it can be shown that an extremum of m is located at

$$\xi_0 = \frac{1}{6} (3 - \nu + \sqrt{9 + \nu^2}) \tag{4.26}$$

and the inequality $|m(\xi, \tau)| \leq 1$ is satisfied if

$$\nu^4 - 6\nu^3 + 9\nu^2 - 216 \leq 0. \tag{4.27}$$

It is interesting to remark that (4.26) and (4.27) coincide with those obtained for rigid-plastic beams loaded and fixed at the same manner as the considered shell [11].

The inequality (4.27) is satisfied if $0 \leq \nu \leq 5.6166$.

4.3.2 Case II

4.3.2.1 First phase of motion

If $\nu \geq \nu_2 = 5.6166$ the inequality $|m| < 1$ is not satisfied at $\xi = \xi_*$, where ξ_* is a coordinate which depends on geometrical and material parameters

of the shell. Now at $\xi = \xi_*$ a plastic hinge circle crops up which remains stationary during the first phase of motion. The transverse velocity distribution can be presented as (Fig. 4.5)

$$\dot{w} = \frac{1}{\xi_*} [\dot{w}_1(\xi_* - \xi) + \dot{w}_0\xi] \quad (4.28)$$

for $\xi \in (0, \xi_*)$ and

$$\dot{w} = \frac{1}{(1 - \xi_*)} [\dot{w}_2(\xi - \xi_*) + \dot{w}_0(1 - \xi)] \quad (4.29)$$

for $\xi \in (\xi_*, 1)$.

Substituting (4.28), (4.29) in (4.4) and integrating with appropriate boundary (4.6), (4.7) leads to

$$\begin{aligned} q &= \frac{1}{\nu} \left[(\omega + \ddot{w}_1)\xi + \frac{\ddot{w}_0 - \ddot{w}_1}{2\xi_*} \xi^2 + \nu \right], \\ m &= -\frac{\xi^2}{2} (\omega + \ddot{w}_1) - \frac{\ddot{w}_0 - \ddot{w}_1}{6\xi_*} \xi^3 - \nu\xi + 1 \end{aligned} \quad (4.30)$$

for $\xi \in (0, \xi_*)$ and

$$\begin{aligned} q &= \frac{1}{\nu} \left[\omega + \ddot{w}_2 + \frac{\ddot{w}_0 - \ddot{w}_2}{2} (\xi_* - 1) \right] (\xi - 1) - 1, \\ m &= -\frac{1}{2} (\omega + \ddot{w}_2) (\xi - 1)^2 - \frac{\ddot{w}_0 - \ddot{w}_2}{6(\xi_* - 1)} (\xi - 1)^3 + \nu(\xi - 1) \end{aligned} \quad (4.31)$$

for $\xi \in (\xi_*, 1)$.

Inserting $q(\xi_*, \tau) = 0$, $m(\xi_*, \tau) = -1$ in Eqs. (4.30) and (4.31), respectively, one obtains

$$\begin{aligned} \ddot{w}_0 &= -\omega + \frac{2\nu}{\xi_*} - \frac{12}{\xi_*^2}, \\ \ddot{w}_1 &= -\omega - \frac{4\nu}{\xi_*} + \frac{12}{\xi_*^2} \end{aligned} \quad (4.32)$$

and

$$\begin{aligned} \ddot{w}_0 &= -\omega - \frac{2\nu}{\xi_* - 1} - \frac{6}{(\xi_* - 1)^2}, \\ \ddot{w}_1 &= -\omega + \frac{4\nu}{\xi_* - 1} + \frac{6}{(\xi_* - 1)^2}. \end{aligned} \quad (4.33)$$

The acceleration \ddot{w}_0 presented by (4.32) and (4.33) has a unique value if

$$2\nu\xi_*^3 - 3(1 + \nu)\xi_*^2 + (12 + \nu)\xi - 6 = 0. \quad (4.34)$$

The first phase lasts as long as shear sliding takes place at the simply supported edge. Let the sliding stop at $\tau = \tau_1$, e.g. $\dot{w}_2(\tau_1) = 0$. Integrating (4.32) and (4.33) and satisfying initial conditions one can recheck that

$$\tau_1 = \frac{(1 - \xi_*)^2}{-4\nu(\xi_* - 1) + \omega(1 - \xi_*)^2 - 6} \quad (4.35)$$

and

$$\begin{aligned} \dot{w}_0(\tau) &= \left(\frac{2\nu}{\xi_*} - \omega + \frac{12}{\xi_*^2} \right) \tau + 1, \\ w_0(\tau) &= \left(\frac{2\nu}{\xi_*} - \omega + \frac{12}{\xi_*^2} \right) \frac{\tau^2}{2} + \tau, \\ \dot{w}_1(\tau) &= \left(-\frac{4\nu}{\xi_*} - \omega + \frac{12}{\xi_*^2} \right) \tau + 1, \\ w_1(\tau) &= \left(-\frac{4\nu}{\xi_*} - \omega + \frac{12}{\xi_*^2} \right) \frac{\tau^2}{2} + \tau, \\ \dot{w}_2(\tau) &= \left(\frac{4\nu}{(\xi_* - 1)} - \omega + \frac{6}{(\xi_* - 1)^2} \right) \tau + 1, \\ w_2(\tau) &= \left(\frac{4\nu}{(\xi_* - 1)} - \omega + \frac{6}{(\xi_* - 1)^2} \right) \frac{\tau^2}{2} + \tau. \end{aligned} \quad (4.36)$$

Relations (4.35) and (4.36) are to be considered as initial conditions for the subsequent motion. No more sliding takes place at $\xi = 1$ and a generator of the shell turns around the simply supported edge.

4.3.2.2 Second phase of motion

During the second phase of motion shear sliding continues at the clamped end and a travelling bending hinge occurs at $\eta = \eta(\tau)$ (Fig. 4.6). The velocity field can be presented as

$$\dot{w} = \frac{1}{\eta} [\dot{w}_1(\eta - \xi) + \dot{w}_0\xi] \quad (4.37)$$

for $\xi \in (0, \eta)$ and

$$\dot{w} = \dot{w}_0 \frac{\xi - 1}{\eta - 1} \quad (4.38)$$

for $\xi \in (\eta, 1)$.

From (4.37) and (4.38) one easily obtains the transverse acceleration as

$$\ddot{w} = \ddot{w}_1 + (\ddot{w}_0 - \ddot{w}_1) \frac{\xi}{\eta} - \frac{\dot{\eta}}{\eta^2} (\dot{w}_0 - \dot{w}_1) \xi, \quad (4.39)$$

for $\xi \in (0, \eta)$ and

$$\ddot{w} = \ddot{w}_0 \frac{\xi - 1}{\eta - 1} - \frac{\dot{\eta} \dot{w}_0}{(\eta - 1)^2} (\xi - 1), \quad (4.40)$$

for $\xi \in (\eta, 1)$.

Inserting (4.39), (4.40) in (4.4) and making use of (4.6), (4.7) yields

$$\begin{aligned} q &= \frac{1}{\nu} \left[(\omega + \ddot{w}_1) \xi + (\ddot{w}_0 - \ddot{w}_1) \frac{\xi^2}{2\eta} - \frac{\dot{\eta}}{2\eta^2} (\dot{w}_0 - \dot{w}_1) \xi^2 + \nu \right], \quad (4.41) \\ m &= -\frac{1}{2} (\omega + \ddot{w}_1) \xi^2 - (\ddot{w}_0 - \ddot{w}_1) \frac{\xi^3}{6\eta} + \frac{\dot{\eta}}{6\eta^2} (\dot{w}_0 - \dot{w}_1) \xi^3 - \nu \xi + 1, \end{aligned}$$

for $\xi \in (0, \eta)$ and

$$\begin{aligned} q &= \frac{1}{\nu} \left[\omega (\xi - 1) + \ddot{w}_0 \frac{(\xi - 1)^2}{2(\eta - 1)^2} - \frac{\dot{\eta} \dot{w}_0}{2(\eta - 1)^2} (\xi - 1)^2 + C \right], \quad (4.42) \\ m &= -\frac{1}{2} \omega (\xi - 1)^2 - \ddot{w}_0 \frac{(\xi - 1)^3}{6(\eta - 1)} + \frac{\dot{\eta} \dot{w}_0}{6(\eta - 1)^2} (\xi - 1)^3 - C (\xi - 1), \end{aligned}$$

for $\xi \in (\eta, 1)$, where C is an arbitrary constant.

Transverse velocity and acceleration fields (4.37)-(4.40) envisage a plastic hinge at $\xi = \eta(\tau)$. Thus $m(\eta, \tau) = -1$, $q(\eta, \tau) = 0$ and according to (4.41), (4.42)

$$C = \frac{3}{2(\eta - 1)} - \frac{\omega}{4} (\eta - 1) \quad (4.43)$$

and

$$\begin{aligned} \ddot{w}_0 &= \frac{-3}{(\eta - 1)^2} + \frac{\dot{\eta} \dot{w}_0}{\eta - 1} - \frac{3}{2} \omega, \\ \ddot{w}_1 &= \frac{12}{\eta^2} - \frac{4\nu}{\eta} - \omega, \\ \dot{\eta} &= \frac{\frac{3\eta}{\eta-1} + 2(\eta-1)(\nu + \frac{\omega}{4}\eta - \frac{6}{\eta})}{\dot{w}_0\eta - (1-\eta)(\dot{w}_1 - \dot{w}_0)}. \end{aligned} \quad (4.44)$$

The system of Eqs. (4.44) can be integrated numerically accounting for the initial conditions (4.35), (4.36) and $\eta(\tau_1) = \xi_*$. The second phase of motion terminates at the moment $\tau = \tau_2$ when the bending hinge at $\eta(\tau)$ disappears. The time τ_2 can be found numerically from the equation

$$\dot{w}_0(\tau_2) = \dot{w}_1(\tau_2)(1 - \eta(\tau_2)). \quad (4.45)$$

4.3.2.3 Third phase of motion

During the third phase the velocity distribution is presented as (Fig. 4.4)

$$\dot{w} = \dot{w}_1(\tau)(1 - \xi). \quad (4.46)$$

It is easy to recheck that the subsequent motion coincides with that corresponding to the case I, phase 2. Thus, (4.21)-(4.23) hold good in present case, as well. However, in Eqs. (4.24) and (4.25) τ_1 and τ_2 must be replaced by τ_2 and τ_3 , respectively. Here τ_3 stands for the final moment of motion when $\dot{w}_1(\tau_3) = 0$. It easily follows from (4.23)-(4.25) that

$$\tau_3 = \tau_2 + \frac{\dot{w}_1(\tau_2)}{3\nu + \frac{3}{2}\omega - 3}. \quad (4.47)$$

and

$$w_1(\tau_3) = \frac{\dot{w}_1^2(\tau_2)}{2(3\nu + \frac{3}{2}\omega - 3)} + w_1(\tau_2). \quad (4.48)$$

4.3.3 Case III

4.3.3.1 First phase of motion

The first phase (case III) coincides with the first phase of case II. Relations (4.28)-(4.36) hold good in the present case.

4.3.3.2 Second phase of motion

Also the second phase of motion is similar to the second phase in case II so that (4.37)-(4.44) remain valid in the present case. However, the second phase persists as long as shear sliding at the clamped end ceases. Thus the motion is prescribed by the system of Eqs. (4.44) until $\dot{w}_1(\tau_2) = 0$.

4.3.3.3 Third phase of motion

During the third phase no shear sliding takes place at supports. The transverse velocity distribution corresponds to the triangular pattern (Fig. 4.7).

Now at $\xi = \eta(\tau)$ a travelling bending hinge is located. The velocity distribution can be presented as

$$\dot{w} = \frac{1}{\eta} \dot{w}_0 \xi \quad (4.49)$$

for $\xi \in (0, \eta)$ and

$$\dot{w} = \dot{w}_0 \frac{\xi - 1}{\eta - 1} \quad (4.50)$$

for $\xi \in (\eta, 1)$. The acceleration field corresponding to (4.49) and (4.50) can be presented as

$$\ddot{w} = \left(\frac{\ddot{w}_0}{\eta} - \frac{\dot{\eta} \dot{w}_0}{\eta^2} \right) \xi \quad (4.51)$$

for $\xi \in (0, \eta)$ and

$$\ddot{w} = \left(\frac{\ddot{w}_0}{(\eta - 1)} - \frac{\dot{\eta} \dot{w}_0}{(\eta - 1)^2} \right) (\xi - 1) \quad (4.52)$$

for $\xi \in (\eta, 1)$.

Inserting (4.51), (4.52) in the equations of motion (4.4) and integrating under appropriate boundary conditions (now nowhere $|q| = 1$) leads to the expressions for the shear force and bending moment. Taking into account that at $\xi = \eta$ a plastic hinge circle is located, e.g. $m(\eta, \tau) = -1$, $q(\eta, \tau) = 0$ one has

$$\begin{aligned} \ddot{w}_0 &= 3 \left(-\frac{2}{\eta} - \frac{1}{1 - \eta} - \frac{\omega}{2} \right), \\ \dot{\eta} &= \frac{-3}{\dot{w}_0} \left(\frac{2(\eta - 1)}{\eta} + \frac{\eta}{1 - \eta} \right). \end{aligned} \quad (4.53)$$

The third phase of motion terminates at the moment when the travelling hinge reaches the modal position, e.g.

$$\eta(\tau_3) = \beta = \frac{\sqrt{2}}{1 + \sqrt{2}}. \quad (4.54)$$

4.3.3.4 Fourth phase of motion

The subsequent motion is a modal form motion with triangular velocity distribution (Fig. 4.7), where $\eta = \text{const} = \beta$.

Now the velocity distribution is

$$\dot{w} = \frac{\dot{w}_0(\tau)}{\beta} \xi \quad (4.55)$$

for $\xi \in (0, \beta)$ and

$$\dot{w} = \dot{w}_0(\tau) \frac{\xi - 1}{\beta - 1} \quad (4.56)$$

for $\xi \in (\beta, 1)$. The acceleration can be obtained when differentiating (4.55) and (4.56) with respect to time.

The equilibrium Eqs. (4.4) with Eqs. (4.55) and (4.56) lead to the relations

$$\ddot{w}_0 = -\frac{3\omega}{2} - \frac{6}{\beta^2} = \frac{-3}{(\beta - 1)^2} - \frac{3\omega}{2} \quad (4.57)$$

which in turn yield

$$\begin{aligned} \dot{w}_0(\tau) &= \left(-\frac{6}{\beta^2} - \frac{3\omega}{2} \right) (\tau - \tau_3) + \dot{w}_0(\tau_3) \quad (4.58) \\ w_0(\tau) &= \left(-\frac{6}{\beta^2} - \frac{3\omega}{2} \right) \frac{(\tau - \tau_3)^2}{2} + \dot{w}_0(\tau_3) (\tau - \tau_3) + w_0(\tau_3). \end{aligned}$$

The motion stops at the moment τ_4 when $\dot{w}_0(\tau_4) = 0$. Thus

$$\tau_4 = \tau_3 + \frac{2\beta^2 \dot{w}_0(\tau_3)}{12 + 3\omega\beta^2}. \quad (4.59)$$

4.3.4 Case IV

4.3.4.1 First phase of motion

During the first phase (Fig. 4.8)

$$\dot{w} = \dot{w}_1 \frac{\beta_1 - \xi}{\beta_1} + \frac{\xi}{\beta_1} \quad (4.60)$$

for $\xi \in (0, \beta_1)$ and

$$\dot{w} = \dot{w}_2 \frac{\beta_2 - \xi}{\beta_2 - 1} + \frac{\xi - 1}{\beta_2 - 1} \quad (4.61)$$

for $\xi \in (\beta_2, 1)$, whereas in the central part of the shell $\dot{w} = 1$. In Eqs. (4.60) and (4.61) $\beta_1 = \text{const}$, $\beta_2 = \text{const}$ whereas \dot{w}_1 and \dot{w}_2 are certain functions of time. Making use of (4.60), (4.61) and (4.4) it is easy to recheck that

$$\begin{aligned}
q &= \frac{1}{\nu} \left[(\omega + \ddot{w}_1) \xi - \frac{\ddot{w}_1}{2\beta_1} \xi^2 + \nu \right], \\
m &= -\frac{\xi^2}{2} (\omega + \ddot{w}_1) + \frac{\ddot{w}_1}{6\beta_1} \xi^3 - \nu \xi + 1
\end{aligned} \tag{4.62}$$

for $\xi \in (0, \beta_1)$ and

$$\begin{aligned}
q &= \frac{1}{\nu} \left[(\omega + \ddot{w}_2) (\xi - 1) - \frac{\ddot{w}_2}{2(\beta_2 - 1)} (\xi - 1)^2 - \nu \right], \\
m &= -\frac{(\xi - 1)^2}{2} (\omega + \ddot{w}_2) + \frac{\ddot{w}_2}{6(\beta_2 - 1)} (\xi - 1)^3 + \nu (\xi - 1)
\end{aligned} \tag{4.63}$$

for $\xi \in (\beta_2, 1)$. In the central part of the shell $q = 0$, $m = 1$, $n = 0$.

Inserting $q(\beta_j, \tau) = 0$, $m(\beta_j, \tau) = -1$ in Eqs. (4.62) and (4.63) leads to the relations (here $j = 1, 2$)

$$\begin{aligned}
\ddot{w}_1 &= -\omega + \frac{12}{\beta_1^2} - \frac{4\nu}{\beta_1}, \\
\ddot{w}_2 &= -\omega + \frac{6}{(\beta_2 - 1)^2} + \frac{4\nu}{\beta_2 - 1}
\end{aligned} \tag{4.64}$$

and

$$\begin{aligned}
\beta_1 &= \frac{\nu - \sqrt{\nu^2 - 12\omega}}{\omega}, \\
\beta_2 &= \frac{\omega - \nu + \sqrt{\nu^2 - 6\omega}}{\omega}.
\end{aligned} \tag{4.65}$$

It is worthwhile to mention that the accelerations \ddot{w}_1 , \ddot{w}_2 in Eq. (4.64) are similar to those for the first phase of case II (formulae (4.32) and (4.33)). The first phase of motion ends when $\dot{w}_2(\tau_1) = 0$. Thus

$$\tau_1 = \frac{(1 - \beta_2)^2}{4\nu(1 - \beta_2) + \omega(1 - \beta_2)^2 - 6} \tag{4.66}$$

and

$$\dot{w}_j(\tau_1) = \ddot{w}_j \tau_1 + 1 \tag{4.67}$$

whereas

$$w_j(\tau_1) = \ddot{w}_j \frac{\tau_1^2}{2} + \tau_1. \tag{4.68}$$

Here $j = 1, 2$.

4.3.4.2 Second phase of motion

Now a bending hinge starting from the position $\eta(\tau_1) = \beta_2$ moves towards the center of the shell. The another bending hinge remains stationary at $\xi = \beta_1$ (Fig. 4.9). Shear sliding also takes place at the clamped end of the shell.

The motion of the left part of the shell for $\xi \in (0, \beta_1)$ is similar to the former phase. Thus the relations (4.60) and (4.62) remain valid for the present case as well. For $\xi \in (\beta_2, 1)$ instead of (4.61) and (4.63) one has

$$\dot{w} = \frac{\xi - 1}{\eta_2 - 1}, \quad \ddot{w} = \frac{-\dot{\eta}_2}{(\eta_2 - 1)^2}(\xi - 1) \quad (4.69)$$

and

$$q = \frac{1}{\nu} \left[\omega(\xi - \eta_2) - \frac{\dot{\eta}_2}{2(\eta_2 - 1)^2} [(\xi - \eta_2)^2 + 2(\xi - \eta_2)(\eta_2 - 1)] \right], \quad (4.70)$$

$$m = -\frac{\omega}{2}(\xi - \eta_2)^2 + \frac{\dot{\eta}_2}{6(\eta_2 - 1)^2} [(\xi - \eta_2)^3 + 3(\xi - \eta_2)^2(\eta_2 - 1)] - 1$$

where conditions $q(\eta_2, \tau) = 0$, $m(\eta_2, \tau) = -1$ are taken into account.

Inserting the boundary conditions $m(1, \tau) = 0$ and $\eta_2(\tau_1) = \beta_2$ in Eq. (4.70) leads to the relation

$$\eta_2 = 1 - \sqrt{-\frac{2}{\omega} + \left[\frac{2}{\omega} + (\beta_2 - 1)^2 \right] e^{3\omega(\tau - \tau_1)}}. \quad (4.71)$$

Assume that the second phase of motion end at $\tau = \tau_2$ when the travelling hinge at $\xi = \eta_2$ reaches the position $\xi = \beta_1$. Making use of (4.71) one can define the time

$$\tau_2 = \frac{1}{3\omega} \ln \frac{2 + \omega(\beta_1 - 1)^2}{2 + \omega(\beta_2 - 1)^2} + \tau_1 \quad (4.72)$$

where β_1, β_2 are given by (4.65) and τ_1 by (4.66).

Evidently, the central displacement $w_0(\tau) = \tau$ and according to (4.64)-(4.68)

$$\begin{aligned} \dot{w}_1(\tau_2) &= \left(-\omega + \frac{12}{\beta_1^2} - \frac{4\nu}{\beta_1} \right) \tau_2 + 1, \\ w_1(\tau_2) &= \left(-\omega + \frac{12}{\beta_1^2} - \frac{4\nu}{\beta_1} \right) \frac{\tau_2^2}{2} + \tau_2, \\ \dot{w}_0(\tau_2) &= 1, \quad w_0(\tau_2) = \tau_2, \quad \eta(\tau_2) = \beta_1. \end{aligned} \quad (4.73)$$

4.3.4.3 Third phase of motion

During this phase the bending hinge $\eta(\tau)$ being at $\xi = \beta_1$ initially moves towards the clamped end. At the same time shear sliding takes place at the clamped end. This deformation mechanism coincides with that of the second phase of case III (Fig. 4.6). Now $\eta_e = \eta$.

For determination of quantities w_0 , w_1 and η one can use the system (4.44) which corresponds to the velocity pattern presented in Fig. 6. However, initial conditions for the set (4.44) are given by (4.72) and (4.73). This phase of motion terminates at the moment $\tau = \tau_3$ when shear sliding ceases, e.g. $\dot{w}_1(\tau_3) = 0$.

4.3.4.4 Fourth phase of motion

During this phase the velocity distribution has a triangular shape with the single moving hinge travelling towards the clamped end (Fig. 4.7). This type of motion coincides with that of the third phase of case III. Thus the relations (4.49)-(4.54) hold good in the present case, as well. However, the time τ_3 in (4.54) is to be replaced by τ_4 , for which $\eta(\tau_4) = \beta$.

4.3.4.5 Fifth phase of motion

This phase of motion coincides with the fourth phase of case III. Thus (4.55)-(4.58) hold good, provided τ_3 is replaced by τ_4 . The motion stops at τ_5 when $\dot{w}_0(\tau_5) = 0$. It follows from (4.58) that

$$\tau_5 = \tau_4 + \frac{2\beta^2\dot{w}_0(\tau_4)}{12 + 3\omega\beta^2}. \quad (4.74)$$

4.3.5 Case V

4.3.5.1 First phase of motion

This phase of motion coincides with the first phase of case IV. Thus the relations (4.60)-(4.68) hold good in the present case.

4.3.5.2 Second phase of motion

The motion of the shell during the second phase also coincides with that corresponding to the second phase of case IV. However, the second phase terminates now at the moment when shear sliding stops at the clamped end, e.g. $\dot{w}_1(\tau_2) = 0$, or

$$\tau_2 = \frac{\beta_1^2}{\omega\beta_1^2 + 4\nu\beta_1 - 12} \quad (4.75)$$

and

$$w_1(\tau_2) = \frac{\beta_1^2}{2(\omega\beta_1^2 + 4\nu\beta_1 - 12)}. \quad (4.76)$$

Note that during the second phase of motion relations (4.69)-(4.71) hold good for the right-hand part and (4.60) and (4.62) for the left hand part of the shell.

4.3.5.3 Third phase of motion

At the moment τ_2 defined by (4.75) the third phase of motion can be promulgated. Now the deformation mechanism follows the scheme depicted in Fig. 4.10. Both hinges, located at $\xi = \eta_1$ and $\xi = \eta_2$, respectively, are travelling hinges.

For the region $\xi \in (\eta_2, 1)$ relations (4.69)-(4.71) remain valid in the present case as well. However, for $\xi \in (0, \eta)$ one has (Fig. 4.10)

$$\dot{w} = \frac{\xi}{\eta_1}, \quad \ddot{w} = -\frac{\dot{\eta}_1}{\eta_1^2}\xi. \quad (4.77)$$

The acceleration (4.77) and equations of motion (4.4) lead to stress distributions

$$\begin{aligned} q &= \frac{1}{\nu} \left[\omega\xi - \frac{\dot{\eta}_1}{2\eta_1^2}\xi^2 + \frac{\dot{\eta}_1}{2} - \omega\eta_1 \right], \\ m &= -\frac{\omega}{2}\xi^2 + \frac{\dot{\eta}_1}{6\eta_1^2}\xi^3 + \left(\omega\eta_1 - \frac{\dot{\eta}_1}{2} \right) \xi \end{aligned} \quad (4.78)$$

where

$$\dot{\eta}_1 = \frac{3}{2}\omega\eta_1 + \frac{6}{\eta_1}. \quad (4.79)$$

The solution of (4.79) satisfying the initial condition $\eta_1(\tau_2) = \beta_1$ can be presented as

$$\eta_1 = \sqrt{-\frac{4}{\omega} + \left(\frac{4}{\omega} + \beta_1^2 \right) e^{3\omega(\tau - \tau_2)}}. \quad (4.80)$$

The third phase of motion ends at the moment $\tau = \tau_3$ when the travelling hinges meet each other, e.g. $\eta_1(\tau_3) = \eta_2(\tau_3)$. Making use of (4.71) and (4.80) one can recheck that

$$e^{3\omega(\tau_3 - \tau_2)} = \frac{1}{A} \left[B \pm \sqrt{B^2 - A \left[\frac{8}{\omega} + \left(1 + \frac{2}{\omega} \right)^2 \right]} \right] \quad (4.81)$$

where

$$\begin{aligned} A &= \left[\frac{2}{\omega} + \beta_1^2 - (\beta_2 - 1)^2 \right]^2, \\ B &= \left(1 + \frac{2}{\omega} \right) \left(\frac{2}{\omega} + \beta_1^2 \right) + (\beta_2 - 1)^2 \left(1 - \frac{2}{\omega} \right) + \frac{4}{\omega}. \end{aligned} \quad (4.82)$$

From (4.81) one easily obtains

$$\tau_3 = \tau_2 + \frac{1}{3\omega} \ln \left\{ B \pm \sqrt{B^2 - A \left[\frac{8}{\omega} + \left(1 + \frac{2}{\omega} \right)^2 \right]} \right\} - \frac{\ln A}{3\omega}. \quad (4.83)$$

At the final moment of the third phase of motion

$$\dot{w}_0(\tau_3) = 1, \quad w_0(\tau_3) = \tau_3.$$

4.3.5.4 Fourth phase of motion

Now the motion takes place with a single moving hinge. The transverse velocity pattern corresponds to Fig. 4.7. This type of motion was considered earlier (the phase four, case IV).

4.3.5.5 Fifth phase of motion

This phase of motion coincides with the fifth phase of case IV.

4.4 Discussion

The results of calculations are presented in Table 4.1 and 4.2 and Figs. 4.11-4.15.

In Table 4.1 the values of the coordinates ξ_0 and ξ_* are presented for different values of the parameter ν . Here $\omega = 2$.

Distributions of the longitudinal bending moment m and shear force q at the initial moment of time are presented in Figs. 4.11-4.13. Fig. 4.11 corresponds to the case I, Fig. 4.12 to the case III and Fig. 4.13 to the case V. It can be seen from Figs. 4.11-4.13 that the stress distributions do not exceed the limits of admissible values. Calculations carried out showed that the stress distributions varied only slightly in time.

Maximal displacements as functions of time τ are presented in Figs. 4.14 and 4.15. Fig. 4.14 corresponds to the case I whereas Fig. 4.15 is associated with the cases II and III.

It can be seen from Figs. 4.12-4.15 that the bending moment, shear force and permanent transverse deflections are more sensitive to the parameter ν in the case of smaller values of ν .

On the other hand, the results of calculations bear out the corollary that shear effects become more important for shorter shells and less important for longer shells. The same conclusion was drawn by Jones and Oliveira [16] and Li and Jones [15] when studying cylindrical shells with symmetrical boundary conditions, subjected to impulsive and blast loading, respectively. Similar observations have been found previously by Li and Jones [10, 22] for clamped beams and circular plates subjected to distributed blast loadings of finite intensity.

Following Li and Jones [10] the cubic yield surface was used in the present study. Li and Jones [10, 22] suggested extension of the yield surface corresponding to the Tresca yield criterion to include the transverse shear force as an independent quantity. This yield surface circumscribes other proposed yield surface to give an upper bound solution. A lower bound solution may be obtained when the size of the cubic yield surface is multiplied by 0.75.

Theoretical predictions presented above are valid under the assumption that the stress distribution is admissible everywhere and the flow law is violated nowhere. This means that the bending moment and the shear force must meet inequalities $|m(\xi, \tau)| \leq 1$, $|q(\xi, \tau)| \leq 1$, provided the yield regime corresponds to the face $n = 1$ of the yield surface. The kinematical admissibility of the solution is controlled by the energy criterion

$$\dot{E}_j = P_j \dot{\delta}_j \geq 0 \quad (4.84)$$

at each hinge circle. Here \dot{E}_k stands for energy dissipation rate at a hinge circle $\xi = \xi_j$, P_j is a generalized stress (bending moment or shear force) and $\dot{\delta}_j$ stands for the corresponding generalized strain.

It is assumed herein that the shells under consideration are short but remaining "reasonably short" so that the length of the tube cannot be much less than the thickness of the shell wall. Using the notations (4.3) we confined our attention to shells with $\nu > 1$. The minimum value of $\nu = \nu_1$ is obtained from the condition that $\ddot{w}_1 < 0$ during the final phase of case I. From (4.23) it follows that

$$\nu_1 = 1 - \frac{1}{2}\omega.$$

The values of $\nu = \nu_j$, such that for $\nu_j \leq \nu \leq \nu_{j+1}$ for $j = 1, 2, 3, 4, 5$ the solution corresponds to the case number j , are accommodated in Table 2 for different values of the parameter ω . Although $\nu_1 = 0$ in Table 2 for smaller values of ω one has $\nu_1 > 0$. For instance, in the case when $\omega = 1$ evidently $\nu_1 = 0.5$.

As it was mentioned above ν_2 is obtained as a solution of (4.27) whereas ν_3 is defined as $max\nu$ for which $\tau_{22} \leq \tau_{23}$. Here τ_{22} stands for the solution of (4.44) with respect to τ_2 and τ_{23} satisfies the equation $\dot{w}_1(\tau_2) = 0$. However, ν_4 is determined according to the requirement $\beta_1 = \beta_2$ and ν_5 from the condition that the travelling hinge η_2 reaches the position β_1 earlier than shear sliding stops at the clamped edge. Thus according to (4.66), (4.71)-(4.73) and (4.75) $\nu_5 = max\nu$ for which

$$\frac{1}{3\omega} \ln \frac{2 + \omega(\beta_1 - 1)^2}{2 + \omega(\beta_2 - 1)^2} + \frac{(1 - \beta_2)^2}{4\nu(1 - \beta_2) + \omega(1 - \beta_2)^2 - 6} \leq \frac{\beta_1^2}{\omega\beta_1^2 + 4\nu\beta_1 - 12}.$$

It is worthwhile to mention that the final modal form stage of motion (the third phase for case II, the fourth phase for case III and the fifth phase for case IV and case V) is very short in time. Due to this the contribution of last phase in the total permanent displacements is small. It is somewhat surprising because in the pure bending theory the modal form motions are predominant among others [3].

4.5 Concluding remarks

The dynamic plastic response of rigid-plastic cylindrical shells to initial impulsive loadings is studied above. The transverse shear force, the circumferential membrane force and the longitudinal bending moment are retained in the simplified yield condition. Theoretical solutions are obtained for cylindrical shells clamped at the left and simply supported at the right-hand end.

It is interesting to note that the obtained solutions substantially differ from those corresponding to shells with both simply supported or clamped ends, respectively. It was noted by Li and Jones [15] that in the case of tubes with identical supports at both ends the solution (except of the longitudinal bending moment) is not sensitive to the support conditions. The same regards to beams and circular plates [10, 22].

The solution procedure revealed the matter that shear sliding is more essential for shorter shells as might be expected. On the other hand, deformation process begins with shear sliding at supports in each shell subjected to the impulsive loading. However, the share of shear in the bulk deformation is less in the case of longer shells.

Tabel 4.1. Values of ξ_0 and ξ_*

ν	ξ_0	ξ_*
2	0.7676	-
2.5	0.7342	-
3	0.7071	-
3.5	0.6849	-
4	0.6667	-
4.5	0.6514	-
5	0.6385	-
5.6166	0.6252	0.6252
6	-	0.6290
6.5	-	0.6344
7	-	0.6404
7.5	-	0.6464
8	-	0.6256
8.5	-	0.6594
9	-	0.6667
9.5614	-	0.6752

Tabel 4.2. Boundaries of cases I-V

ω	ν_1	ν_2	ν_3	ν_4	ν_5
2	0	5.6166	6.79	9.5614	10.7017
3	0	5.6166	6.78	9.8468	10.9386
4	0	5.6166	6.78	10.242	11.1805
5	0	5.6166	6.78	10.4289	11.42771
6	0	5.6166	6.78	10.7261	11.6785

Acknowledgement

The support from Estonian Science Foundation by Grant Project N^o 4377 is gratefully acknowledged.

4.6 References

- [1] Hodge P. Impact pressure loading of rigid-plastic cylindrical shells. *J Mech Phys Solids* 1955; 3: 176-188.
- [2] Song GH, Wang R. Rigid plastic analysis of cantilever cylindrical shells under transverse and axial impact. *Proceeding of the First Symposium on Limit Analysis and Plasticity Theory*. Beijing: Science Press; 1965. p. 77-85.
- [3] Jones N. *Structural Impact*. Cambridge, UK: Cambridge University Press; 1989.
- [4] Jones N. On the dynamic inelastic failure of beams. In: Wierzbicki T, Jones N, editors. *Structural Failure*. New York: Wiley; 1989. p. 133-159.
- [5] Jones N. Bounds on the dynamic plastic behaviour of structures including transverse shear effects. *Int J Impact Eng* 1985; 3(4): 273-291.
- [6] Stronge WJ, Yu TX. *Dynamic Models for Structural Plasticity*. London: Springer; 1993.
- [7] Yu TX, Chen FL. Failure of plastic structures under intense dynamic loading: modes, criteria and thresholds. *Int J Mech Sci* 2000; 42(8): 1537-1554.
- [8] Symonds PS. Plastic shear deformations in dynamic load problems. In: Heyman J, Leckie FA, editors. *Engineering Plasticity*. Cambridge: CUP; 1968. p. 647-664.
- [9] Nonaka T. Shear and bending response of a rigid-plastic beam to blast-type loading. *Ing Arch* 1977; 46: 35-52.
- [10] Li QM, Jones N. Blast loading of fully clamped beams with transverse shear effects. *Mech Struct Mach* 1995; 23(1): 59-86.
- [11] Jones N, Song B. Shear and bending response of a rigid-plastic beam to partly distributed blast-type loading. *J Struct Mech* 1986; 14(3): 275-320.
- [12] Jones N, de Oliveira JG. The influence of rotatory inertia and transverse shear on the dynamic plastic behaviour of beams. *J Appl Mech* 1979; 46: 303-310.
- [13] Jones N, de Oliveira JG. Dynamic plastic response of circular plates with transverse shear and rotatory inertia. *J Appl Mech* 1980; 47: 27-34.
- [14] Duffey TA. Dynamic rupture of shells. In: Wierzbicki T, Jones N, editors. *Structural Failure*. New York: Wiley; 1989. p. 161-172.
- [15] Li QM, Jones N. Blast loading of a "short" cylindrical shell with transverse shear effects. *Int J Impact Eng* 1995; 16(2): 331-353.
- [16] Jones N, de Oliveira JG. Impulsive loading of a cylindrical shell with transverse shear and rotatory inertia. *Int J Solids Struct* 1983; 19: 263-279.
- [17] Lellep J, Torn K. Shear and bending response of a rigid-plastic beam subjected to impulsive loading. *Int J Impact Eng* 2005; 31(9): 1081-1105.
- [18] Haydl HM, Sherbourne AN. Some approximations to the Ilyushin yield surface for circular plates and shells. *Angew Math Mech* 1979; 59(2): 131-

132.

[19] Ilyushin AA. Plasticite. Paris: Eurolles; 1957.

[20] Robinson M. An evaluation of the errors in the yield surface for a rotationally symmetric thin shell due to neglecting transverse normal stresses and shell curvature. *Int J Mech Sci* 2000; 42(6): 1087-1095.

[21] Zyczkowski M. Combined loadings in the theory of plasticity. Warszawa: PWN; 1981.

[22]. Li QM, Jones N. Blast loading of fully clamped circular plates with transverse shear effects. *Int J Solids Struct* 1994; 31: 1861-1876.

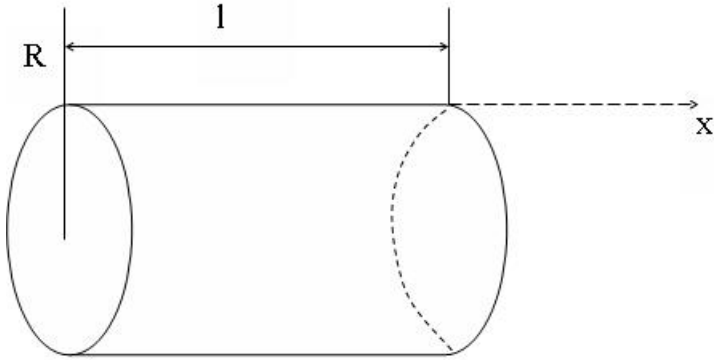


Figure 4.1: A cylindrical shell.

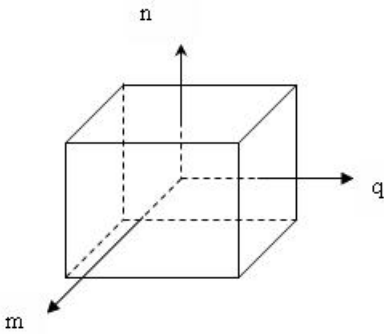


Figure 4.2: The yield surface.

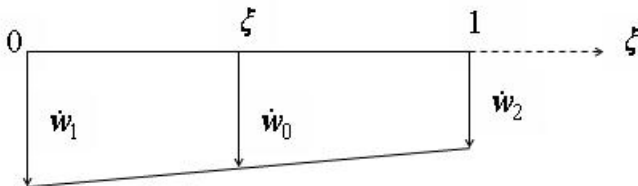


Figure 4.3: Velocity field for Case I, phase I.

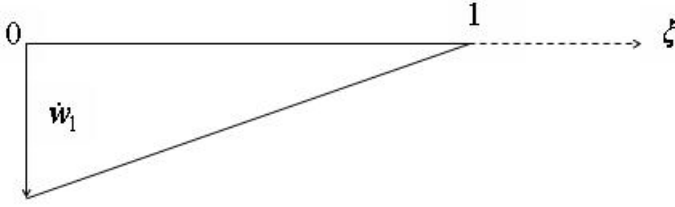


Figure 4.4: Velocity field for Case I, phase II.

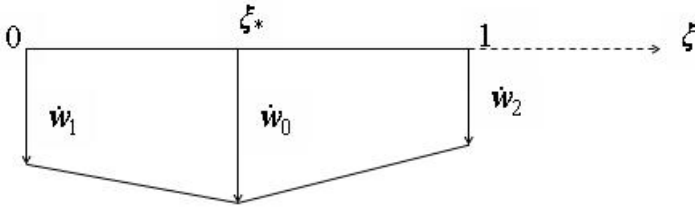


Figure 4.5: Velocity field for Case II, phase I.

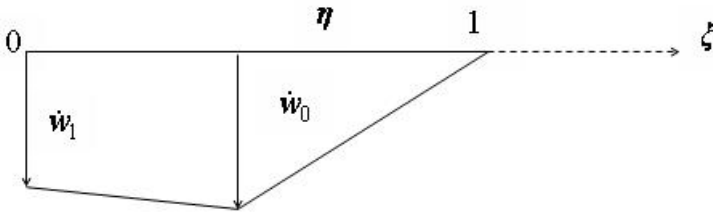


Figure 4.6: Velocity field for Case II, phase II.

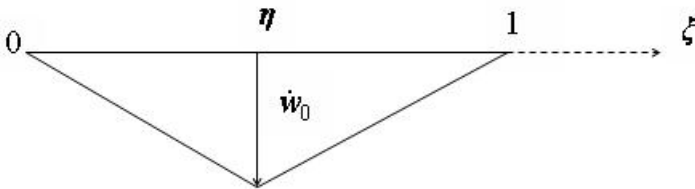


Figure 4.7: Velocity field for Case III, phase III.

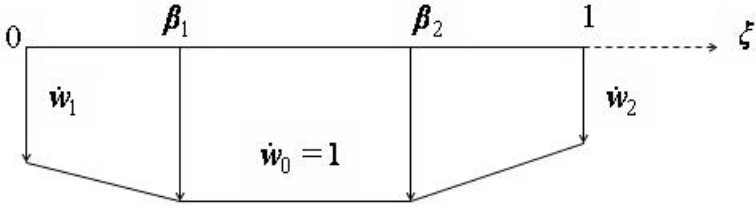


Figure 4.8: Velocity field for Case IV, phase I.

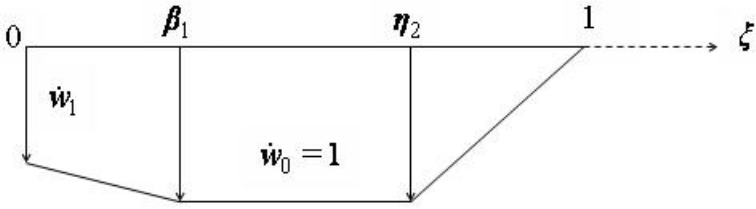


Figure 4.9: Velocity field for Case IV, phase II.

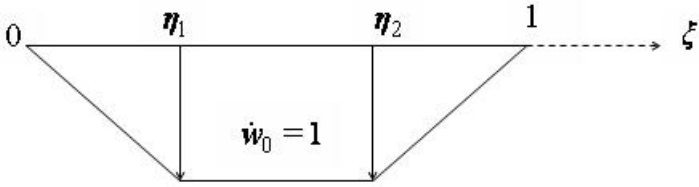


Figure 4.10: Velocity field for Case V, phase III.

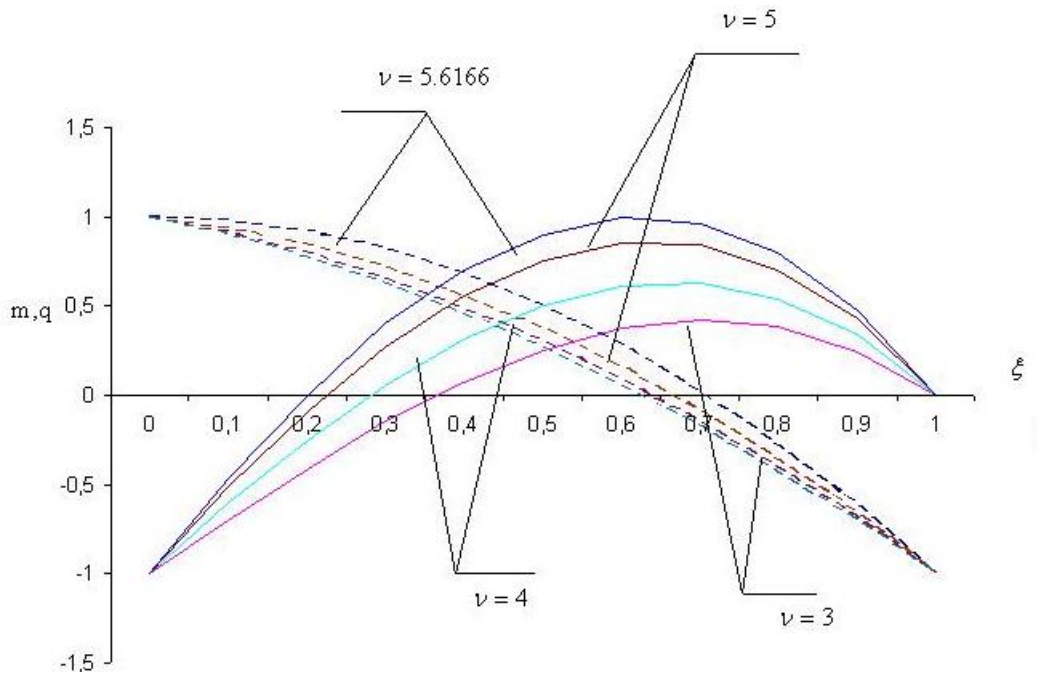


Figure 4.11: Bending moment and shear force (case I).

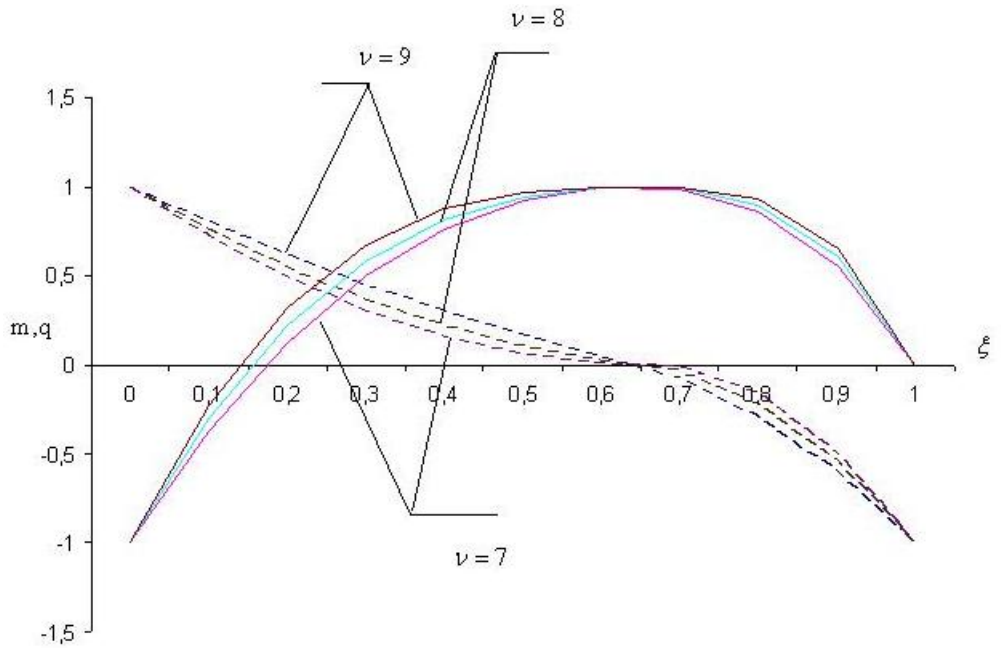


Figure 4.12: Bending moment and shear force (case III).

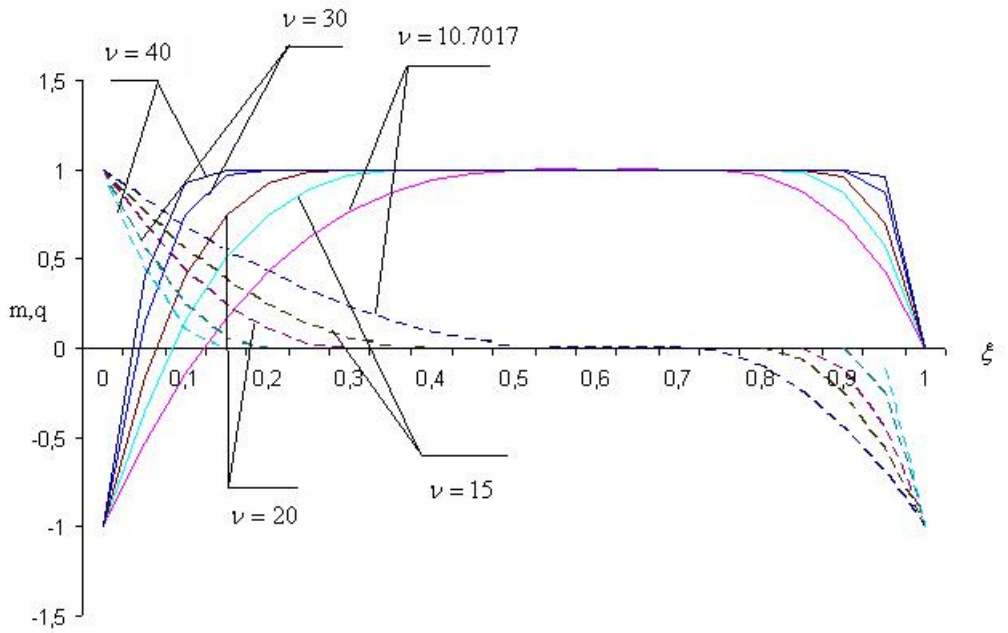


Figure 4.13: Bending moment and shear force (case V).

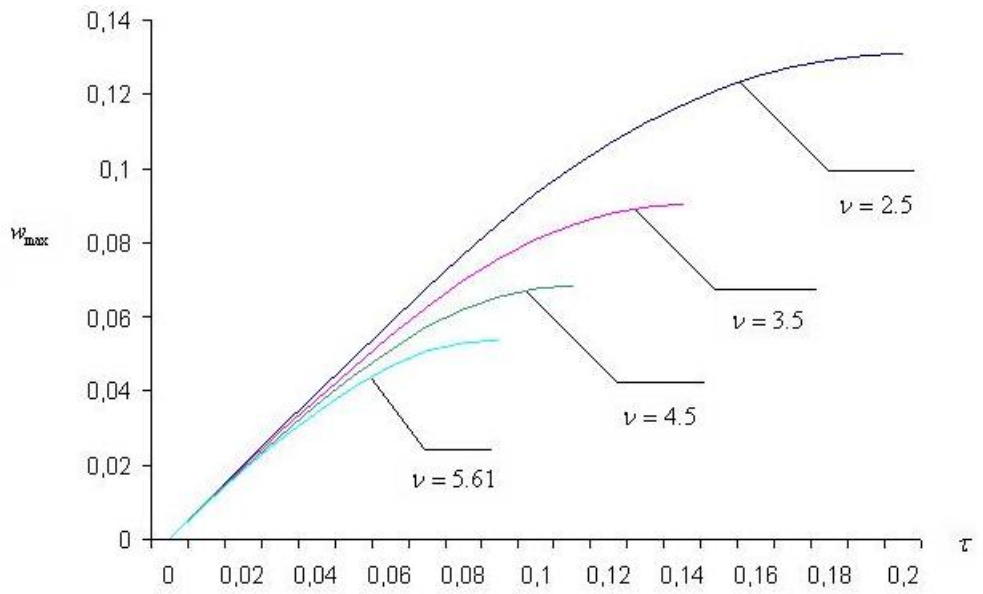


Figure 4.14: Maximal deflections (case I).

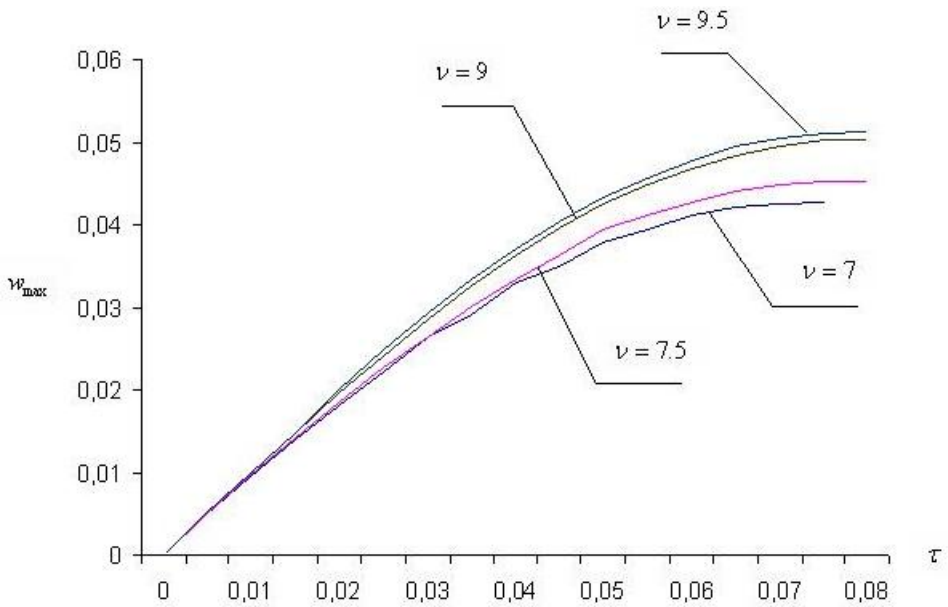


Figure 4.15: Maximal deflections (case III).

REFERENCES

- [1] Aggarwal HR, Ablow CM. Plastic bending of an annular plate by uniform impulse. *Int J Non-Linear Mech* 1971, 6(1): 69-80.
- [2] Calladine CR. *Plasticity for Engineers*. New York: Ellis Hoewood, Chichester; John Wiley 1985.
- [3] Campbell JD. *Dynamic Plasticity of Metals*. CISM, Springer 1972.
- [4] Chakrabarty J. *Applied Plasticity* . New York: Springer-Verlag 2000.
- [5] Chen WF, Liu XL. *Limit Analysis in Soil Mechanics*. Amsterdam: Elsevier 1990.
- [6] Dinno KS, Robinson M. Limit analysis of thick and thin circular plates subjected to transverse pressure. *World Conf Space Enclosures Montreal* 1976.
- [7] Drucker D. The effect of shear on the plastic bending of beams. *J Appl Mech* 1956; 23: 509-514.
- [8] Duffey TA. Dynamic rupture of shells. In: Wierzbicki T, Jones N, (Editors). *Structural Failure* New York: Wiley; 1989; 161-172.
- [9] Florence AL. Annular plate under a transverse line impulse. *AIAA J* 1965; 3(9): 1729-1732.
- [10] Florence AL. Clamped circular rigid-plastic plates under blast loading. *ASME J Appl Mech* 1966; 33: 256-260.
- [11] Florence AL. Clamped circular rigid-plastic plates under central blast loading. *Int J Solids Struct* 1966; 2: 319-335.
- [12] Florence AL. Response of circular plates to central pulse loading. *Int J Solids Struct* 1977; 13: 1091-1102.
- [13] Guowei Ma, Shoji Iwasaki, Yutaka Miyamoto and Hideaki Deto. Dynamic plastic behavior of circular plate using unified yield criterion. *Int J Solids Struct* 1999; 33(22): 3257-3275.

- [14] Haydl HM, Sherbourne AN. Rigid-plastic collapse of compression-bent shallow shells. *Int J Mech Sci* 1973; 15(9): 727-739.
- [15] Haydl HM, Sherbourne AN. Some approximations to the Ilyushin yield surface for circular plates and shells. *Angew Math Mech* 1979; 59(2): 131-132.
- [16] Heyman J. The full plastic moment of an I-beam in the response of shear force. *J Mech Phys Solids* 1970; 18: 359-365.
- [17] Hodge PG. Impact pressure loading of rigid-plastic cylindrical shells. *J Mech Phys Solids* 1955; 3: 176-188.
- [18] Hodge PG. *Plastic Analysis of Structures*. New York: Krieger 1981.
- [19] Hopkins HG, Prager W. On the dynamics of plastic circular plates. *J Appl Math Phys (ZAMP)* 1954; 5(4): 317-330.
- [20] Horne MR. *Plastic Theory of Structures*. Cambridge: MIT 1971.
- [21] Hu YQ. Application of response number for dynamic plastic response of plates subjected to impulsive loading. *Int J Pressure Vessels Piping* 2000; 77: 711-714.
- [22] Ilyushin AA. *Plasticite*. Paris: Eurolles; 1957.
- [23] Johnson W, Mellor PB. *Engineering Plasticity*. Ellis Horwood, Chichester 1986.
- [24] Jones N. Finite deflections of a simply supported rigid-plastic annular plate loaded dynamically. *Int J Solids Struct* 1968; 4: 593-603.
- [25] Jones N. Rigid-plastic behaviour of plates. *Bull Mech Eng Educ* 1970; 9(3): 235-248.
- [26] Jones N. Bounds on the dynamic plastic behaviour of structures including transverse shear effects. *Int J Impact Eng* 1985; 3(4): 273-291.
- [27] Jones N. *Structural Impact*. Cambridge, UK: Cambridge University Press; 1989.
- [28] Jones N. On the dynamic inelastic failure of beams. In: Wierzbicki T., Jones N. (Editors). *Structural Failure*. New York: Wiley; 1989; 133-159.
- [29] Jones N, Kim SB, LI QM. Response and failure of ductile circular plates struck by a mass. *J Pressure Vessel Technol* 1997; 119: 332-342.
- [30] Jones N, de Oliveira JG. The influence of rotatory inertia and transverse shear on the dynamic plastic behaviour of beams. *J Appl Mech* 1979; 46: 303-310.

- [31] Jones N, de Oliveira JG. Dynamic plastic response of circular plates with transverse shear and rotatory inertia. *J Appl Mech* 1980; 47(1): 27-34.
- [32] Jones N, de Oliveira JG. Impulsive loading of a cylindrical shell with transverse shear and rotatory inertia. *Int J Solids Struct* 1983; 19: 263-279.
- [33] Jones N, Song B. Shear and bending response of a rigid-plastic beam to partly distributed blast-type loading. *J Struct Mech* 1986; 14(3): 275-320.
- [34] Jones N, Wierzbicki T. *Structural Crashworthiness*. London: Butterworths 1983.
- [35] Kaliszky S. *Plasticity. Theory and Engineering Applications*. Amsterdam: Elsevier 1989.
- [36] Kumar A, Reddy VVK. Dynamic plastic response of circular plates with transverse shear. *J Appl Mech* 1986; 53: 952-953.
- [37] Landgraf G. Aufstellung von Fließbedingungen für Schnittgrößen von Flächentragwerken. *ZAMM* 1968; 48(5): 317-327.
- [38] Lee KH, Reddy JN, Wang CM. *Shear Deformable Beams and Plates Relationships with Classical Solutions*. Pergamon 2000.
- [39] Lellep J. Optymalizacja położenia podpor belki sztywno-plastycznej obciążonej impulsem predkości. *Mech Teoret Stosow* 1978; 16(4): 573-582.
- [40] Lellep J. Optimal location of additional supports for plastic cylindrical shells subjected to impulsive loading. *Int J Non-Linear Mech* 1984; 19(4): 323-330.
- [41] Lellep J, Mürk A. Inelastic stepped plates under impulsive loading. *Plasticity and Impact Mechanics*. (Ed. N.K. Gupta). Phoenix Publ House 2003: 577-588.
- [42] Lellep J, Sakkov E. Optimizations of cylindrical shells of fiber-reinforced composite materials. *Mech Compos Mat* 1996; 32(1): 65-71.
- [43] Lellep J, Torn K. Dynamic plastic response of circular cylindrical shells to dynamic loads. *Proc. 13th Nordic Sem Comp Mech, Mech Appl Math Series*, 7. Univ Oslo, Oslo 2000: 222-225.
- [44] Lellep J, Torn K. Plastic response of a circular cylindrical shell to dynamic loadings. *Int J Impact Eng* 2004; 30(5): 555-576.

- [45] Lellep J, Torn K. Shear, bending response of a rigid-plastic beam subjected to impulsive loading. *Int J Impact Eng* 2005; 31(9): 1081-1105.
- [46] Lellep J, Torn K. Dynamic plastic response of annular plates with transverse shear effects. *Int J Impact Eng* (in press)
- [47] Li QM. Continuity condition at bending and shearing interfaces of rigid, perfectly plastic structural elements. *Int J Solids Struct* 2000; 37: 3651-3665.
- [48] Li QM, Huang YG. Dynamic plastic response of thin circular plates with transverse shear and rotatory inertia subjected to rectangular pulse loading. *Int J Impact Eng* 1989; 8: 219-228.
- [49] Li QM, Huang YG. Dynamic plastic response of circular plates with transverse shear. *ASME, J Appl Mech* 1990; 57: 1077-1078.
- [50] Li QM, Jones N. Blast loading of fully clamped circular plates with transverse shear effects. *Int J Solids Struct* 1994; 31(14): 1861-1876.
- [51] Li QM, Jones N. Blast loading of fully clamped beams with transverse shear effects. *Mech Struct Mach* 1995; 23(1): 59-86.
- [52] Li QM, Jones N. Blast loading of a "short" cylindrical shell with transverse shear effects. *Int J Impact Eng* 1995; 16(2): 331-353.
- [53] Li QM, Jones N. Formation of a shear localization in structural elements under transverse dynamic loads. *Int J Solids Struct* 2000; 37(45): 6683-6704.
- [54] Li QM, Jones J. On dimensionless number for dynamic plastic response of structural members. *Arch Appl Mech* 2000; 70: 245-254.
- [55] Lin TH. *Theory of Inelastic Structures*. New York: Wiley 1968.
- [56] Liu D, Stronge WJ. Shear and bending deformation of rigid-plastic circular plates by central pressure pulse. *Int J Impact Eng* 1996; 18(4): 383-402.
- [57] Liu D, Stronge WJ. Deformation of simply supported circular plate by central pressure pulse. *Int J Solids Struct* 1996; 33(2): 283-299.
- [58] Ma G, Iwasaki S, Miyamoto Y, Deto H. Dynamic plastic behavior of circular plate using unified yield criterion. *Int J Solids Struct* 1999; 36: 3257-3275.
- [59] Martin J. *Plasticity: Fundamentals and General Results*. Cambridge: MIT Press 1975.
- [60] Mazalov VN, Nemirovski JV. Dynamical bending of circular piece-wise non-homogeneous plates. *Arch mech Stosow* 1973; 25(3): 469-490.

- [61] Mazalov VN, Nemirovsky JV. Dynamical bending of rigid-plastic annular plates. *Int J Non-Linear Mech* 1976; 11(1): 25-39.
- [62] Mohaghegh MM, Coon MD. Plastic analysis of thick circular plates. *Int J Mech Sci* 1973; 15(11): 935-938.
- [63] Mroz Z. Plastic deformation of annular plates under dynamic loads. *Arch Mech Stosow* 1958; 10: 499-516.
- [64] Nguyen Dang N. Variational and computational plastic limit and shakedown analysis. Birkhauser-Verlag 1995.
- [65] Niepostyn D, Stańczyk A. Impulsowe obciążenie plastycznej płyty pierścieniowej opartej na brzegu zewnętrznym. Część I. Impuls ciśnienia. *Biul WAT* 1979; 28(10): 61-76.
- [66] Niepostyn D, Stańczyk A. Impulsowe obciążenie plastycznej płyty pierścieniowej opartej na brzegu zewnętrznym. Część II. Wymyslenia kinematyczne. *Biul WAT* 1979; 28(10): 77-88.
- [67] Nonaka T. Some interaction effects in a problem of plastic beam dynamics. Parts 1-3. *ASME J Appl Mech* 1967; 34: 623-643.
- [68] Nonaka T. Shear and bending response of a rigid-plastic beam to blast-type loading. *Ing Arch* 1977; 46: 35-52.
- [69] de Oliveira JG, Jones N. Some remarks on the influence of transverse shear on the plastic yielding of structures, *Int J Mech Sci* 1978; 20: 759-765.
- [70] de Oliveira JG, Jones N. A numerical procedure for the dynamic plastic response of beams with rotatory inertia and transverse shear effects. *J Struct Mech* 1979; 7: 193-2230.
- [71] Robinson M. The effect of transverse shear stresses on the yield surface for thin shells. *Int J Solids and Struct* 1973; 9(7): 819-828.
- [72] Robinson M. An evaluation of the errors in the yield surface for a rotationally symmetric thin shell due to neglecting transverse normal stress and shell curvature. *Int J Mech Sci* 2000; 42(6): 1087-1095.
- [73] Save MA, Massonnet CE, Saxce GDe. *Plastic Limit Analysis of Plates, Shells and Disks*. Amsterdam: Elsevier 1997.
- [74] Sawczuk A, Duszek M. A note on the interaction of shear and bending in plastic plates. *Arch Mech Stosow* 1963; 15: 411-426.
- [75] Sawczuk A. *Mechanics and Plasticity of Structures*. PWN - Ellis Horwood, Chichester 1989.

- [76] Sawczuk A, Sokół-Supel J. Limit Analysis of Plates. Warszawa: PWN 1993.
- [77] Shen WQ, Jones N. Dynamic response and failure of fully clamped circular plates under impulsive loading. *Int J Impact Eng* 1993; 13(2): 259-278.
- [78] Shi XH, Gao YG. Generalization of response number for dynamic plastic response of shells subjected to impulsive loading. *Int J Pressure Vessels Piping* 2001; 78: 453-459.
- [79] Skrzypek J, Hetnarski RB. Plasticity and Creep. Theory, Examples and Problems. London, Tokyo: CRC press, Boca Raton 1993.
- [80] Song GH, Wang R. Rigid plastic analysis of cantilever cylindrical shells under transverse and axial impact. *Proceeding of the First Symposium on Limit Analysis and Plasticity Theory*. Beijing: Science Press 1965; 77-85.
- [81] Stańczyk A. Impuls brzegowy w plastycznej płycie pierścieniowej. *Rozpr Inżyn* 1982; 30(2): 201-226.
- [82] Stronge WJ, Yu TX. Dynamic Models for Structural Plasticity. London: Springer 1993.
- [83] Symonds PS. Plastic shear deformations in dynamic load problems. In: Heyman J, Leckie FA, (Editors). *Engineering Plasticity*. Cambridge: CUP 1968; 647-664.
- [84] Zaera R, Arias A, Navarro C. Analytical modelling of metallic circular plates subjected to impulsive loads. *Int J Solids Struct* 2002; 39(3): 659-672.
- [85] Zhao Y-P, Fang J, Yu TX. Dynamic plastic shear failure analysis for an infinitely large plate with a centred cylinder under impulsive loading. *Int J Solids Struct* 1994; 31(11): 1585-1595.
- [86] Zyczkowski M. Combined loadings in the theory of plasticity. Warszawa: PWN 1981.
- [87] Wang AJ. The permanent deflection of a plastic plate under blast loading. *J Appl Mech* 1955; 22: 375-376.
- [88] Wang AJ, Hopkins HG. The plastic deformation of built-in circular plates under impulsive load. *J Mech Phys Solids* 1954; 3: 22-37.
- [89] Wang Y, Yu M, Xiao Y, Li L. Dynamic plastic response of a circular plate based on unified strength theory. *Int J Impact Eng* 2005; 31(1): 25-40.

- [90] Wen HM. Deformation and tearing of clamped circular work-hardening plates under impulsive loading. *Int J Pressure Vessels Piping* 1998; 75(1): 67-73.
- [91] Wen HM, Yu TX, Reddy TY. Failure maps of clamped beams under impulsive loading. *Mech Struct Mach* 1995; 23: 453-472.
- [92] Wen HM, Yu TX, Reddy TY. A note on clamped circular plates under impulsive loading. *Mech Struct Mach* 1995; 23(3): 331-342.
- [93] Wierzbicki T, Jones N. *Structural Failure*. New York: Joh Wiley 1989.
- [94] Yu TX, Chen FL. Failure of plastic structures under intense dynamic loading: modes, criteria and thresholds. *Int J Mech Sci* 2000; 42(8): 1537-1554.
- [95] Yu TX, Chen FL. A further study of plastic shear failure of impulsively loaded clamped beams. *Int J Impact Eng* 2000; 24: 613-629.
- [96] Yu TX, Zang LC. *Plastic Bending: Theory and Applications*. World Scientific 1996.
- [97] Ерхов МИ. Теория идеально пластических элементов конструкций. М, Наука, 1978.
- [98] Комаров КЛ, Немировский ЮВ. Динамика жесткопластических элементов конструкций. Наука, Сиб отд Новосибирск 1984.
- [99] Леллеп Я. Импульсивное нагружение круглых пластин, материал которых имеет различные пределы текучести при растяжении и сжатии. *Tartu Riikl Ülik Toim* 1971; 281: 261-269.
- [100] Лепик Ю. Оптимальное проектирование неупругих конструкций в случае динамического нагружения. Таллинн: Валгус 1982.
- [101] Немировский ЮВ, Скворода АР. Динамический узиб жесткопластических защамленных круглых пластин при учете эффектов сдвига и инерции вращения. *Ж прикл мех техн физ* 1978; 2: 124-133.
- [102] Шаблий ОН, Жук НП. Предельное равновесие цилиндрической оболочки с учетом напряжений сдвига. *Прикл мех* 1974; 10(7): 69-76.
- [103] Шапиро ГС. Удар по кольцевой жестко-пластической пластинке. *Прикл мат мех* 1959; 23: 234-241.
- [104] Жук НП, Шаблий ОН. О предельном равновесии оболочек вращения и круглых пластин с учетом напряжений сдвига. *Прикл мех* 1972; 8(7): 35-41.

- [105] Жук НП, Шаблей ОН. Предельное равновесие круглой пластинки с учетом напряжений сдвига. Прикл механика 1973; 9(3): 47-54.

SUMMARY

In the present study problems of dynamic plastic behaviour of structural elements subjected to impulsive loading are studied. The attention is focused on structures (beams, annular plates, circular cylindrical shells) with non-symmetrical end conditions accounting for shear deformations. The latter means that in contrast to classical solutions shear forces are retained in the equations of yield surfaces and associated flow law.

In the introduction a review of existing literature in this area is presented.

In the first chapter equations for analysis of beams, axisymmetric plates and circular cylindrical shells are presented. Basic equations consist of a set of equilibrium equations and the yield surface with the associated flow law.

In the second chapter the dynamic response of a rigid-plastic beam is considered. The beam is subjected to the initial impulsive loading. Plastic yielding of the material is controlled by the square yield criterion which retains the transverse shear force as well as the bending moment. The beam under consideration is clamped at the left and simply supported at the right hand end.

In the third chapter the dynamic response of a rigid-plastic annular plate clamped at the outer edge and free at the inner edge is considered. The plate is subjected to initial impulsive loading so that at the initial moment of time all points of the plate have the uniform transverse velocity. It is assumed that the behaviour of a rigid perfectly plastic material is controlled by a cubic yield condition and the associated flow law in the space of bending moments and the transverse shear force. Theoretical predictions are developed and compared with an upper bound solution.

In the fourth chapter the dynamic plastic behaviour of a circular cylindrical shell subjected to an initial impulsive loading is studied. It is assumed that the thin walled tube is clamped at the left end and simply supported at the right-hand end. The behaviour of the rigid, perfectly plastic material is controlled by a cubic yield condition which retains the axial bending moment, circumferential membrane force as well as the transverse shear force. Theoretical predictions are presented for a wide range of geometrical and material parameters of the shell.

The Chapters 2-4 consist of three original journal papers published in recent years.

KOKKUVÕTE

Impulsiivselt koormatud konstruktsioonide käitumine arvestades nihkepingeid

Käesolevas töös uuritakse impulsiivselt koormatud plastsete kehade dünaamilist käitumist. Tähelepanu all on konstruktsioonid (talad, ümarplaadid, ringsilindrilised koorikud), millel on mittesümmeetrilised rajatingimused ja mille korral võetakse arvesse nihkepinged. See tähendab, et erinevalt klassikalistest lahendustest nihkepinged jäävad voolavuspinna ja assotseeritud voolavusseaduse võrranditesse.

Sissejuhatuses on toodud ülevaade plastsete talade, plaatide ja koorikute dünaamilist koormamist käsitleva kirjanduse kohta.

Esimese peatükis on toodud põhivõrrandid talade, ümarplaatide ja ringsilindriliste koorikute kohta. Põhivõrrandid koosnevad tasakaaluvõrranditest, voolavustingimustest ja assotseeritud voolavusseadusest.

Teises peatükis on vaadeldud jäik-plastsete talade dünaamilist käitumist. Tala on impulsiivselt koormatud. Eeldatakse, et materjali käitumine vastab ruudukujulisele voolavustingimusele. Tala üks ots on vabalt toetatud ja teine on jäigalt kinnitatud. Töös näidatakse, et sõltuvalt parameetri $\nu = Q_0 l / M_0$ väärtusest võib deformatsiooni mehhanism olla erinev, ent kõigil juhtudel lõpeb liikumine modaalse liikumise faasiga. Huvitav on märkida, et antud tala korral, st kui tala üks ots on jäigalt kinnitatud ja teine vabalt toetatud, on deformeerumise mehhanism täiesti erinev sellest juhust, kui tala mõlemad otsad on ühte moodi kinnitatud.

Samale järeldusele jõutakse ka ringsilindrilise kooriku ja rõngasplaadi uurimise korral. Rõngasplaadi korral oleks sümmeetriliselt kinnitatud plaadiks ümarplaat.

Kolmandas peatükis on uuritud jäik-plastse rõngasplaadi dünaamilist käitumist. Plaadi välisserv on jäigalt kinnitatud ja siseserv vabalt toetatud. Plaadile on rakendatud impulsiivne koormus, mis tähendab, et liikumise algmomendil on plaadi kõikidele punktidele rakendatud ühtlane kiirus. Eeldatakse, et materjali plastsust kontrollitakse kuubikujulise voolavustingimusega.

Neljandas peatükis käsitletakse impulsiivselt koormatud ringsilindrilise kooriku dünaamilist käitumist. Eeldatakse, et kooriku üks ots on jäigalt kinnitatud ja teine vabalt toetatud.

Käesoleva töö teine, kolmas ja neljas peatükk on iseseisva uurimistöö tulemus, mis on avaldatud trükis 3 artiklina.

ACKNOWLEDGEMENT

I am very grateful to professor Jaan Lellep for supervising this work.

CURRICULUM VITAE

Kadre Torn

Born: June 02, 1969, Tartu, Estonia.

Nationality: Estonian.

Marital Status: Married, 4 children.

Address: Liivi 2, 50409 Tartu, Estonia,

phone: +37 27 440 312, e-mail: kadre@bose.ee.

Education

1987 Tartu Secondary School No. 2.

1987 - 1994 Faculty of Mathematics, University of Tartu.

1998 - 2006 PhD student of the Institute of Applied Mathematics,
University of Tartu.

Professional employment

1994 - 1999 Secretary of the chair of Theoretical mechanics,
University of Tartu.

From 2000 Data operator of Backoffice Services Estonia OÜ.

Scientific work

Dynamics and optimization of plastic shells accounting for shear forces.

List of publications

1. Lellep J, Torn K. Plastic response of a circular cylindrical shell to dynamic loadings. *Int. J. Impact Eng.* 2004; 30(5): 555-576.
2. Lellep J, Torn K. Shear, bending response of a rigid-plastic beam subjected to impulsive loading. *Int. J. Impact Eng.* 2005; 31(9): 1081-1105.
3. Lellep J, Torn K. Dynamic plastic response of circular cylindrical shells to dynamic loads. *Proc. 13th Nordic Sem. Comp. Mech., Mech. Appl. Math. Series, 7. Univ. Oslo, Oslo.* 2000: 222-225.
4. Lellep J, Torn K. Dynamic plastic response of annular plates with transverse shear effects. *Int. J. Impact Eng.* (in press)

CURRICULUM VITAE

Kadre Torn

Sünniaeg ja -koht: 02. juuni 1969, Tartu, Eesti.

Kodakondsus: Eestlane.

Perekonnaseis: Abielus, 4 last.

Aadress: Liivi 2, 50409 Tartu, Eesti,

tel: +37 27 440 312, e-mail: kadre@bose.ee.

Haridus

- 1987 Tartu 2. Keskkool, keskharidus.
1987 - 1994 Tartu Ülikool, Matemaatikateaduskond, kõrgharidus.
1998 - 2006 Doktoriõpe, Tartu Ülikool, Matemaatikateaduskond.

Teenistuskäik

- 1994 - 1999 Tartu Ülikooli teoreetilise mehaanika kateedri vanemlaborant.
Alates 2000 Backoffice Services Estonia OÜ, vanemandmeoperaator.

Teaduslik tegevus

Teadustöö teema on plastsete koorikute dünaamika ja optimeerimine arvestades nihkepingeid.

Teaduspublikatsioonid

1. Lellep J, Torn K. Plastic response of a circular cylindrical shell to dynamic loadings. *Int. J. Impact Eng.* 2004; 30(5): 555-576.
2. Lellep J, Torn K. Shear, bending response of a rigid-plastic beam subjected to impulsive loading. *Int. J. Impact Eng.* 2005; 31(9): 1081-1105.
3. Lellep J, Torn K. Dynamic plastic response of circular cylindrical shells to dynamic loads. *Proc. 13th Nordic Sem. Comp. Mech., Mech. Appl. Math. Series, 7. Univ. Oslo, Oslo.* 2000: 222-225.
4. Lellep J, Torn K. Dynamic plastic response of annular plates with transverse shear effects. *Int. J. Impact Eng.* (in press)